Dissertation

Femtosecond UV-VIS Absorption Studies of Retinal

フェムト秒時間分解紫外・可視吸収分光によるレチナールの研究

Shoichi Yamaguchi

山口　祥一

December, 1997

Dissertation

Femtosecond UV-VIS Absorption Studies of Retinal

フェムト秒時間分解紫外・可視吸収分光によるレチナールの研究

Shoichi Yamaguchi

山口　祥一

December, 1997

Contents

1. Introduction

1-1. Background

In 1949, when lasers were not yet invented, Porter and Norrish developed the flash photolysis method which employs discharge tubes in order to study photofragmentation reactions of gaseous molecules such as biacetyl and carbon disulfide [1, 2]. They acquired millisecond time-resolved UV-VIS absorption spectra of those molecules, and in the case of biacetyl, for example, they found acetyl radical as a reaction intermediate. Time-resolved spectroscopy, which they initiated, has made great advances since then in terms of time resolution, detection sensitivity, and applicability. Their original method that a first flash excites molecules to start a reaction and a second flash probes the excited molecules to detect a reaction intermediate is presently called pump-probe spectroscopy, and even now it is still a major method of time-resolved spectroscopy. In other words, the advances of time-resolved spectroscopy so far are not ascribed to the progress of experimental principles, but supported by the development of lasers and electronics. Researches into chemical reaction dynamics, which were Porter's main purpose in originating flash photolysis, have been demanding excellent technique of time-resolved spectroscopy and strongly motivating the development of it.

Time-resolved UV-VIS absorption spectroscopy is at present reaching the limit of time resolution. Pump-probe spectroscopy utilizing femtosecond pulses has the fastest time resolution among all kinds of time-resolved UV-VIS absorption spectroscopy. The time resolution of pump-probe absorption spectroscopy is determined by the pulse width of a pump pulse and that of a probe pulse. The generation of ultrashort pulses as short as 6 fs was reported in 1987 [3], and recently 10-fs pulses have been acquired with more stability by using far simpler laser systems [4, 5]. After we consider that, for instance, a Fourier transform-limited 1-fs pulse has spectral width of as much as 10000 cm^{-1}, we do not anticipate any great future improvement of the time resolution of pump-probe UV-VIS absorption spectroscopy based on the same experimental principle. In fact, the recent progress of the generation of ultrashort optical pulses is directed toward the improvement of stability and tuning range rather than the shortening of pulse width. It is due to the fact that the replacement of dye solutions with ion-doped crystals as a laser gain medium did not enlarge gain band width, but brought about the distinct improvement of the optical stability of a gain medium against light and heat.

Nevertheless there is still sufficient room for improvement in time-resolved UV-VIS absorption spectroscopy even based on the same experimental principle, that is, the pump-probe method. An ideal situation for studying chemical reaction dynamics, where there is no room for improvement in lasers, is imagined as follows: The center wavelength and the peak power of ultrashort pump pulses can be arbitrarily chosen, and transient absorption spectrum can be recorded by using ultrashort probe pulses simultaneously in the wide wavelength

region extending from 200 nm to 1000 nm. Though the recent advance of the nonlinear optical mixing technique is making it possible to arbitrarily choose the center wavelength of pump pulses, it is still difficult to acquire arbitrary peak power and the fastest time resolution with pump wavelength arbitrarily chosen. The only way to generate wide-band ultrashort probe pulses is to focus intense ultrashort pulses into a transparent medium in order to induce self-phase modulation (SPM). The group velocity dispersion (GVD) in the SPM medium makes time resolution worse, and the band width of the acquired probe pulses is usually limited within the wavelength region from 400 nm to 1000 nm. Nishioka and co-workers have reported the generation of ultrabroadband femtosecond pulses ranging from 150 nm to 1000 nm [6], but the application of these pulses to time-resolved spectroscopy has not yet been performed. Femtosecond time-resolved UV absorption spectra in the wavelength region shorter than 400 nm has never been reported so far to the best of my knowledge. It is probable that all the above-mentioned problems are solved in the near future and ultrafast time-resolved UV-VIS absorption spectroscopy becomes a general handy experimental technique just like UV-VIS and FTIR spectrometers at present.

1-2. What will be reported and clarified

In this thesis, the construction of a femtosecond time-resolved pump-probe UV-VIS absorption spectrometer and its application to the ultrafast chemical dynamics of retinal in solution are reported.

In Chap. 2, the construction of the femtosecond absorption spectrometer is described. The time resolution of the constructed spectrometer is about 300 fs. The center wavelength of the pump pulses can be tuned at 267 ± 6 nm, 400 ± 10 nm, and 800 ± 20 nm. Time-resolved spectra can be recorded by way of multichannel detection in the VIS region of 400 nm ~ 800 nm and the UV region of 300 nm ~ 400 nm. Especially femtosecond time-resolved absorption spectra in the UV region have been measured for the first time to the best of my knowledge. I have also developed a novel method to measure the chirp structure of the wide-band probe pulses which is important in the data processing of the femtosecond time-resolved absorption spectra. This method is based on optical Kerr effect (OKE), and is superior in several aspects over the sum or difference frequency generation (SFG, DFG) cross-correlation method which is being used widely: The OKE cross-correlation method is more handy, more accurate, and much less time-consuming, and is especially powerful when the probe pulses are in the UV region.

By using this femtosecond UV-VIS spectrometer, the ultrafast dynamics of retinal and terthiophene have been studied from the following perspectives, (a), (b), and (c):

(a) trans → cis photoisomerization reactions of retinal in non-polar solvents

Since retinal has four C=C double bonds in its polyenic backbone, there are sixteen possible

cis-trans isomers associated with it. Among these various isomers, the all-trans isomer is the most stable one. Depending upon the nature of the solvents, isomerization of the all-trans isomer to the other isomers takes place in the excited states. As depicted in Fig. 1-1, all-trans retinal in aerated non-polar solvents such as hexane isomerizes upon UV irradiation to yield 13-cis and 9-cis retinal [7-9]. This photoisomerization reaction mechanism has not yet been clarified because of the complicated electronic structure and the ultrashort lifetimes of the electronic excited singlet states of retinal. In the present study, the femtosecond time-resolved VIS absorption spectroscopy of all-trans, 13-cis, and 9-cis retinal and the femtosecond time-resolved UV absorption spectroscopy of all-trans retinal have been performed. It will be shown in Sect. 3-1 that an excited singlet state having a twisted structure at the C_{12}=C_{13} double bond participates as a reaction intermediate in the all-trans → 13-cis photoisomerization.

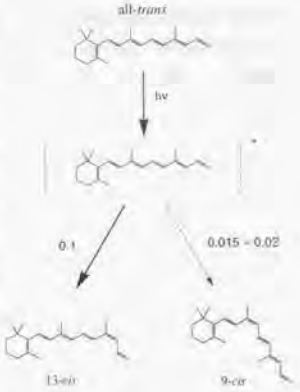

Fig. 1-1 Photoisomerization of all-trans retinal in aerated nonpolar solvents to the 13-cis and 9-cis isomers with their respective quantum yields.

(b) dynamic hydrogen-bonding between retinal and protic solvents in the excited states

As retinal has a carbonyl group, it is able to form a hydrogen-bond (H-bond) with a protic solvent molecule. H-bonded all-trans retinal photoisomerizes to yield the 11-cis isomer as well as 13-cis and 9-cis, and the quantum yield of all-trans → 11-cis reaction is lower than that of all-trans → 13-cis but higher than that of all-trans → 9-cis. It means that the H-bond formation greatly influences the electronic structure and the potential surface of the excited states of retinal. In Sect. 3-2, the ground-state UV-VIS absorption spectra and the femtosecond time-resolved VIS absorption spectra of all-trans retinal in the mixed solvents of 1-butanol and cyclohexane are shown. It will be shown that chemical equilibrium is established between free and H-bonded retinal in the ground (S_0) and the lowest excited triplet state (T_1) but that all the retinal molecules are H-bonded and free retinal does not exist in the first and second lowest excited singlet states (S_1, S_2).

(c) ultrafast vibrational relaxation in α-terthiophene

The dissipation of vibrational excess energy of photoexcited polyatomic molecules in liquids occurs in the femto- or picosecond time range. Such ultrafast energy dissipation is caused by solvent-solute interaction. Vibrational relaxation is followed by subsequent physical and chemical processes, and the distribution of vibrational energy strongly influences a chemical

reaction. Therefore, a chemical reaction in the solution phase is vastly different from that in the gas phase. In Chap. 4, the femtosecond time-resolved VIS absorption spectra and the picosecond time-resolved Raman spectra of α-terthiophene in cyclohexane are presented. It will be shown that the vibrational energy redistribution and relaxation processes are clearly observed in α-terthiophene.

In Chap. 5, all the studies in this thesis are summarized shortly.

1-3. References

[1] R. G. W. Norrish and G. Porter, *Nature* **164** (1949) 658.

[2] G. Porter, *Proc. Roy. Soc. London* **A200** (1949) 284.

[3] R. L. Fork, C. H. Brito Cruz, P. C. Becker and C. V. Shank, *Opt. Lett.* **12** (1987) 483.

[4] J. Zhou, G. Taft, C.-P. Huang, M. M. Murnane, H. C. Kapteyn and I. P. Christov, *Opt. Lett.* **19** (1994) 1149.

[5] M. T. Asaki, C.-P. Huang, D. Garvey, J. Zhou, H. C. Kapteyn and M. M. Murnane, *Opt. Lett.* **18** (1993) 977.

[6] H. Nishioka, W. Odajima, K. Ueda and H. Takuma, *Opt. Lett.* **20** (1995) 2505.

[7] S. Ganapathy and R. S. H. Liu, *J. Am. Chem. Soc.* **114** (1992) 3459.

[8] S. Ganapathy and R. S. H. Liu, *Photochem. Photobiol.* **56** (1992) 959.

[9] W. H. Waddell and K. Chihara, *J. Am. Chem. Soc.* **103** (1981) 7389.

2. Femtosecond time-resolved UV-VIS absorption spectrometer

In order to obtain pico- or femtosecond time resolution, a special technique based on correlation between optical pulses is used. There are two kinds of pulses employed in the correlation method. One is incoherent nanosecond pulses of which correlation time is short. The other is ultrashort pulses of which pulse width is in the pico- or femtosecond time range. The latter is far more useful and general at present. Then, the generation of femtosecond pules is the first and foremost important factor in femtosecond time-resolved spectroscopy. The next is optical measurement techniques and data processing. This chapter consists of two parts describing the construction of the femtosecond time-resolved UV-VIS absorption spectrometer. In Sect. 2-1, the working principles of the femtosecond laser is explained. In Sect. 2-2, the optical measurement setup and the performance of the constructed spectrometer are described. Especially, the measurement technique of the chirp structure of wide-band ultrashort pulses and the estimation of the time resolution are described in detail.

2-1. Femtosecond laser

2-1-1. Overview

Lasers have to satisfy the following three requisites in order to be able to generate stable ultrashort optical pulses of which the pulse width is less than 100 fs.

(a) The gain band width should be sufficiently wide.

(b) The phases of the oscillating longitudinal modes should be locked.

(c) An optical element having negative GVD should be included in the cavity.

These requisites are deduced from the fact that the Fourier transformation of the time representation of the electric field of optical pulses corresponds to the frequency representation of it and vice versa. For requisite (a), it is important that the gain medium has a wide absorption or fluorescence band just as dye solutions and ion-doped crystals. The mode-locking technique enables requisite (b). The advance of the ultrashort pulse generation technique has been accompanied by the development of various mode-locking techniques. A prism pair is the best-known optical element for requisite (c) [1]. The colliding-pulse mode-locked (CPM) ring dye laser reported by Fork et al. in 1981 [2] satisfied these three requisites for the first time and generated stable ultrashort pulses of which the pulse width is less than 100 fs. The gain medium and the passive mode locker of the CPM laser were both dye solutions. The CPM laser was dominantly used in femtosecond time-resolved spectroscopy for about ten years, but it has two drawbacks: troublesome maintenance and difficulty in the alteration of oscillating wavelength. Both of them are due to the simultaneous use of the two dye solutions.

Ti:sapphire lasers have overcome these two drawbacks and have spread rapidly. The mode-locked operation of Ti:sapphire lasers was first reported in 1989, and since then various new mode-locking methods have been developed [3-7]. Though all these methods gave stable

femtosecond pulses, the most prevailing method among them is self mode locking which is a mode-locking technique without any special mode locker such as an electro-optic modulator or a saturable absorber. Therefore, the cavity of self mode-locked lasers is very simple in spite of their femtosecond-pulse generation, and their tuning range of oscillating wavelength is not limited by mode lockers at all but determined by solely the coating of the mirrors in the cavity. Though the mechanism of the femtosecond-pulse generation by self mode locking has not yet been clarified thoroughly, significant contribution of third-order nonlinear optical effect such as Kerr-lens effect has been pointed out as the possible mechanism for mode locking. It is noted that the replacement of a liquid gain medium with solid one is of great effect, not only in the stabilization of the output but also in the improvement of tunability and the simplification of mode locking. Recently, it has been shown that positive GVD in a Ti:sapphire crystal prevents output pulses from being shortened further, and that by using a crystal of shorter optical path length one can produce pulses as short as 10 fs [8, 9].

The excitation light sources of the above-mentioned femtosecond lasers are continuous-wave (CW) lasers such as Ar^+ lasers. The output pulse energy of CW mode-locked femtosecond lasers is usually about 0.1 nJ ~ 10 nJ which is insufficient for wide-band continuum generation by means of SPM. For use in femtosecond time-resolved UV-VIS absorption spectroscopy, the amplification of the output of CW mode-locked femtosecond lasers is indispensable. The gain band width of amplifiers has to cover the spectrum of input femtosecond pulses. The repetition rate of CW mode-locked femtosecond lasers is usually about 100 MHz, but it is impossible at present to keep this repetition rate until after the amplification. In the amplification process, high pulse energy is achieved at the expense of the reduced repetition rate. Using dye lasers as mode-locked femtosecond lasers, typically high pulse energy of about 100 μJ ~ 200 μJ was obtained by making use of multi-stage dye amplifiers at low repetition rates of about 10 Hz, and pulse energy of 1 μJ ~ 10 μJ was obtained by multi-pass dye amplifiers at higher repetition rates of about 10 kHz. In the amplification of the output of mode-locked Ti:sapphire lasers, Ti:sapphire crystals are generally used as gain media, and the regenerative amplification method is often adopted by taking advantage of their longer excited-state lifetime than that of dye molecules. The Ti:sapphire regenerative amplifiers gives pulse energy of about 500 μJ ~ 1 mJ at a repetition rate of 1 kHz. The output of the Ti:sapphire regenerative amplifiers is generally more stable and has better beam quality than that of dye amplifiers. These advantages has enabled stable wavelength conversion by optical parametric amplification (OPA) seeded with the output of the regenerative amplifiers [10-13].

2-1-2. Ti:sapphire laser

2-1-2-1. Self mode-locked laser

In the present study, a CW self mode-locked Ti:sapphire laser was constructed by

modifying a commercial CW Ti:sapphire laser (Spectra Physics, Model 3900S). Its cavity configuration is shown in Fig. 2-1. The excitation light source of the Ti:sapphire crystal was a multi-line CW Ar^+ laser (Spectra Physics, Model 2060 BeamLok). The Ar^+ laser was operated at average power of about 3.3 W, though its specified maximum power was 8 W. The linear polarization direction of the output of the Ar^+ laser was vertical, but was altered to be horizontal by a pair of mirrors before entering the cavity. A Ti:sapphire crystal R, a concave mirror M5 for focusing the Ar^+ laser output into R, and all the mirrors M1 ~ M4 inside the cavity were used as they were in the commercial CW laser. There were four points of the modification for mode-locking operation.

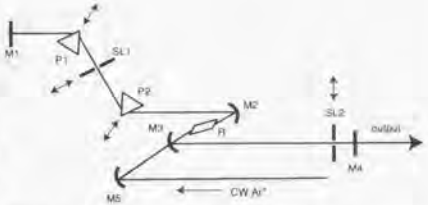

Fig. 2-1 CW self mode-locked Ti:sapphire laser cavity. M1, end mirror; M2, concave mirror; M3, dichroic concave mirror; M4, output coupler; M5 , concave mirror; P1 and P2, Brewster dispersion prism; R, Ti:sapphire rod; SL1, variable slit for tuning; SL2, variable slit for mode locking.

(a) The cavity length was extended by putting M1 and M4 further from R.

(b) A pair of Brewster dispersing prisms P1 and P2 was put between M1 and M2.

(c) A movable and variable slit SL1 was put between P1 and P2 as an alternative of a built-in birefringent filter for wavelength tuning.

(d) A movable and variable slit SL2 was put just in front of M4 for mode-locking operation.

P1 and P2 were identical and made of LaFN28 glass. The prism angle was determined to set the angle of incidence which gave the minimum deviation being equal to the Brewster angle at a wavelength of 800 nm.

When SL2 was opened fully, the laser oscillated in the CW mode with the output average power of about 0.5 W. The mode-locking operation of the laser was obtained by gradually closing SL2 until the CW output power decreased to about 0.1 W and then tapping the optical table on which the laser was placed. The typical output of the self mode-locked Ti:sapphire laser was as follows: pulse width, 100 fs; center wavelength, 800 ± 20 nm; repetition rate, 84 MHz; average power, 0.1 W. The repetition rate was the inverse of the time during which a pulse goes round the cavity once. The pulse width was determined by the nonlinear optical effect and the positive GVD in the crystal R and the negative GVD provided by the pair of P1 and P2. The extent of the nonlinear optical effect in R could not be varied effectively because the power was almost fixed. The extent of the positive GVD in R also could not be varied effectively because the length of R was fixed. The extent of the negative GVD provided by the prism pair could be varied by changing the distance between P1 and P2, and consequently the shortest pulse width obtained so far was about 60 fs. The center wavelength could be varied by moving SL1, and the tuning range was limited by the coating of the mirrors M1 ~ M4.

The SHG intensity auto-correlation trace of the output of the constructed self mode-

locked Ti:sapphire laser is shown in Fig. 2-2 which was measured by using a home-made rapid-scanning auto-correlator. The spectrum of the output of the laser is shown in Fig. 2-3 which was measured by using a polychromator and a CCD of a time-resolved absorption spectroscopy setup described in Sect. 2-2-2. On the assumption that the envelope of the electric field of the output pulse is expressed by a Gaussian function, the full width at half maximum (FWHM) of the auto-correlation trace was obtained as 140 fs by way of fitting in Fig. 2-2, and then the pulse width was calculated at 100 fs. On the assumption that the band shape in Fig. 2-3 is expressed by a Gaussian function, the band width was obtained as 210 cm^{-1} by way of fitting. Then, the product of the pulse width and the band width is 21 ps cm^{-1}. That of an ideal Fourier-transform limited pulse with a Gaussian envelope is 15 ps cm^{-1}. This means that a chirp was impressed on the output pulse of the present self mode-locked Ti:sapphire laser. If a proper GVD compensation is done on the output pulse, a compressed pulse of 70 fs can be obtained with the same band width.

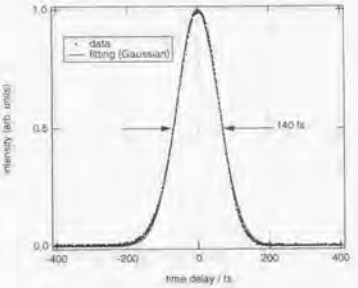

Fig. 2-2 SHG intensity auto-correlation trace of the output of the constructed self mode-locked Ti:sapphire laser.

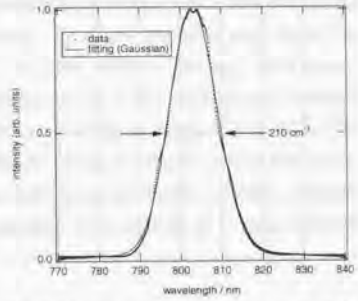

Fig. 2-3 Intensity spectrum of the output of the constructed self mode-locked Ti:sapphire laser.

2-1-2-2. Regenerative amplifier

A commercial regenerative amplifier (Clark-MXR, CPA-1) was used to amplify the output of the self mode-locked Ti:sapphire laser. The details of the regenerative amplifier is not described in this thesis. The typical output of the regenerative amplifier was as follows: pulse width, 210 fs; center wavelength, 800 ± 20 nm; repetition rate, 1 kHz; average power, 0.5 W. The SHG intensity auto-correlation trace of the amplified output is shown in Fig. 2-4. The spectrum of the amplified output is shown in Fig.

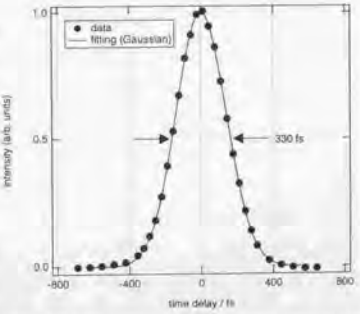

Fig. 2-4 SHG intensity auto-correlation trace of the regenarative amplifier output.

2-5. The auto-correlation trace and the spectrum were both measured by utilizing a time-resolved absorption spectroscopy setup described in Sect. 2-2-2. The band width in Fig. 2-5 is 0.8 times as much as that before the amplification in Fig. 2-3, and the sharp edges of the band feature the spectrum of the amplified output. The narrower band width and the sharp edges are primarily due to the insufficient band width of the transmittance of the pulse stretcher in the regenerative amplifier. The gain band width of the regenerative amplifier cavity itself is probably enough. The pulse width of the amplified output is twice as much as that before the amplification. The longer pulse width is caused by the pulse stretcher and the pulse compressor in the regenerative amplifier. Though the pulse width of the amplified output strongly depends on the alignments of the pulse stretcher and the pulse compressor, it was not possible to acquire the amplified output of which the pulse width is shorter than 210 fs. The product of the pulse width and the band width was finally 34 ps cm^{-1} which is more than twice as large as the ideal value. Though such a large product is not preferable for time-resolved spontaneous Raman spectroscopy [14], no serious problem is brought about in time-resolved UV-VIS absorption spectroscopy.

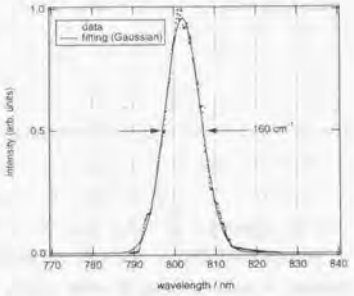

Fig. 2-5 Intensity spectrum of the regenerative amplifier output.

2-2. UV-VIS absorption spectroscopy

2-2-1. Introduction

Femtosecond time-resolved UV-VIS absorption spectroscopy is the most fundamental method to study ultrafast excited-state dynamics among a lot of femtosecond time-resolved spectroscopic techniques developed so far. Molecules in condensed phases at room temperature usually have wide UV-VIS absorption bands of which the band width ranges from about 100 cm^{-1} to 5000 cm^{-1}. It gives UV-VIS absorption spectroscopy both an advantage and a disadvantage simultaneously. The former is that it is in principle possible to obtain sufficient time resolution as fast as 10 fs or 100 fs without any sacrifice of spectral information, because spectral resolution as high as 1 cm^{-1} or 10 cm^{-1} is unnecessary at all in UV-VIS absorption spectroscopy. The latter is that it is mostly difficult to obtain decisive information about the molecular structure of a reaction intermediate from UV-VIS absorption spectra, because broad absorption bands are usually not sensitive enough to the molecular structure. Vibrational spectroscopy has an opposite advantage and disadvantage. Picosecond time-resolved Raman spectroscopy has already been established [14, 15] and also several femtosecond time-resolved Raman measurements have been done. At present, the variable range of the excitation wavelength of ultrafast Raman spectroscopy is still not wide enough. Ultrafast IR spectroscopy has been making a great advance in these five years [16-18], but measurable wavenumber range is still limited. Therefore, time-resolved UV-VIS absorption spectroscopy as well as fluorescence spectroscopy is still one of the most powerful tools to study chemical reaction dynamics which includes an intermediate of which the lifetime is in the subpicosecond or femtosecond time range.

In femtosecond time-resolved UV-VIS absorption spectroscopy, pump and probe light have to be femtosecond pulses. In measuring a time-resolved absorption spectrum, it is desirable to employ wide-band probe pulses and a multichannel detector. The only known way to obtain wide-band femtosecond pulses of which the band width is more than 1000 cm^{-1} is to focus intense femtosecond pulses whose pulse energy is at least 1 μJ into a transparent medium such as water, glass, and so on and broaden the band width by means of SPM [19]. The spectrum of wide-band femtosecond pulses obtained in this way depends on the pulse width, the pulse shape, the peak power of the input femtosecond pulses, and the third nonlinear optical susceptibility and the path length of the transparent medium. Though the generation of wide-band femtosecond pulses in the VIS-NIR region extending from wavelength 400 nm to 1000 nm has already been reported by a lot of groups, that in the UV region shorter than 400 nm has been reported only by Nishioka et al. [20] who used 250-mJ femtosecond pulses and a 9-m tube filled with rare gases as SPM media. As far as the pump pulses are concerned, it is highly desirable that the center wavelength of the pump pulses are tunable over a wide range to study various molecular systems. The wavelength conversion of femtosecond pulses has been performed by continuum amplifiers [21-23], parametric

conversion techniques such as OPA [10-13], and harmonic generation. It is possible at present to obtain femtosecond pump pulses of almost any arbitrary center wavelength within a range from 260 nm to 1000 nm.

2-2-2. Optical measurement setup

The optical measurement setup of femtosecond time-resolved pump-probe UV-VIS absorption spectroscopy was constructed using the output of the Ti:sapphire regenerative amplifier as a light source that was described in Sect. 2-1. In this section, a measurement setup which employs femtosecond pump pulses with a center wavelength of about 400 nm is described.

In Fig. 2-6, a schematic representation of the optical measurement setup for femtosecond time-resolved VIS absorption spectroscopy is shown. The output of the regenerative amplifier whose center wavelength is about 800 nm was divided into two beams by a beam splitter. One of the beams with a pulse energy of about 200 ~ 300 μJ was focused into water in a flow-type cuvette and converted into wide-band femtosecond pulses by means of SPM. The wide-band beam thus generated was further split into two which were used as probe and reference light. The path length of the cuvette was 10 mm. The second beam with a pulse energy of about 100 μJ was focused into a KDP crystal to obtain pump light of which the center wavelength was about 400 nm. The path length of the KDP crystal used was 1 mm. Time delay between the pump and the probe was controlled by a translation stage driven by a stepper motor. Sample solutions were spouted by a magnet-gear pump as a jet sheet from a nozzle specially designed for use in CW dye lasers. The diameter of the pump beam on the jet sheet was about 0.6 mm, and that of the probe beam was about 0.4 mm. The flow speed of sample solutions was sufficiently rapid to exchange them between laser shots. The probe beam which transmitted the photoexcited sample area (0.3 mm^2) and the reference beam were focused onto different positions of the entrance slit of a single polychromator (Jobin Yvon, HR320) by which both of the beams were dispersed, and detected simultaneously by the different stripes of a liquid nitrogen cooled CCD of 1100 (horizontal) × 330 (vertical) pixels (Princeton Instruments, LN/CCD-1100PB/UVAR). The grating of the polychromator had 150

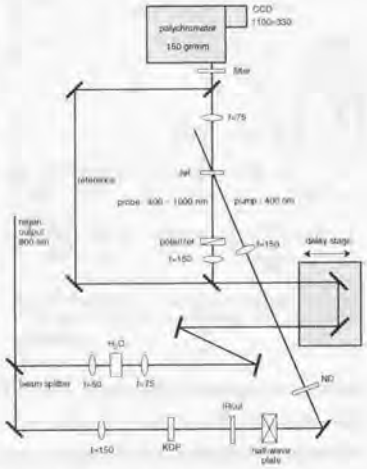

Fig. 2-6 Schematic of the optical measurement setup of femtosecond time-resolved VIS absorption spectroscopy.

grooves per 1 mm. A mechanical shutter was used to switch the pump beam on and off. All the beams were linearly polarized. A sheet polarizer was used for the wide-band probe continuum to minimize the effect of GVD. The polarization direction of the pump beam was rotated by a half-wave plate so that it formed an angle of 55 degree with that of the probe beam.

A schematic representation of the optical measurement setup of femtosecond time-resolved UV absorption spectroscopy is shown in Fig. 2-7. In what is following, a brief description of the UV experimental setup is given with emphasis on the aspects different from those in the VIS setup already described above. The output of the regenerative amplifier was frequency-doubled using a BBO crystal of 3-mm path length to generate UV femtosecond pulses. The center wavelength of the UV pulses was about 400 nm, and the pulse energy was about 100 μJ. These intense UV femtosecond pulses were focused into water and converted to wide-band continuum by means of SPM. After the spectral component of which the wavelength was longer than 390 nm was removed by the U-340 optical filter (HOYA), the wide-band continuum was used as a probe beam. This was done especially because an intense component at 400 nm which was not preferable for the present purpose still remained even after the SPM continuum generation. The fundamental output of the regenerative amplifier which was the residual after the SHG was again frequency-doubled by a KDP crystal of 1-mm path length, and was used as a pump beam. No reference beam was prepared because of the lack of a proper beam splitter. The beam diameter of the pump beam and that of the probe on the jet sheet were both about 0.2 mm. The grating of the polychromator had 600 grooves per 1 mm.

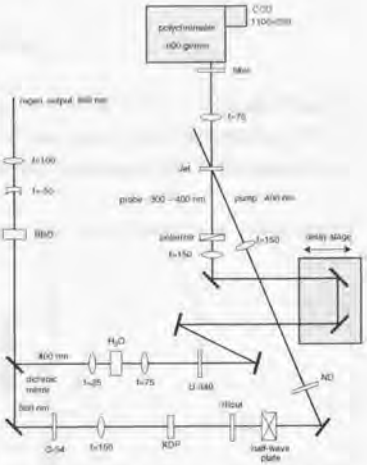

Fig. 2-7 Schematic of the optical measurement setup of femtosecond time-resolved UV absorption spectroscopy.

In both the VIS and the UV setup, the angle between the linear polarization direction of the pump beam and that of the probe beam was set to 55 degree. It is for the purpose of removing the influence of rotational relaxation from time-resolved absorption spectra. It is well-known technique in fluorescence spectroscopy, and an angle of 55 degree is generally called a magic angle. If the direction of a transition dipole moment interacting with pump light is parallel to that of a transition dipole moment interacting with probe light as in the case of fluorescence spectroscopy, it is self-evident that the magic-angle technique removes the influence of rotational relaxation. In fact, even if they are not parallel as in the general case of

time-resolved absorption spectroscopy, it can be easily shown that the influence of rotational relaxation is removed by the magic-angle technique in the same way. The angle between the directions of those two transition dipole moments only influences the initial anisotropy of pump-induced absorbance.

2-2-3. Performance of spectrometer

2-2-3-1. Measurable range and accuracy of wavelength

Since the CCD used in this study had enough sensitivity in the wavelength range 200 nm ~ 1100 nm, the measurable wavelength range of the constructed femtosecond UV-VIS absorption spectrometer was determined by the intensity spectrum of the femtosecond wide-band probe light.

In Fig. 2-8, the spectrum of the wide-band probe light used in the VIS setup is shown. The sensitivity of the detection system was not corrected. The intensity in the wavelength range 700 nm ~ 800 nm was rather weak because of a NIR-cut filter just in front of the polychromator. The wavelength range from 400 nm to 800 nm was simultaneously measurable in femtosecond time-resolved VIS absorption measurements. Since the slit width was as narrow as 10 μm, the pixel size of the CCD determined the spectral resolution which was about 0.5 nm. Wavelength calibration was done by using the emission spectrum of a Hg lamp (Fig. 2-9) and that of a Ne lamp (Fig. 2-10). The maximum deviation of the calibrated wavelengths from the wavelengths of the emission lines in literature was about 0.2 nm.

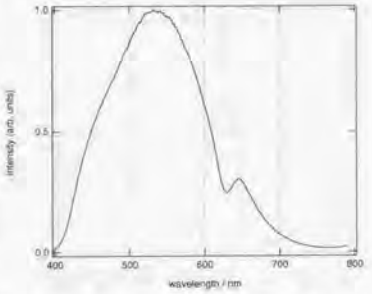

Fig. 2-8 Intensity spectrum of femtosecond VIS wide-band probe pulses.

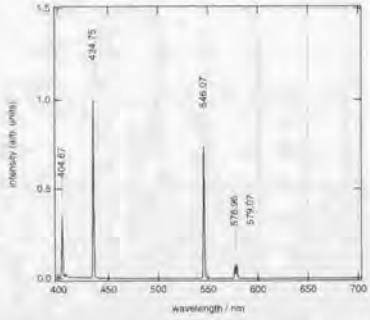

Fig. 2-9 Emission spectrum of a Hg lamp for VIS wavelength calibration.

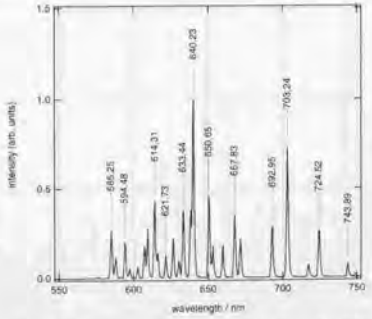

Fig. 2-10 Emission spectrum of a Ne lamp for VIS wavelength calibration.

The spectrum of the wide-band probe light used in the UV setup is shown in Fig. 2-11. The sensitivity of the detection system was not corrected. The U-340 optical filter was used as mentioned in Sect. 2-2-2. This filter absorbs light of which the wavelength is longer than 390 nm. The wavelength range 310 nm ~ 390 nm was simultaneously measurable in femtosecond time-resolved UV absorption measurements. Since the U-340 filter is not transparent in the wavelength range shorter than 260 nm, another optical filter (ASAHI, UV long-cut filter) transparent in the wavelength range 200 nm ~ 340 nm but not in the range 350 nm to 410 nm was used instead to check the UV probe intensity in the range 200 nm ~ 300 nm as shown in Fig. 2-12. It is recognized that a spectral component of which the wavelength was shorter than 300 nm was not sufficient enough for absorption measurements. Though several conditions including focal distance of the focusing lens used in the SPM continuum generation, the SPM medium itself, and path length of the flow-type cuvette were varied, wide-band UV light which had enough intensity in the wavelength range shorter than 300 nm was not obtained. Since the UV probe light was absorbed by samples, the slit width was set to be as wide as 200 μm. Thus the spectral

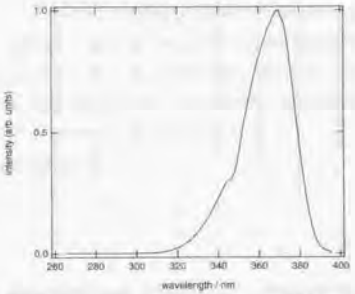

Fig. 2-11 Intensity spectrum of femtosecond UV wide-band probe pulses.
A U-340 filer (HOYA) was used to cut an intense 400-nm component.

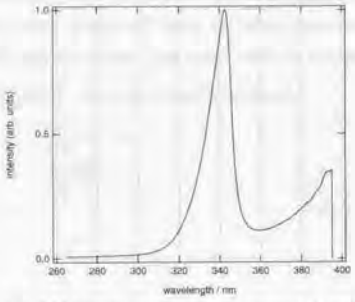

Fig. 2-12 Intensity spectrum of femtosecond UV wide-band probe pulses.
A UV long-cut filer (ASAHI) was used to cut an intense 400-nm component.

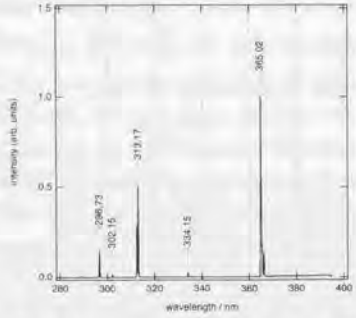

Fig. 2-13 Emission spectrum of a Hg lamp for UV wavelength calibration.

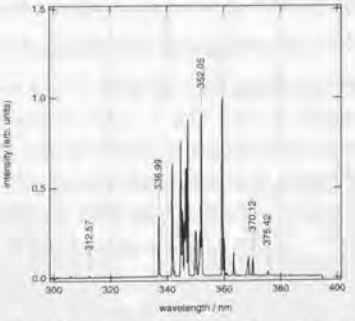

Fig. 2-14 Emission spectrum of a Ne lamp for UV wavelength calibration.

resolution was about 1 nm, which was worse than that in the VIS setup in spite of the grating of higher dispersion. Wavelength calibration was done by using the emission spectrum of a Hg lamp (Fig. 2-13) and that of a Ne lamp (Fig. 2-14). The maximum deviation of the calibrated wavelengths from the wavelengths of the emission lines in literature was about 0.06 nm.

All the wavelengths reported in this thesis are values in air.

2-2-3-2. Accuracy of absorbance

The first purpose of time-resolved UV-VIS absorption spectroscopy is to measure the UV-VIS absorption spectra of molecules in electronic excited states or that of reaction intermediates. In this case, the measurement of a base line which is usually necessary for acquiring ground-state absorption spectra is not essential. In the present spectrometer, the spectrum of the probe light and that of the reference were measured twice; (i) when samples were not irradiated with the pump light (pump off), and (ii) when they were irradiated with the pump light (pump on). Absorbance A at wavelength λ, was expressed as follows:

$$A = \log_{10} \frac{\sum_{i=1}^{N} \frac{I^{off}_{probe,i}}{I^{off}_{refe,i}}}{\sum_{i=1}^{N} \frac{I^{on}_{probe,i}}{I^{on}_{refe,i}}}, \qquad (2\text{-}1)$$

where $I^{off}_{probe,i}$ was the intensity of the probe light at λ on the ith exposure of the CCD when the pump was off, $I^{off}_{refe,i}$ was the intensity of the reference light at λ on the ith exposure of the CCD when the pump was off, and the others in which *off* was replaced with *on* were those when the pump was on. N was the total number of the exposures of the CCD. In the UV setup, $I^{off}_{refe,i} = I^{on}_{refe,i} = 1$, since no reference beam was prepared as mentioned in Sect. 2-2-2. The most desirable method for the data accumulation is to synchronize the exposure of the CCD with the laser shots. However the laser repetition rate of 1 kHz was too high to synchronize the CCD exposure. Therefore, the CCD was operated in an asynchronous mode without decreasing the repetition rate of the laser. The exposure time of the CCD was about 0.1 s ~ 1 s. If it was 1 s, for example, the accumulation of 1000 laser shots was achieved in every exposure. The total number of the exposures N was typically about 5 ~ 20.

The accuracy of absorbance in pump-probe measurements is determined by the fluctuation of pump intensity and that of probe spectra. In the present spectrometer, the former was easily kept within ±5% which was regarded as stable enough. As a result, the

accuracy of absorbance of the present spectrometer was primarily determined by the latter, and was estimated in the following way: Absorption measurements were performed with the pump off all time instead of switching it on and off in a typical measurement procedure as described in Eq. (2-1). If the probe spectrum was perfectly stable, absorbance at all the wavelengths acquired in this method must be equal to 0. Thus, the absorption spectrum acquired in this method exactly expressed the accuracy of absorbance at each wavelength. An accuracy spectrum of the VIS setup and that of the UV setup are shown in Fig. 2-15 and 16 respectively. The exposure time of the CCD was 1 s, and the total number of the exposures was 10. It can be easily recognized from Fig. 2-15 that the fluctuation of absorbance in the wavelength range 430 nm ~ 710 nm was about ±0.003, that in the range 400 nm ~ 430 nm was about ±0.01, and that in the range 710 nm ~ 800 nm was about ±0.015. The larger fluctuation in the range 400 nm ~ 430 nm and 710 nm ~ 800 nm was due to the weakness of the probe and the reference intensity in this range. It is realized from Fig. 2-16 that the fluctuation of absorbance in the wavelength range 310 nm ~ 385 nm was about ±0.004, that in the range 300 nm ~ 310 nm and 385 nm ~ 395 nm was about ±0.02. The larger fluctuation in the latter was due to the weakness of the probe intensity in those ranges, and especially the probe intensity spectrum in the range 300 nm ~ 310 nm was unstable.

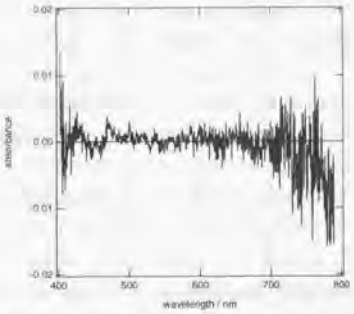

Fig. 2-15 Typical VIS absorption spectrum without pump light, illustrating the accuracy of absorbance (see text).
CCD exposure time, 1 s; number of exposures, 10.

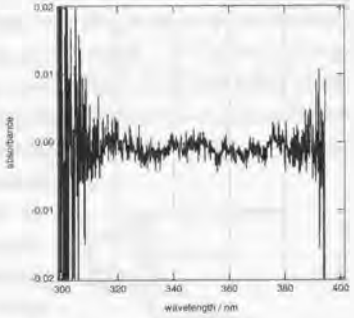

Fig. 2-16 Typical UV absorption spectrum without pump light, illustrating the accuracy of absorbance (see text).
CCD exposure time, 1 s; number of exposures, 10.

2-2-3-3. Time-resolution and chirp correction by OKE method

The refractive index of materials depends on the frequency of light. In the UV-VIS region, the higher the frequency is, generally the larger the refractive index becomes. Then, light of higher frequency has a slower phase velocity. Ultrashort light pulses travel at a group velocity that also becomes smaller in materials with an increase in the optical frequency. Then group velocity dispersion (GVD) is defined as positive or normal. When a Fourier transform-limited pulse passes through a material having GVD, a chirp is impressed on it and

it is not Fourier transform-limited any more. Since a chirp, or frequency sweep, which originates from positive GVD is in a direction that the frequency becomes higher toward the trailing edge of a pulse, it is called an upchirp.

The broader the spectral width, the larger the effect of GVD. Wide-band probe pulses used in femtosecond time-resolved UV-VIS absorption spectroscopy almost always have an upchirp impressed on them because of the positive GVD of optical elements on their optical path and of an SPM medium itself. Thus, the longer-wavelength component of probe pulses reaches a sample earlier than the shorter-wavelength component. Such a wavelength-dependent temporal structure of wide-band probe continuum is not suitable for pump-probe time-resolved absorption measurements. In principle, the upchirp of femtosecond wide-band continuum pulses can be compensated so that they are compressed into Fourier-transform limited pulses by applying proper negative GVD [1, 24]. The whole VIS region over 10000 cm^{-1} is usually required for practical absorption measurements. This spectral width corresponds to 1 fs in temporal width, which is much shorter than the minimum pulse width (6 fs) realized so far [25]. Therefore, it is unrealistic to totally compensate the upchirp of femtosecond wide-band probe pulses by applying proper negative GVD. As a practical alternative, the temporal structure of the wide-band probe pulses is measured before or after an absorption measurement, and the probe-wavelength-dependence of the time delay between pump and probe is corrected on data processing to acquire "real" time-resolved absorption spectra [26-28]. Let this procedure be called chirp correction.

The best-known available technique for measuring the temporal structure of femtosecond wide-band continuum pulses is the sum or difference frequency generation (SFG or DFG) cross-correlation method using a nonlinear crystal such as KDP and BBO [19, 26, 27]. A schematic representation of the optical measurement setup of the SFG cross-correlation method constructed according to the literature [19, 26, 27] is shown in Fig. 2-17. In the SFG cross-correlation measurement, the sample of the absorption measurements (Fig. 2-6, 7) was replaced with a nonlinear crystal in which pump and probe light were optically mixed. The light intensity at the sum frequency of the monochromatic pump pulse and the wide-band probe pulse was measured while scanning time delay. A spectral portion of the continuum probe pulse was selected by changing the phase-matching angle of the nonlinear crystal. A monochromator was used for extracting the generated sum frequency. The cross-correlation traces thus measured at different wavelengths which correspond to the

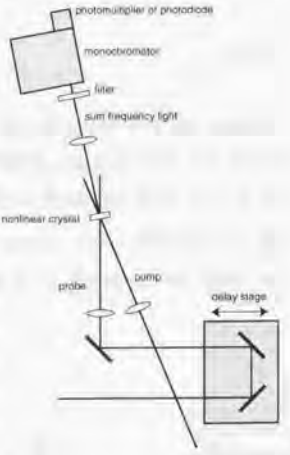

Fig. 2-17 Schematic of the optical measurement setup of the SFG cross-correlation method.

sum frequencies of the pump pulse and different spectral components of the wide-band probe pulse have their peaks at different time delays. The time delays thus obtained are generally regarded as the origins of time delay for those spectral components of the probe, because SFG in a transparent nonlinear crystal is an instantaneous process.

The intensity of the SFG signal I_{SFG} obtained using the setup shown in Fig. 2-17 can be written as a function of angular frequency of the SFG light ω_{SFG} and time delay t_{delay}. At first, let the electric field of the pump pulse E_{pump} and that of the probe pulse E_{probe} be written as a function of time t in a complex form as follows:

$$E_{pump}(t) = Ev_{pump}(t)\exp\left(i\omega_{pump}t\right), \tag{2-2}$$

$$E_{probe}(t) = Ev_{probe}(t)\exp\left[i\left\{\omega_{probe}t + \phi(t)\right\}\right], \tag{2-3}$$

where Ev_{pump} and Ev_{probe} are the envelopes of the electric fields, ω_{pump} and ω_{probe} are the central frequencies, and $\phi(t)$ is a real function which represents the chirp of the probe pulse. If the probe pulse is Fourier transform-limited, $\phi(t)$ is equal to 0. It is assumed that the pump pulse is Fourier transform-limited. The electric field of the SFG light $E_{SFG}(t)$ is given by

$$E_{SFG}(t) = E_{pump}(t + t_{delay})E_{probe}(t), \tag{2-4}$$

where t_{delay} is positive when the pump pulse reaches the crystal earlier than the probe. In writing Eq. (2-4), coefficients of less importance are omitted, and also they will not be considered in the further discussions. Let the Fourier transform of electric field $E(t)$ in the time domain be expressed as $\tilde{E}(\omega)$ in the frequency domain. In the SFG method, the spectrally resolved intensity of the SFG light is measured as mentioned above. Then, the following equation is obtained:

$$\begin{aligned} I_{SFG}(\omega_{SFG}, t_{delay}) &= \left|\tilde{E}_{SFG}(\omega_{SFG})\right|^2 \\ &= \int_{-\infty}^{\infty} dt_1 \int_{-\infty}^{\infty} dt_2 E_{SFG}(t_1) E_{SFG}^{*}(t_2) \exp\left\{i\omega_{SFG}(t_2 - t_1)\right\} \\ &= \int_{-\infty}^{\infty} dt_2 \exp\left(i\omega_{SFG}t_2\right) \\ &\cdot \int_{-\infty}^{\infty} dt_1 E_{pump}(t_1 + t_{delay}) E_{pump}^{*}(t_1 + t_2 + t_{delay}) E_{probe}(t_1) E_{probe}^{*}(t_1 + t_2) \end{aligned}$$

$$= \int_{-\infty}^{\infty} dt_2 \exp\left\{i\left(\omega_{SFG} - \omega_{pump} - \omega_{probe}\right)t_2\right\}$$

$$\cdot \int_{-\infty}^{\infty} dt_1 Ev_{pump}(t_1 + t_{delay}) Ev_{pump}(t_1 + t_2 + t_{delay}) Ev_{probe}(t_1) Ev_{probe}(t_1 + t_2)$$

$$\cdot \exp\left[i\left\{\phi(t_1) - \phi(t_1 + t_2)\right\}\right]. \qquad (2\text{-}5)$$

The trace of time-delay dependence of the signal intensity I_{SFG} at a fixed angular frequency ω_{SFG} is regarded as the cross-correlation trace between the pump pulse and the probe spectral component of which the angular frequency is $\omega_{SFG} - \omega_{pump}$. The time delay $t_{SFG}^{MAX}(\omega_{SFG})$ which gives the maximum of the cross-correlation trace is interpreted as the origin of time delay for that spectral component of the probe pulse. The FWHM of the cross-correlation trace, $T_{SFG}^{fwhm}(\omega_{SFG})$, corresponds to the time-resolution of the pump-probe measurement. The derivation of $t_{SFG}^{MAX}(\omega_{SFG})$ and $T_{SFG}^{fwhm}(\omega_{SFG})$ is described later in this section.

There are following three practical drawbacks in the SFG (or DFG) cross-correlation technique as a method of measuring chirp structures for the purpose of the chirp correction of femtosecond time-resolved UV-VIS absorption spectra:

(a) The amount of GVD which broadens the temporal width of the wide-band probe pulse in the SFG cross-correlation measurement (Fig. 2-17) is not exactly the same as that in the time-resolved absorption measurements (Fig. 2-6, 7), because the sample of the absorption measurements has to be replaced by a nonlinear crystal.

(b) The SFG cross-correlation measurement is time-consuming. The adjustment of the phase-matching angle of a nonlinear crystal and the scanning of time delay are necessary each time the SFG light intensity of different wavelengths is measured. It is difficult to obtain more than twenty SFG cross-correlation traces in an hour. It also takes about half an hour or more to change the setup from the absorption measurement to the SFG cross-correlation measurement.

(c) Especially in the case of the UV probe pulses, it is sometimes impossible to measure the chirp structure in all the wavelength range of the wide-band probe with only one nonlinear crystal. In this case, it is necessary to use several sets of not only a nonlinear crystal but also a monochromator and a detector.

The drawback (a) is particularly noticeable, when samples are in a cuvette or a cryostat, or when 10-fs ultrashort pulses are used. As regards the drawback (b), in fact there has been no paper so far that reported more than twenty SFG cross-correlation traces at different wavelengths. As one example of the drawback (c), there is no crystal with which a 400-nm pump pulse and a 350-nm component of a UV probe pulse are optically mixed for SFG. Though it is not impossible to generate the difference frequency of this pair of the pulses which is about 3600 cm^{-1}, it is too troublesome to generate and detect the IR signal for the

purpose of chirp correction.

A precise and convenient cross-correlation method which overcomes all these three drawbacks has been recently developed by the author [29]. This method utilizes non-resonant optical Kerr effect (OKE) instead of SFG or DFG. Let this method be called OKE cross correlation. A schematic representation of the optical measurement setup of the OKE cross-correlation method is shown in Fig. 2-18. When a solution sample was used in the absorption measurements, the sample used for the OKE cross-correlation measurement was just the solvent without a solute. The difference between the OKE setup in Fig. 2-18 and the absorption setup in Fig. 2-6 or Fig. 2-7 was only an analyzer polarizer of a Glan prism which was introduced between a sample and the polychromator. Experimental conditions in these two setups were exactly identical except for slit width and some optical filters in front of the polychromator. Thus the drawback (a) was already overcome. The OKE setup shown in Fig. 2-18 is what is called a homodyne-detected optical-Kerr-shutter configuration: The pump-induced anisotropy of the refractive index of the sample changes the polarization state of the wide-band probe beam, and the resultant change of the probe transmittance through the crossed polarizer-analyzer pair is detected by the CCD with the polychromator. Let the signal thus detected be called an OKE spectrum. The femtosecond time-resolved non-resonant OKE of liquids has been studied extensively by several groups, and it has already been established that the OKE responses have two components: an instantaneous electronic response and a nuclear response with a finite time constant [30]. As the instantaneous component dominates the transient OKE signal of liquids, it always has a peak at the zero time delay [30]. Therefore, it was expected that the OKE cross-correlation method provides information equivalent to that given by the SFG or DFG method. The idea of utilizing OKE for characterizing the chirp structure of wide-band probe pulses was first reported by Sala et al. [31] to the best of my knowledge. Although they pointed out the advantage of the OKE cross-correlation method for the purpose of the chirp correction of time-resolved absorption spectra, the obtained information on the chirp structure of wide-band probe pulses was limited by their experimental restrictions and they could not show the overwhelming superiority of the OKE method above the SFG or DFG method.

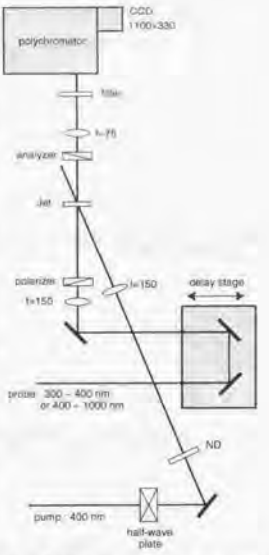

Fig. 2-18 Schematic of the optical measurement setup of the OKE cross-correlation method.

Let the expression of the OKE spectrum $I_{OKE}(\omega_{OKE}, t_{delay})$ be derived analytically in

order to confirm information obtained by the OKE cross-correlation method. ω_{OKE} is observed angular frequency. It is assumed that the OKE responses consist of only an instantaneous electronic component. The electric field of light passing through the analyzer $E_{OKE}(t)$ in the homodyne detection is expressed as follows:

$$E_{OKE}(t) = \left|E_{pump}(t + t_{delay})\right|^2 E_{probe}(t) . \tag{2-6}$$

After deriving $\tilde{E}_{OKE}(\omega_{OKE})$ from Eq. (2-6) and replacing $\tilde{E}_{SFG}(\omega_{SFG})$ with $\tilde{E}_{OKE}(\omega_{OKE})$ in Eq (2-5), $I_{OKE}(\omega_{OKE}, t_{delay})$ is obtained as follows:

$$\begin{aligned} I_{OKE}(\omega_{OKE}, t_{delay}) &= \int_{-\infty}^{\infty} dt_2 \exp(i\omega_{OKE} t_2) \\ &\cdot \int_{-\infty}^{\infty} dt_1 \left|E_{pump}(t_1 + t_{delay})\right|^2 \left|E_{pump}(t_1 + t_2 + t_{delay})\right|^2 E_{probe}(t_1) E_{probe}^{*}(t_1 + t_2) \\ &= \int_{-\infty}^{\infty} dt_2 \exp\left\{i\left(\omega_{OKE} - \omega_{probe}\right) t_2\right\} \\ &\cdot \int_{-\infty}^{\infty} dt_1 Ev_{pump}{}^2(t_1 + t_{delay}) Ev_{pump}{}^2(t_1 + t_2 + t_{delay}) Ev_{probe}(t_1) Ev_{probe}(t_1 + t_2) \\ &\cdot \exp\left[i\left\{\phi(t_1) - \phi(t_1 + t_2)\right\}\right] . \end{aligned} \tag{2-7}$$

The trace of time-delay dependence of the signal intensity I_{OKE} at a fixed angular frequency ω_{OKE} is regarded as the OKE cross-correlation trace between the pump pulse and the probe spectral component of which angular frequency is ω_{OKE}. The time delay which gives the maximum of the OKE cross-correlation trace is written as $t_{OKE}^{MAX}(\omega_{OKE})$, and the FWHM of the OKE cross-correlation trace is expressed as $T_{OKE}^{fwhm}(\omega_{OKE})$.

There remains one important problem before proceeding further: What is really necessary for chirp correction is the origins of time delay at different wavelengths in pump-probe time-resolved absorption measurements, and it is not self-evident that they are identical with those in the OKE measurement, that is, $t_{OKE}^{MAX}(\omega_{OKE})$, or in the SFG measurement, $t_{SFG}^{MAX}(\omega_{SFG})$. First of all, it is necessary to define the origins of time delay in time-resolved absorption measurements. Since there is no general definition, the following definition is adopted in this thesis: The origins of time delay in time-resolved absorption measurements are time delays when the absolute signal intensity of the bleaching of ground-state absorption has its maximum on the assumption that excited states generated by the pump pulse decay to

the ground state with a time constant much shorter than the pulse width of the pump and that of the probe. This definition is based on a hypothetical system which has instantaneous relaxation of population. Since the absolute value of the transient absorption signal in the unit of absorbance is equal to that in the unit of transmittance when the electric field of the pump pulse is regarded as a perturbation, the absorption signal A as a function of observed angular frequency ω_{abs} and time delay t_{delay} is written as follows:

$$A(\omega_{abs}, t_{delay}) = \frac{\left|\tilde{E}_{probe}(\omega_{abs}) + \tilde{E}_{abs}(\omega_{abs})\right|^2 - \left|\tilde{E}_{probe}(\omega_{abs})\right|^2}{\left|\tilde{E}_{probe}(\omega_{abs})\right|^2}$$

$$= \frac{\tilde{E}_{probe}(\omega_{abs})\tilde{E}_{abs}^{*}(\omega_{abs}) + c.c.}{\left|\tilde{E}_{probe}(\omega_{abs})\right|^2}, \qquad (2\text{-}8)$$

where $c.c.$ is the complex conjugate of the first term. $E_{abs}(t)$ is the electric field from which the absorption signal originates. When the ground-state absorption band width of the hypothetical system in the above definition is wide enough, $E_{abs}(t)$ is determined by only $E_{pump}(t + t_{delay})$ and $E_{probe}(t)$ as follows:

$$E_{abs}(t) = \left|E_{pump}(t + t_{delay})\right|^2 E_{probe}(t)$$

$$= E_{OKE}(t) . \qquad (2\text{-}9)$$

Since the absorption bleaching signal is due to an absorbance change proportional to the pump light intensity and the OKE signal is due to a refractive index change also proportional to the pump light intensity, the fact that $E_{abs}(t)$ is equal to $E_{OKE}(t)$ is natural. However A is not equal to I_{OKE} because the absorption bleaching signal is heterodyne-detected while the OKE signal is homodyne-detected. From the above arguments, A is expressed after omitting the unimportant denominator of Eq. (2-8) in the following way:

$$A(\omega_{abs}, t_{delay}) = \int_{-\infty}^{\infty} dt_2 \exp\left\{i\left(\omega_{probe} - \omega_{abs}\right)t_2\right\}$$

$$\cdot \int_{-\infty}^{\infty} dt_1 Ev_{pump}^{\ 2}(t_1 + t_{delay}) Ev_{probe}(t_1) Ev_{probe}(t_1 + t_2)$$

$$\cdot \exp\left[i\left\{\phi(t_1 + t_2) - \phi(t_1)\right\}\right] + c.c. \qquad (2\text{-}10)$$

A can be regarded as a heterodyne-detected instantaneous OKE signal. The time delay which gives the maximum of the trace of time-delay dependence of the signal A at a fixed angular frequency ω_{abs} is written as $t_{abs}^{MAX}(\omega_{abs})$, and the FWHM of that trace is expressed as $T_{abs}^{fwhm}(\omega_{abs})$.

In fact, it is difficult to analytically derive $t_{SFG}^{MAX}(\omega_{SFG})$, $t_{OKE}^{MAX}(\omega_{OKE})$, $t_{abs}^{MAX}(\omega_{abs})$, $T_{SFG}^{fwhm}(\omega_{SFG})$, $T_{OKE}^{fwhm}(\omega_{OKE})$, $T_{abs}^{fwhm}(\omega_{abs})$ from Eq. (2-5), (2-7), (2-10) against general Ev and ϕ. Accordingly the following simplifications as regards the pump pulse and the probe pulse are introduced:

$$Ev_{pump}(t) = \varepsilon_{pump} \exp\left\{-\left(\frac{t}{\tau_{pump}}\right)^2\right\}, \tag{2-11}$$

$$Ev_{probe}(t) = \varepsilon_{probe} \exp\left\{-\left(\frac{t}{\tau_{probe}}\right)^2\right\}, \tag{2-12}$$

$$\phi(t) = \kappa t^2 . \tag{2-13}$$

In Eq. (2-11) and (2-12), both of the electric-field envelopes are expressed as Gaussian functions, ε_{pump} and ε_{probe} are the electric-field amplitudes and are positive real constants, and τ_{pump} and τ_{probe} are also positive real constants $\frac{1}{\sqrt{2\ln 2}}$ times as much as the pulse widths. In Eq. (2-13), the chirp of the wide-band probe pulse is assumed to be a linear chirp, and κ is a positive real constant because of the upchirp of the probe. By substituting Eq. (2-11), (2-12), (2-13) for Eq. (2-5), (2-7), (2-10), it is realized that the trace of time-delay dependence at a fixed angular frequency is expressed as a Gaussian function for all the signals. The center position and FWHM of these traces are derived as follows:

SFG,

$$t_{SFG}^{MAX}(\omega_{SFG}) = -\frac{1}{2} \cdot \frac{\kappa\left(\omega_{SFG} - \omega_{probe} - \omega_{probe}\right)}{\frac{1}{\tau_{probe}^{\ 2}}\left(\frac{1}{\tau_{pump}^{\ 2}} + \frac{1}{\tau_{probe}^{\ 2}}\right) + \kappa^2}, \tag{2-14}$$

$$T_{SFG}^{fwhm} = \tau_{pump} \sqrt{\frac{2\ln 2\left\{\left(\frac{1}{\tau_{pump}^{\ 2}} + \frac{1}{\tau_{probe}^{\ 2}}\right)^2 + \kappa^2\right\}}{\frac{1}{\tau_{probe}^{\ 2}}\left(\frac{1}{\tau_{pump}^{\ 2}} + \frac{1}{\tau_{probe}^{\ 2}}\right) + \kappa^2}}\ ; \tag{2-15}$$

OKE,

$$I_{OKE}^{MAX}(\omega_{OKE}) = -\frac{1}{2} \cdot \frac{\kappa\left(\omega_{OKE} - \omega_{probe}\right)}{\frac{1}{\tau_{probe}^{\ 2}}\left(\frac{2}{\tau_{pump}^{\ 2}} + \frac{1}{\tau_{probe}^{\ 2}}\right) + \kappa^2}\ , \tag{2-16}$$

$$T_{OKE}^{fwhm} = \tau_{pump} \sqrt{\frac{\ln 2\left\{\left(\frac{2}{\tau_{pump}^{\ 2}} + \frac{1}{\tau_{probe}^{\ 2}}\right)^2 + \kappa^2\right\}}{\frac{1}{\tau_{probe}^{\ 2}}\left(\frac{2}{\tau_{pump}^{\ 2}} + \frac{1}{\tau_{probe}^{\ 2}}\right) + \kappa^2}}\ ; \tag{2-17}$$

Absorption,

$$I_{abs}^{MAX}(\omega_{abs}) = -\frac{1}{2} \cdot \frac{\kappa\left(\omega_{abs} - \omega_{probe}\right)}{\frac{1}{\tau_{probe}^{\ 2}}\left(\frac{2}{\tau_{pump}^{\ 2}} + \frac{1}{\tau_{probe}^{\ 2}}\right) + \kappa^2}\ , \tag{2-18}$$

$$T_{abs}^{fwhm} = \tau_{pump} \sqrt{\frac{2\ln 2\left\{\left(\frac{2}{\tau_{pump}^{\ 2}} + \frac{1}{\tau_{probe}^{\ 2}}\right)^2 + \kappa^2\right\}}{\frac{1}{\tau_{probe}^{\ 2}}\left(\frac{2}{\tau_{pump}^{\ 2}} + \frac{1}{\tau_{probe}^{\ 2}}\right) + \kappa^2}}\ . \tag{2-19}$$

On the basis of Eq. (2-14), (2-16), and (2-18), let us first discuss the origin of time delay. As regards the origin of time delay of the ω_c spectral component of the probe pulse, ω_c reasonably satisfies $\omega_c = \omega_{SFG} - \omega_{pump}$ in the SFG measurement, $\omega_c = \omega_{OKE}$ in the OKE measurement, and $\omega_c = \omega_{abs}$ in the absorption measurement. Then, the origin of time delay

of the ω_c component is proportional to $\omega_c - \omega_{probe}$, which is natural because of the assumption of the linear chirp. The coefficient of proportionality of the origin of time delay to $\omega_c - \omega_{probe}$ in the OKE measurement and that in the absorption measurement are equal, but that in the SFG measurement is different. This is due to the fact that whereas SFG is a three-wave-mixing process, OKE and absorption are both four-wave-mixing processes. However, the difference is very small. In the present setup, for example, where the pulse width of the pump pulse was about 200 fs, the spectral width of the probe pulse was about 10000 cm^{-1}, and the proportional coefficient of $t_{OKE}^{MAX}(\omega_{OKE})$ to $\omega_c - \omega_{probe}$ was about 1300 fs^2 which was calculated from Fig. 2-20 shown below, the difference between $t_{OKE}^{MAX}(\omega_{OKE})$ and $t_{SFG}^{MAX}(\omega_{SFG})$ is calculated as follows:

$$\frac{t_{SFG}^{MAX}(\omega_{SFG}) - t_{OKE}^{MAX}(\omega_{OKE})}{t_{SFG}^{MAX}(\omega_{SFG})} = 5.5 \times 10^{-5}, \tag{2-20}$$

which is definitely not important at all. The value of Eq. (2-20) becomes larger when the chirp is smaller, but probably has no reason to be important in femtosecond time-resolved UV-VIS absorption measurements utilizing wide-band probe pulses. It is concluded from Eq. (2-14), (2-16), and (2-18) that the OKE method is applicable to the chirp correction of time-resolved absorption spectra according to our expectations, and to be theoretically exact, the OKE method is preferable to the SFG method.

Let us now discuss the time resolution. As regards all the signals, the FWHM T^{fwhm} of Eq. (2-15), (2-17), and (2-19) does not depend on observed angular frequency. It is also due to the assumption of the linear chirp of the probe pulse. T^{fwhm} can be regarded as the time resolution. The time resolution of the absorption measurement T_{abs}^{fwhm} is just $\sqrt{2}$ times as much as T_{OKE}^{fwhm} of the OKE method. However, it is impossible to derive T_{abs}^{fwhm} directly from T_{SFG}^{fwhm} of the SFG method. Again the OKE method is preferable to the SFG method.

Before the experimental results of the OKE method are shown, the influence of widening of the probe band width on the time resolution is discussed. On the assumption that both SPM and GVD induce a linear chirp approximately, the dependence of the time resolution T^{fwhm} on the probe band width with GVD fixed is calculated in the following way. τ_{probe} and κ defined above are expressed as a function of GVD (ϕ_{GVD}) and the proportional coefficient of a linear chirp by means of SPM (κ_{SPM}) as follows:

$$\tau_{probe} = \sqrt{\frac{\left(\frac{1}{4}\cdot\frac{\frac{1}{\tau_{pump}^{2}}}{\frac{1}{\tau_{pump}^{4}}+\kappa_{SPM}^{2}}\right)^{2}+\left(\frac{1}{4}\cdot\frac{\kappa_{SPM}}{\frac{1}{\tau_{pump}^{4}}+\kappa_{SPM}^{2}}+\phi_{GVD}\right)^{2}}{\frac{1}{4}\cdot\frac{\frac{1}{\tau_{pump}^{2}}}{\frac{1}{\tau_{pump}^{4}}+\kappa_{SPM}^{2}}}}, \tag{2-21}$$

$$\kappa = \frac{1}{4}\cdot\frac{\frac{1}{4}\cdot\frac{\kappa_{SPM}}{\frac{1}{\tau_{pump}^{4}}+\kappa_{SPM}^{2}}+\phi_{GVD}}{\left(\frac{1}{4}\cdot\frac{\frac{1}{\tau_{pump}^{2}}}{\frac{1}{\tau_{pump}^{4}}+\kappa_{SPM}^{2}}\right)^{2}+\left(\frac{1}{4}\cdot\frac{\kappa_{SPM}}{\frac{1}{\tau_{pump}^{4}}+\kappa_{SPM}^{2}}+\phi_{GVD}\right)^{2}}, \tag{2-22}$$

By using the same values of the parameters as those used in deriving Eq. (2-20), it can be shown that κ_{SPM} =4.7 × 10^{-3} fs^{-2} and ϕ_{GVD}=6.0 × 10^{2} fs^{2}. In Fig. 2-19, the probe band-width dependence of T^{fwhm} and the probe pulse width are shown when κ_{SPM} is varied from 0 fs^{-2} to 5 × 10^{-3} fs^{-2} and ϕ_{GVD} is fixed at 6.0 × 10^{2} fs^{2}. It is clear from Fig. 2-19 that when the probe band width is increased by means of a larger κ_{SPM} value with positive GVD kept constant, higher time resolution is obtained though the probe pulse width is broadened more. There are two methods to increase κ_{SPM} without increasing ϕ_{GVD}: to use a material as an SPM medium which has a larger third-order nonlinear optical susceptibility, or to increase the peak power of the input femtosecond pulse for SPM. In either case, spectral information obtained from a pump-probe time-resolved absorption measurement increases when the probe band width becomes wider, and higher time resolution is also obtained even without any special GVD compensation. This is an

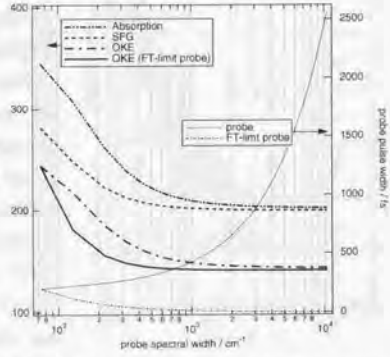

Fig. 2-19 Probe spectral-width dependence of the time-resolution (absorption, SFG, OKE) and the probe pulse width (chirped, FT-limit).
The extent of SPM was varied while the amount of GVD was fixed.

important advantage for absorption measurements. Fig. 2-19 shows also T_{OKE}^{fwhm} and the probe pulse width when the probe pulse is formed into a Fourier transform-limited pulse by applying proper negative GVD. Though the probe pulse width in this case is naturally extremely short due to the GVD compensation, T_{OKE}^{fwhm} which is essential is not influenced so much by whether GVD is compensated or not. Especially in the range where the probe band width is more than 1000 cm^{-1}, T_{OKE}^{fwhm} of the Fourier transform-limited probe and that of the chirped probe are almost equal. It is also applicable to T_{abs}^{fwhm} and T_{SFG}^{fwhm}. It is noted that the time resolution is limited by the pump pulse width and extreme pulse compression of the probe is not effective. Thus it is concluded that any GVD compensation of the wide-band probe is not necessary at all if only chirp correction is properly done.

The chirp structure of the femtosecond wide-band probe pulses was measured by using the OKE method. In Fig. 2-20, the time-resolved OKE spectra of hexane measured in the VIS setup are shown. Background which was independent of time delay was subtracted. The exposure time of the CCD at one time delay point was 2 s. The sharp peak at wavelength 450 nm in Fig. 2-20 was a Raman-induced OKE (RIKES) peak assigned to the CH stretching vibration modes of hexane. It is easily seen from Fig. 2-20 that the spectral component of the probe pulse which passed through the optical Kerr shutter shifted to the longer wavelength side as time delay increased. The OKE cross-correlation traces of the pump and the probe at different wavelengths were made from the OKE spectra of Fig. 2-20 by summing up over 10 CCD pixels for each wavelength region of about 5 nm, and are shown in Fig. 2-21 where intensity is normalized. Though only some representative cross-correlation traces are shown in Fig. 2-21, in fact more than 70 traces were obtained. t_{OKE}^{MAX} and T_{OKE}^{fwhm} was obtained by a Gaussian fitting. T_{OKE}^{fwhm} was about 0.3 ps though it depended a little on wavelength because of a nonlinear chirp. The wavelength dependence of t_{OKE}^{MAX} thus determined is shown in Fig. 2-22. The overall tendency of the t_{OKE}^{MAX} curve in Fig. 2-22 agrees very well with that measured by the SFG cross-correlation method. A t_{OKE}^{MAX} curve obtained by the SFG method is usually well fitted with simple expressions such as $a + b\lambda^{-2} + c\lambda^{-4}$ where

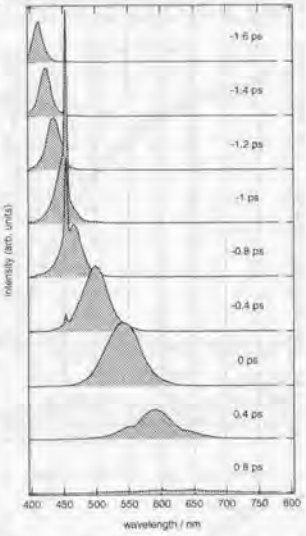

Fig. 2-20 Femtosecond time-resolved VIS OKE spectra of hexane at various time delays.

λ is wavelength and a,b,c are constants, but small structures that exist at wavelength 550 nm, 610 nm, 670 nm, and 710 nm in the t_{OKE}^{MAX} curve of Fig. 2-22 cannot be fitted with such a simple expression. This finding is ascribed to the advantage of the OKE method; it gives five or ten times more data points in a t_{OKE}^{MAX} curve on the wavelength axis than the SFG method. It is presumed that these small structures in the t_{OKE}^{MAX} curve are related with the wide-band pulse generation process, because these structures were also observed similarly when hexane was replaced with cyclohexane, acetonitrile, or acetone.

The OKE cross-correlation traces in the UV setup which utilized the 400-nm pump pulse and the UV wide-band probe pulse are shown in Fig. 2-23. As in the case of the VIS setup, T_{OKE}^{fwhm} was about 0.3 ps though it depended a little on wavelength because of a nonlinear chirp. In Fig. 2-24, the wavelength dependence of t_{OKE}^{MAX} is shown. Small structures exist in the t_{OKE}^{MAX} curve of Fig. 2-24 which cannot be fitted with the simple expression.

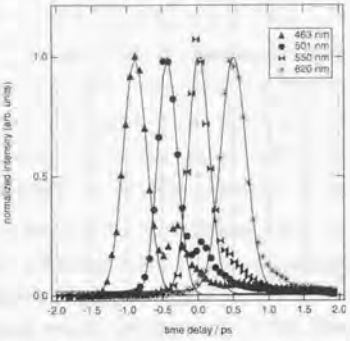

Fig. 2-21 Femtosecond time-resolved VIS OKE cross-correlation traces obtained from Fig. 2-20.

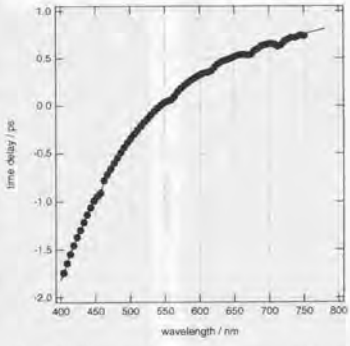

Fig. 2-22 Wavelength dependence of time delay in the VIS wavelength region obtained from the OKE cross-correlation traces in Fig. 2-21.

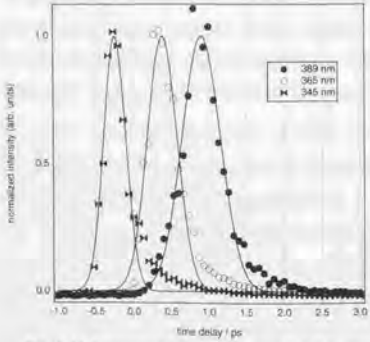

Fig. 2-23 Femtosecond time-resolved UV OKE cross-correlation traces.
Hexane was used as an OKE medium.

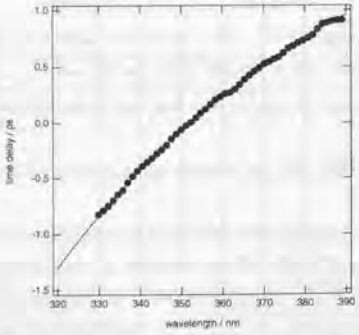

Fig. 2-24 Wavelength dependence of time delay obtained from the OKE cross-correlation traces in Fig. 2-23.

It took about five minutes to obtain the t_{OKE}^{MAX} curve in Fig. 2-22 or that in Fig. 2-24 by using the OKE cross-correlation method including the procedure of changing the setup from the absorption measurements. On the other hand, it probably takes about five hours or more to obtain the equivalent results by using the SFG method. It is because $I_{SFG}(\omega_{SFG}, t_{delay})$ is measured in the SFG method by way of sequential acquisitions as regards both of the parameters ω_{SFG} and t_{delay}, but $I_{OKE}(\omega_{OKE}, t_{delay})$ is measured in the OKE method by way of multichannel acquisition as regards ω_{OKE}. Thus, it is affirmed that the drawback (b) of the SFG method mentioned above has been completely overcome. Since the phase-matching condition of OKE does not depend on wavelength and the wavelength range of the absorption measurements is identical with that of the OKE measurements, the drawback (c) has been also completely overcome.

Chirp correction of time-resolved absorption spectra was performed during the data processing as given below: A curve which expressed the time-delay dependence of transient absorbance at wavelength λ_0 (corresponding to one pixel of the CCD) was made, and the time-delay axis of the curve was shifted to set t_{OKE}^{MAX} at λ_0 coincident with its origin, and finally the curve on the shifted time-delay axis was made by a linear interpolation to yield the chirp-corrected time-resolved absorption spectra. In Fig. 2-25, a set of time-resolved absorption spectra before chirp correction and that after chirp correction are shown as an example. Chirp correction drastically changed absorption band shape especially in the subpicosecond time range. In the chirp-correction procedure, a t_{OKE}^{MAX}-curve detailed on the wavelength axis is essential to perform precise chirp correction. The OKE method is effective in this regard as well.

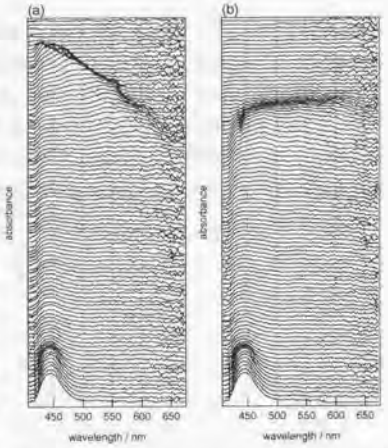

Fig. 2-25 Femtosecond time-resolved VIS absorption spectra of all-trans retinal in hexane at -4 ps ~ 120 ps after photoexcitation. (a) before chirp correction, (b) after chirp correction. In the subpicosecond time range, S – S transitions exhibit broad bands extending from 450 nm to 650 nm.

For the purpose of chirp correction of femtosecond time-resolved UV-VIS absorption spectra, the OKE cross-correlation method developed here is superior in theoretical and practical experimental aspects to the SFG or DFG method. It is expected that the OKE method becomes a standard method of chirp correction in the future.

2-3. Summary

A femtosecond time-resolved UV-VIS absorption spectrometer based on Ti:sapphire laser as a light source was constructed. This spectrometer enabled the measurements of transient spectra such as excited-state absorption spectra and ground-state bleaching spectra in the UV-VIS range with time-resolution of about 300 fs. The accuracy of absorbance obtained in a typical measurement was about 0.01. Further improvements to acquire faster time resolution by using pulse compression technique and to extend the measurable wavelength range to the shorter wavelength side will be needed in the future.

The OKE cross-correlation method was established as a chirp-structure measurement technique for the purpose of chirp correction of time-resolved UV-VIS absorption spectra. The origin of time delay obtained by the OKE method was exactly identical with that of the time-resolved absorption measurements. The time resolution of the OKE method was also identical with that of the absorption measurements except for a factor $\sqrt{2}$. It was concluded that the OKE method was more preferable than the SFG or DFG method in theoretical aspects. From an experimental point of view, the OKE method required still shorter measurement time and afforded much more data points on the wavelength axis than the SFG or DFG method. The OKE method which provides detailed information of chirp structure with less task is valuable as a requisite for the femtosecond time-resolved UV-VIS absorption measurements.

2-4. References

[1] R. L. Fork, O. E. Martinez and J. P. Gordon, *Opt. Lett.* **9** (1984) 150.

[2] R. L. Fork, B. I. Greene and C. V. Shank, *Appl. Phys. Lett.* **38** (1981) 671.

[3] D. E. Spence, P. N. Kean and W. Sibbett, *Opt. Lett.* **16** (1991) 42.

[4] J. Squier, F. Salin, G. Mourou and D. Harter, *Opt. Lett.* **16** (1991) 324.

[5] N. Sarukura, Y. Ishida, H. Nakano and Y. Yamamoto, *Appl. Phys. Lett.* **56** (1990) 814.

[6] P. M. W. French, J. A. R. Williams and R. Taylor, *Opt. Lett.* **14** (1989) 686.

[7] J. Goodberlet, J. Wang, J. G. Fujimoto and P. A. Schulz, *Opt. Lett.* **14** (1989) 1125.

[8] M. T. Asaki, C.-P. Huang, D. Garvey, J. Zhou, H. C. Kapteyn and M. M. Murnane, *Opt. Lett.* **18** (1993) 977.

[9] J. Zhou, G. Taft, C.-P. Huang, M. M. Murnane, H. C. Kapteyn and I. P. Christov, *Opt. Lett.* **19** (1994) 1149.

[10] I. M. Bayanov, R. Danielius, P. Heinz and A. Seilmeier, *Opt. Comm.* **113** (1994) 99.

[11] R. Danielius, A. Piskarskas, P. D. Trapani, A. Andreoni, C. Solcia and P. Foggi, *Appl. Opt.* **35** (1996) 5336.

[12] W. S. Pelouch, P. E. Powers and C. L. Tang, *Opt. Lett.* **17** (1992) 1070.

[13] P. D. Trapani, A. Andreoni, D. Podenas, R. Danielius and A. Piskarskas, *Opt. Comm.* **118** (1995) 338.

[14] K. Iwata, S. Yamaguchi and H. Hamaguchi, *Rev. Sci. Instrum.* **64** (1993) 2140.

[15] H. Hamaguchi and T. L. Gustafson, *Annu. Rev. Phys. Chem.* **45** (1994) 593.

[16] P. Hamm, M. Zurek, T. Röschinger, H. Patzelt, D. Oesterhelt and W. Zinth, *Chem. Phys. Lett.* **268** (1997) 180.

[17] H. Okamoto and M. Tasumi, *Chem. Phys. Lett.* **256** (1996) 502.

[18] T. Q. Ye, C. J. Arnold, D. I. Pattison, C. L. Anderton, D. Dukic, R. N. Perutz, R. E. Hester and J. N. Moore, *Appl. Spectrosc.* **50** (1996) 597.

[19] R. L. Fork, C. V. Shank, C. Hirlimann, R. Yen and W. J. Tomlinson, *Opt. Lett.* **8** (1983) 1.

[20] H. Nishioka, W. Odajima, K. Ueda and H. Takuma, *Opt. Lett.* **20** (1995) 2505.

[21] A. Migus, A. Antonetti, J. Etchepare, D. Hulin and A. Orszag, *J. Opt. Soc. Am. B* **2** (1985) 584.

[22] R. W. Schoenlein, J.-Y. Bigot, M. T. Portella and C. V. Shank, *Appl. Phys. Lett.* **58** (1991) 801.

[23] M. Taiji, K. Bryl, M. Nakagawa, M. Tsuda and T. Kobayashi, *Photochem. Photobiol.* **56** (1992) 1003.

[24] E. B. Treacy, *IEEE J. QUANT. ELECTRON.* **QE-5** (1969) 454.

[25] R. L. Fork, C. H. Brito Cruz, P. C. Becker and C. V. Shank, *Opt. Lett.* **12** (1987) 483.

[26] M. Taiji, Master Thesis, Univ. of Tokyo, 1989.

[27] A. Terasaki, Ph. D. Thesis, Univ. of Tokyo, 1991.

[28] S. Yamaguchi and H. Hamaguchi, *Chem. Phys. Lett.* **227** (1994) 255.

[29] S. Yamaguchi and H. Hamaguchi, *Appl. Spectrosc.* **49** (1995) 1513.

[30] D. McMorrow, W. T. Lotshaw and G. A. Kenny-Wallace, *IEEE J. QUANT. ELECTRON.* **24** (1988) 443.

[31] K. L. Sala, R. LeSage and R. W. Yip, *Appl. Spectrosc.* **38** (1984) 87.

3. Ultrafast chemical dynamics of retinal

Retinal, vitamin A aldehyde and the chromophore of light-sensitive proteins known as rhodopsins, is one of the well studied prototypical molecules exhibiting cis-trans photoisomerization reactions. The spectroscopic and photochemical properties of retinal strongly depend on its surrounding environment. Though organic solvents appear to provide simpler environment than proteins, the excited electronic structure of retinal in organic solvents seems to be more complicated than that of rhodopsins. Thus, the cis-trans photoisomerization reaction mechanism of retinal in organic solvents is much less understood than that in proteins [1, 2]. Excited electronic structure affects crucially the selectivity and the rate-determining mechanisms of chemical reactions. It is of considerable interest to look into the relationship between electronic structure and the isomerization pathway/yield of retinal in organic solvents.

The permanent dipole moment of all-trans retinal is as large as about 5 D [3, 4]. The electronic and molecular structure of retinal is greatly influenced by strong intermolecular interactions such as dipole-dipole interaction and H-bond formation. Consequently the chemical reaction dynamics of retinal is solvent-dependent. In this chapter, the ultrafast chemical dynamics of retinal in organic solvents is discussed in the following two sections. In Sect. 3-1, the electronic structure and the cis-trans photoisomerization reaction of retinal in nonpolar solvents are discussed. In Sect. 3-2, the chemical equilibrium of H-bond formation and breakage reactions between all-trans retinal and 1-butanol as a protic solvent are discussed.

3-1. Retinal in nonpolar solvents

3-1-1. Introduction

3-1-1-1. Isomerization quantum yield

Since retinal has four C=C double bonds in its polyenic backbone, there are sixteen possible cis-trans isomers associated with it, including the all-trans and four mono-cis isomers. It is known that all of these isomers in solution undergo cis-trans isomerization upon UV irradiation [5]. The photoisomerization products and quantum yields of retinal depend on solvent polarity and acidity. It is widely accepted that alkane and cycloalkane solvents such as hexane, cyclohexane, 3-methylpentane, and so on can be regarded as similar environment for the excited-state dynamics and the photoisomerization reactions of retinal. Let these solvents be called nonpolar solvents. The products and quantum yields of the cis-trans photoisomerization reactions of the retinal isomers in nonpolar solvents on direct photoexcitation are summarized in Table 3-1 by referring to reported values. Though it has been reported that degassing

starting isomer	product (quantum yield)
all-trans	13-cis (0.09 – 0.10)[a, b], 9-cis (0.015 – 0.02)[a, b]
13-cis	all-trans (0.21)[c]
9-cis	all-trans (0.18)[c], 9,13-dicis (0.06)[c]
11-cis	all-trans (0.3)[b], 11,13-dicis (0.2)[b]
7-cis	all-trans (0.6)[b], 7,13-dicis (0.1)[b]

Table 3-1 Photoisomerization products and quantum yields of the retinal isomers in aerated nonpolar solvents at room temperature by direct photoexcitation.
a) Ref. [17], b) Ref. [7], c) Ref. [8].

of solutions by making use of N_2 or Ar purging gives rise to concentration dependence of the quantum yields (*vide post*) [6, 7], all the values in Table 3-1 are on condition that solutions are aerated, that is, there is no concentration dependence of the quantum yields. While the main photoproduct from the mono-cis isomers always has the all-trans configuration, the all-trans isomer isomerizes to give the 13-cis and 9-cis isomers. If the 9,13-dicis isomer which the 9-cis isomer affords at a very low quantum yield is disregarded, the all-trans, 13-cis, and 9-cis isomers form a closed reaction system. Then it is presumably impossible that the other isomers such as 7-cis and 11-cis appear in the photoisomerization reaction processes among these three isomers. Therefore, the all-trans, 13-cis, and 9-cis isomers are chosen as starting materials to investigate the photoisomerization reactions between these three isomers.

3-1-1-2. 9-cis → all-trans isomerization

The photoisomerization reaction of retinal in nonpolar solvents for which the mechanism has been clarified best so far is the 9-cis → all-trans reaction. As shown in Table 3-1, Waddell et al. reported the quantum yield of this reaction upon direct photoexcitation in aerated 3-methylpentane to be 0.18 by HPLC analysis [8]. Hamaguchi et al. found that the transient Raman spectrum of T_1 species at 20 ns after the photoexcitation of 9-cis retinal in aerated hexane was nearly identical with that of all-trans retinal [9]. Hirata et al. observed that the $T_0 \leftarrow T_1$ absorption spectrum of 9-cis retinal gradually became identical with that of all-trans retinal in a few nanosecond by using picosecond time-resolved VIS absorption spectroscopy [10]. Tahara et al. have demonstrated by picosecond time-resolved 2D-CARS spectroscopy that photoexcited 9-cis retinal in aerated cyclohexane relaxes to the T_1 state with the 9-cis configuration retained (T_1 9-cis retinal), and then isomerizes adiabatically to give the T_1 all-trans isomer with the time constant of 880 ps [11]. All these results are consistent, and it is very clear that the adiabatic one-way 9-cis → all-trans isomerization in the T_1 state has been established. However it has not yet been clarified whether there exists a 9-cis → all-trans isomerization pathway which is complete only in the singlet states.

3-1-1-3. 13-cis → all-trans isomerization

As regards the 13-cis → all-trans isomerization reaction, there still remain many equivocal points. It has been reported that the quantum yield of this reaction upon direct photoexcitation in aerated 3-methylpentane is 0.21 by HPLC [8]. According to the result of nanosecond time-resolved Raman spectroscopy by Hamaguchi et al. [9] and that of picosecond time-resolved VIS absorption spectroscopy by Mukai and co-workers [12], there exist two kinds of T_1 retinal, that is, the T_1 13-cis and all-trans isomers, at 5 ns ~ 20 ns after the photoexcitation of the 13-cis isomer. This fact suggests two different mechanisms of the

13-cis → all-trans isomerization reaction: One is that this reaction is not complete at 20 ns after photoexcitation and is a comparatively slow reaction which takes place as an adiabatic process in the T_1 state. The other possibility is that this reaction is complete in the excited singlet manifold and does not proceed in the T_1 state. The former is deduced from the fact explained below that there is no adiabatic all-trans → 13-cis isomerization reaction pathway in the T_1 state, that is, there is no chemical equilibrium between the T_1 all-trans and T_1 13-cis isomers. The latter is based on the established fact that all-trans retinal in the excited singlet manifold decays to the T_1 state with the all-trans configuration retained by way of intersystem crossing at a quantum yield reported to be as high as 0.4 ~ 0.7 [13-16]. It is not yet known which of these two mechanisms of the 13-cis → all-trans isomerization reaction is correct.

3-1-1-4. All-trans → 13-cis·9-cis isomerization

As shown in Table 3-1, the total quantum yield of the all-trans → 13-cis·9-cis photoisomerization reaction upon direct photoexcitation in aerated hexane or 3-methylpentane is 0.115 ~ 0.12 [7, 17]. Jensen et al. investigated the composition of the photostationary state of triplet-sensitized retinal by HPLC, and found that the photostationary state consisted of the all-trans, four mono-cis, and 9,13-dicis isomers [18]. If all-trans retinal does not isomerize in the T_1 state, the photostationary state of triplet-sensitized retinal should contain nothing but the all-trans isomer. The mono-cis → all-trans one-way isomerization mechanism in the T_1 state [9, 11, 19] is in obvious conflict with the result of Jensen et al. They denied the one-way isomerization mechanism in their conclusions. Ganapathy and Liu investigated the relation between the quantum yield and the concentration of the all-trans isomer as a starting material by using HPLC [7]. According to their result, there was no concentration dependence of the all-trans → 13-cis·9-cis isomerization quantum yield in aerated solutions on direct photoexcitation, but the quantum yield increased with an increase in the concentration of all-trans retinal as a starting isomer in degassed solutions. They also found that the increasing rate of the all-trans → 9-cis isomerization quantum yield was higher than that of the all-trans → 13-cis isomerization quantum yield. They proposed a novel mechanism that the all-trans → 13-cis·9-cis isomerization reaction in aerated solutions took place in the singlet states, but that another reaction pathway participated in this reaction in degassed solutions by way of intermolecular energy transfer between S_0 and T_1 retinal. Apart from confirming the validity of their novel proposal, it is very important in thinking of isomerization mechanisms to determine whether the quantum yields depend on the concentration of all-trans retinal or not. Accordingly a supplementary experiment has been recently performed in our group, and the result of Ganapathy and Liu has been almost reproduced [20]. They also reported that the all-trans isomer isomerized to give 13-cis, 9-cis, and 11-cis isomers in degassed solutions via triplet sensitization, and that the concentration

dependence of these quantum yields showed a similar tendency to that in the isomerization reactions on direct photoexcitation. In this thesis, the experimental results which Ganapathy and Liu obtained [7] are regarded as valid, and the following two propositions (a) and (b) are premised for further discussions:

(a) In aerated solutions, there is no concentration dependence of the all-trans → 13-cis·9-cis isomerization quantum yield upon direct photoexcitation. Then, this reaction is unimolecular.

(b) In degassed solutions, the quantum yield of the all-trans → 13-cis·9-cis isomerization depends on the concentration of the all-trans isomer either upon direct photoexcitation or via triplet sensitization. Then, this reaction includes an elementary process which intermolecular interaction between retinal molecules takes part in.

The quantum yield measurements via triplet sensitization by Jensen et al. [18] reviewed above were performed under the degassed condition. Then, their result is not effective in discussing unimolecular reaction mechanisms of the all-trans → 13-cis·9-cis isomerization because of the proposition (b). The transient Raman measurements of T_1 retinal by Wilbrandt et al. [21] are also not effective in thinking of unimolecular isomerization mechanisms because of the same reason. Hamaguchi et al. showed that the all-trans, 7-cis, 9-cis, and 11-cis isomers as starting materials in aerated hexane afforded an identical Raman spectrum at 20 ns after photoexcitation, and they ascribed that spectrum to the T_1 all-trans isomer [9]. They came to a conclusion that the 7-cis (or 9-cis, 11-cis) → all-trans isomerization was complete in 20 ns after photoexcitation, but the all-trans isomer did not isomerize at all in the T_1 state. The same conclusion was obtained from the picosecond 2-D CARS experiment by Tahara et al. [11]. Hirata et al. measured the picosecond time-resolved VIS absorption spectra of the all-trans and 9-cis isomers [10]. They showed that in both of the isomers, similar absorption bands were obtained with a rise time constant of about 30 ps, and the band of the all-trans isomer did not change after the 30-ps rise until 5 ns, while that of the 9-cis isomer showed a narrowing process to become identical with that of the all-trans isomer in a few nanoseconds. They concluded that the absorption bands which rose with the 30-ps time constant in both of the isomers were due to the T_1 all-trans isomer and the T_1 9-cis isomer respectively, and the latter isomerized to give the former in a few nanoseconds. Though they used degassed hexane solutions, their results have been reproduced by my measurements on the aerated condition shown later in this thesis. Therefore, it is affirmed that only unimolecular processes contributed to the results of Hirata et al. Yuzawa and Hamaguchi have clearly shown by using submicrosecond time-resolved IR spectroscopy that there is no isomerization reaction taking place in the T_1 state when the all-trans isomer is a starting material [22]. According to their result, T_1 all-trans retinal is generated upon direct photoexcitation within the time resolution of 50 ns and decays exclusively to the all-trans isomer in the ground state (S_0 all-trans) with the time constant of 5 μs, and the S_0 13-cis and S_0 9-cis isomers are also generated within the time resolution and do not decay at all. They

concluded that the all-trans → 13-cis·9-cis isomerization does not take place in the T_1 state; in other words, it is complete in the excited and ground singlet states within the time resolution. However, there still remains an incompatibility between the results of Yuzawa and Hamaguchi [22] and those of Ganapathy and Liu [7] or the proposition (b). Yuzawa and Hamaguchi measured the time-resolved IR spectra of photoexcited all-trans retinal in a degassed cyclohexane solution with the concentration of 3.5×10^{-4} mol dm^{-3}. According to the results of Ganapathy and Liu, the all-trans → 13-cis·9-cis isomerization reaction where intermolecular interaction participates should take place under the condition of Yuzawa and Hamaguchi. As a matter of fact, they reported that the all-trans → 13-cis·9-cis isomerization reaction was complete in less than 50 ns and took place not in the triplet state but in the singlet state, and the T_1 all-trans isomer showed a unimolecular decay to the S_0 all-trans isomer. If the proposition (b) and the results of Yuzawa and Hamaguchi are simultaneously taken into account, it is concluded that intermolecular interaction between singlet retinal molecules participates in the all-trans → 13-cis·9-cis isomerization reaction in degassed solutions. Any transient species in the ground state whose lifetime is less than 50 ns has never been found by either UV-VIS absorption or Raman spectroscopy. Then, retinal in the excited singlet states must take part in this intermolecular interaction. However it is not likely that intermolecular interaction plays an important role for retinal in the excited singlet states, because the lifetime of S_1 all-trans retinal is as short as about 30 ps [10, 23-25] and the concentration of solvents is usually more than about 3000 times as high as that of retinal. In addition, any self-association of retinal molecules has never been reported so far. We leave the matter of intermolecular interaction between singlet retinal molecules to future investigations.

It is clear that an aerated solution should be preferably used for the purpose of discussing unimolecular isomerization reaction mechanisms. The following two conclusions concerning the all-trans → 13-cis·9-cis isomerization of retinal in aerated nonpolar solvents upon direct photoexcitation are consistent with all the studies reviewed above:

(i) The all-trans → 13-cis·9-cis isomerization reaction is unimolecular.

(ii) Isomerization does not take place in T_1 all-trans retinal.

These two conclusions are all what have been clarified so far about the all-trans → 13-cis·9-cis isomerization in the aerated condition. There are two possible reaction schemes. One is similar to the trans → cis isomerization mechanism of stilbene [26]: All-trans retinal in the excited singlet states decays to a perpendicular excited singlet state, and its deactivation gives the S_0 all-trans and mono-cis isomers in an almost equal ratio. In the other scheme, the all-trans isomer in the excited singlet states isomerizes to give the mono-cis isomer in the excited singlet states; in other words, the all-trans → 13-cis·9-cis isomerization is complete in the excited singlet manifold, of which adiabatic one-way isomerization in the excited singlet state is a representative [27]. If there is only one excited singlet state (i.e. S_1) in the low

energy part of the UV-VIS absorption spectrum of all-trans retinal up to 30000 cm^{-1}, the all-trans → 13-cis-9-cis isomerization scheme of retinal has to be the former one. It is because the T_1 mono-cis isomers which are expected in the latter scheme have never been observed when the all-trans isomer is the starting material [9-11, 22, 28]. If there are two or more excited singlet states in this low energy region, both of the two isomerization schemes are possible. It is because the T_1 mono-cis isomers are not always expected after the photoexcitation of the all-trans isomer, when the excited singlet states have their own decay pathways.

3-1-1-5. Excited singlet electronic structure

Three excited singlet states in the low energy region of all-trans retinal up to 30000 cm^{-1} have been proposed since more than twenty years ago [29-39]. Though the state ordering is still under discussion, there are surely a B_u^+ (π, π^*) state, an A_g^- (π, π^*) state, and an (n, π^*) state in the excited singlet manifold, which are very close in energy. The Mulliken symbols of the irreducible representations in the point groups such as A_g and B_u in this thesis are approximate and are derived by correlating the properties of an electronic state with those of the analogous state in a polyene of C_{2h} symmetry. The plus and minus signs attached to the Mulliken symbols were first introduced by Pariser [40], and represent a sign of the linear combination of two degenerate electronic configurations. The ground state is expressed as A_g^+ by definition, and only transitions between plus and minus states are one-photon allowed [40]. Polarized UV-VIS absorption spectroscopic study of crystalline all-trans retinal by Drikos et al. [30-32] and two-photon fluorescence excitation spectroscopy by Birge et al. [34, 35] showed that the S_1 state was of A_g^- (π, π^*) character, but fluorescence spectroscopy of hydrogen-bonded retinal by Takemura et al. [29] postulated that an (n, π^*) state is the lowest excited singlet state. Hochstrasser et al. observed the S - S absorption kinetics of all-trans retinal, and proposed a speculative idea of a partitioning mechanism in the excited singlet manifold [23]. Doukas and co-workers performed picosecond time-resolved fluorescence spectroscopy of all-trans retinal and observed only one decay component through the temperature range of 80 K ~ 296 K [41]. They suggested the same idea as that of Hochstrasser et al. Tahara and Hamaguchi has recently shown by using picosecond time-resolved fluorescence spectroscopy that there are at least two fluorescent species generated by the photoexcitation of all-trans retinal and one of them is assigned to the S_1 state whose lifetime is equal to the rise time constant of T_1 [24]. The recent femtosecond time-resolved VIS absorption measurement of all-trans retinal has revealed the presence of two species both of which precede S_1 [25], but an unequivocal assignment was impossible then. Larson et al. measured the time-delay dependence of absorbance after the photoexcitation of all-trans

retinal at several wavelengths in the femtosecond time range. They concluded that the S_1, S_2, and S_3 states of all-trans retinal are of B_u^+ (π, π^*), A_g^- (π, π^*), and (n, π^*) characters respectively [42]. However some strange assumptions were included in their kinetics model, one of which was that the S_2 lifetime was longer than the S_3 lifetime. It seems that their interpretation is not decisive at all. Very recently Takeuchi and Tahara performed femtosecond time-resolved fluorescence up-conversion spectroscopy, and they found that the transient species of the shortest lifetime emitted the strongest fluorescence [43]. They concluded that the S_1 state of all-trans retinal is of B_u^+ (π, π^*) character.

3-1-1-6. Purpose

The purpose of this section 3-1 is to clarify the all-trans → 13-cis-9-cis isomerization mechanism of retinal in aerated nonpolar solvents. In Sect. 3-1-2, the HPLC analysis of retinal used throughout this study and the UV-VIS absorption spectra of the ground-state retinal isomers are presented. In 3-1-3, the femtosecond time-resolved UV-VIS absorption spectroscopy of retinal using the spectrometer described in Chap. 2 is discussed. The femtosecond time-resolved VIS absorption spectra of the all-trans, 9-cis, and 13-cis isomers are shown in Sect. 3-1-3-1. Some correspondence was found between the excited-state absorption bands of these three isomers about their peak positions and band shapes, but those bands were not identical with each other. This fact indicated that any all-trans → 13-cis-9-cis isomerization pathway complete in the excited singlet manifold was not observed within the accuracy of the present measurements. Accordingly it was considered that the isomerization mechanism by way of the deactivation of a perpendicular excited singlet state mentioned above was more promising than the other. In this mechanism, the deactivation of a perpendicular excited singlet state gives simultaneously a starting material and a photoproduct both of which have absorption bands in the UV region. Then, the femtosecond time-resolved UV absorption spectra of all-trans retinal were measured and are shown in Sect. 3-1-3-2. Two time constants were found in the bleaching recovery process of S_0 all-trans retinal. One of them was longer than the lifetime of the S_2 all-trans isomer but shorter than that of the S_1 all-trans isomer, and the other coincided with the T_1 lifetime. This result indicated that the former time constant of the bleaching recovery corresponded to the lifetime of a perpendicular excited singlet state, and its precursor was not the S_1 but the S_2 or S_3 all-trans isomer. The nanosecond time-resolved UV absorption spectra of all-trans retinal were supplementarily measured and are presented in Sect. 3-1-3-3. In Sect. 3-1-4, detailed discussion on the all-trans → 13-cis-9-cis isomerization reaction of retinal is presented on the basis of these newly obtained experimental data.

3-1-2. Experimental

3-1-2-1. Materials

Hexane, cyclohexane, and diethylether were purchased from Kanto Chemical Co. or Wako Chemical Co. and used as received. No precautions were taken to dry these solvents. All the solvents were aerated. Commercial retinal (Sigma Chemical Co.) was used without further purification throughout this study. Retinal samples were analyzed for isomeric composition by using the HPLC system of JASCO which consisted of a pump (880-PU), a column oven with an injector (865-CO), a 25 × 1 cm Column-Lichrosorb Si 60-5 column, and a UV-VIS spectrometer (875-UV). The eluent (2×10^{-3} dm^3 min^{-1}) was hexane (JIS certified grade) containing 18% diethylether (JIS certified grade). Analysis was performed at a wavelength of 360 nm. The following molar absorption coefficients at 360 nm in the unit of mol^{-1} dm^3 cm^{-1} were used for the calculation of isomeric compositions: all-trans, 45400; 13-cis, 37500; 9-cis, 36600; 11-cis, 24800; 9,13-dicis, 34100 [44]. Isomeric compositions were calculated from the peak areas of chromatograms. It has been found that the lowest limit of the detection of the present HPLC system was about 0.09% of the total amount of retinal [45]. The isomeric compositions of the commercial retinal isomers thus obtained are summarized in Table 3-2.

	all-trans	13-cis	11-cis	9-cis	7-cis
all-trans	98.3%	1.7%	-	-	-
13-cis	0.5%	99.2%	-	-	0.3%
9-cis	0.1%	-	0.2%	99.7%	-

Table 3-2 Isomeric composition of the commercial retinal samples (SIGMA) checked by using HPLC.

It is necessary to consider to what extent a cis-trans isomerization mechanism can be discussed accurately when retinal isomers having isomeric compositions shown in Table 3-2 are used as samples. Let us assume that the isomers are distinguished by subscripts such as i, j. The condition $q_{i\to j}C_i >> C_j$ is sufficient for accurately discussing an isomerization reaction mechanism from an isomer i to j where C_i is the concentration of an isomer i, and $q_{i\to j}$ is the photoisomerization quantum yield of this reaction. Therefore $q_{i\to j}C_iC_j^{-1}$ is regarded as a kind of a standard, and a larger value of $q_{i\to j}C_iC_j^{-1}$ is more preferable. The following values were obtained from Table 3-1 and 2 for the three starting materials: all-trans, $q_{i\to j}C_iC_j^{-1} \equiv 7$; 13-cis, $q_{i\to j}C_iC_j^{-1} \equiv 26$; 9-cis, $q_{i\to j}C_iC_j^{-1} \equiv 60$. The value of $q_{i\to j}C_iC_j^{-1}$ decreases when samples are irradiated with UV light during the spectroscopic measurements. The amount of the samples and the numbers of the photons of UV light that irradiated the samples were controlled to preserve the conditions $q_{i\to j}C_iC_j^{-1} > 5$ for the all-trans isomer as a starting material and $q_{i\to j}C_iC_j^{-1} > 8$ for the 9-cis and 13-cis isomers as starting materials. These conditions were confirmed by HPLC measurements after the spectroscopic

measurements, and guaranteed that when the absorption band of the 13-cis isomer was observed in the time-resolved absorption spectra of the all-trans isomer as a starting material, for example, the contribution of the 13-cis isomer as a photoisomerization product to the band was more than five times as large as that of the 13-cis isomer which stationarily existed. However it is also necessary to remember that the absorption band of an intermediate or a product has contributions possibly from a stationary isomer.

The UV-VIS ground-state absorption spectra of the all-trans, 9-cis, and 13-cis isomers in hexane (HPLC grade) were measured at room temperature (294 K) by using a commercial UV-VIS spectrometer (HITACHI, U-3500), and are shown in Fig. 3-1. The absorption bands in the wavelength region 300 nm ~ 400 nm of those three isomers are nearly identical. It is widely accepted that the transitions from the ground state A_g^- to the excited singlet states B_u^+ (π, π^*), A_g^- (π, π^*), and (n, π^*) contribute to these absorption bands [36], and the predominant contribution is naturally made by the $A_g^- \rightarrow B_u^+$ (π, π^*) transition. However the small structures at a wavelength of about 280 nm and the bands at 250 nm of these three isomers are markedly different from one another. The band at 250 nm of 13-cis retinal is especially distinct. Though there have been several proposals regarding the nature of these transitions, such as $A_g^- \rightarrow A_g^+$ (π, π^*) (so-called cis band) and $A_g^- \rightarrow B_u^-$ (π, π^*), the assignments are still under discussion [36, 46, 47].

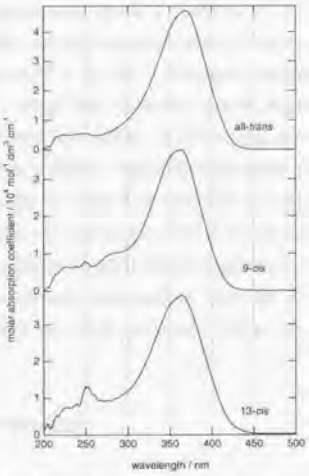

Fig. 3-1 Ground-state molar absorption spectra of all-trans, 9-cis, and 13-cis retinal in hexane.

3-1-2-2. Femtosecond time-resolved VIS absorption spectroscopy

The femtosecond time-resolved VIS absorption spectra of the all-trans, 9-cis, and 13-cis isomers were measured by using the spectrometer described in Chap. 2. The solvent was hexane or cyclohexane (both HPLC grade). All the retinal solutions had nearly the same concentration (2×10^{-3} mol dm^{-3}) and the same volume (0.2 dm^3). The temperature of the solutions just emitted from the jet nozzle in the vicinity of the laser-beam focus point was 293 ± 2 K. The pump pulse was characterized as follows: center wavelength, 400 nm; pulse energy, 6 μJ; excitation density, 2×10 J m^{-2}. The pulse energy of the VIS wide-band probe pulse was less than 0.1 μJ. In a set of time-resolved spectra, there were 70 time-delay points from -4 ps to 120 ps. The exposure time of the CCD was 1 s, and the number of the exposures

at each time delay point was 5. Chirp correction described in Sect. 2-2-3-3 was performed after the measurements to make the final time-resolved spectra.

3-1-2-3. Femtosecond time-resolved UV absorption spectroscopy

The femtosecond time-resolved UV absorption spectra of all-trans retinal were measured by using the spectrometer described in Chap. 2. The solvent was hexane or cyclohexane (both HPLC grade). The concentration of retinal was about 2×10^{-3} mol dm^{-3}, and the volume was about 0.2 dm^3. The pump pulse was characterized as follows: center wavelength, 400 nm; pulse energy, 1.7 μJ; excitation density, 2×10 J m^{-2}. The pulse energy of the UV wide-band probe pulse was less than 0.1 μJ. In a set of time-resolved spectra, there were 70 time-delay points from −4 ps to 120 ps. The exposure time of the CCD was 1 s, and the number of the exposures at each time delay point was 5. Chirp correction described in Sect. 2-2-3-3 was performed after the measurements to make the final time-resolved spectra. As described later, the all-trans → 13-cis-9-cis isomerization total quantum yield was derived from this femtosecond UV absorption measurement. In order to investigate the temperature dependence of the quantum yield, the temperature of the solution just emitted from the jet nozzle in the vicinity of the laser-beam focus point was set at four different points: 269 ± 2 K, 273 ± 2 K, 293 ± 2 K, 298 ± 2 K.

3-1-2-4. Nanosecond time-resolved UV absorption spectroscopy

The nanosecond time-resolved pump-probe UV absorption spectroscopy of all-trans retinal was supplementarily performed by using the spectrometer described in Chap. 2 and a CW Q-switched Nd:YLF laser (Spectra Physics, TFR). Cyclohexane (HPLC grade) was used as the solvent. The concentration was about 2×10^{-3} mol dm^{-3}, and the volume was about 0.2 dm^3. The temperature of the solutions just emitted from the jet nozzle in the vicinity of the laser-beam focus point was 298 ± 2 K. The third harmonic of the Nd:YLF laser was used as the pumping source of all-trans retinal. The pump pulse was characterized as follows: center wavelength, 349 nm; pulse energy, 1 μJ; pulse width, 7 ns; excitation density, 1×10 J m^{-2}. The Nd:YLF laser was synchronized with the Ti:sapphire regenerative amplifier at 1 kHz. The UV wide-band probe pulse in the femtosecond UV setup was used as it was for probing. The probe pulse energy was less than 0.1 μJ. Time delay between the pump and the probe was controlled by using an electronic delay generator (Stanford Research, DG535). The pump pulse width corresponded to the time resolution. The exposure time of the CCD was 1 s, and the number of the exposures at each time delay point was 50. Chirp correction was not necessary at all for these measurements.

3-1-3. Results

3-1-3-1. Femtosecond time-resolved VIS absorption spectra

In Fig. 3-2 ~ 4, several representative femtosecond time-resolved VIS absorption spectra of the retinal isomers in hexane are shown: all-trans, Fig. 3-2; 9-cis, Fig. 3-3; 13-cis, Fig. 3-4. The spectra are shown in the forms of difference spectra. The positive signals correspond to the photoinduced increase of absorbance which is caused by transitions from excited states to higher excited states. The negative signals correspond to the photoinduced decrease of absorbance which is caused by ground-state bleaching and/or stimulated emission gain. Stimulated Raman loss (inverse Raman) may also contribute to the positive signals and stimulated Raman gain to the negative signals.

There are several common features to all the sets of the spectra of Fig. 3-2 ~ 4. First of all, the absorption bands around 450 nm at 100 ps after the photoexcitation in these sets are very similar and undoubtedly assigned to the $T_n \leftarrow T_1$ absorption [10, 12, 25, 48]. As mentioned in Sect. 3-1-1, the T_1 species has exclusively the all-trans configuration when the S_0 all-trans isomer is the starting material [9-12, 22]. It is affirmed that the absorption band at 100 ps around 450 nm in Fig. 3-2 is ascribed to the T_1 all-trans isomer. The band shape and the peak position of this band agree well with the reported results [10, 15, 16, 48]. When the

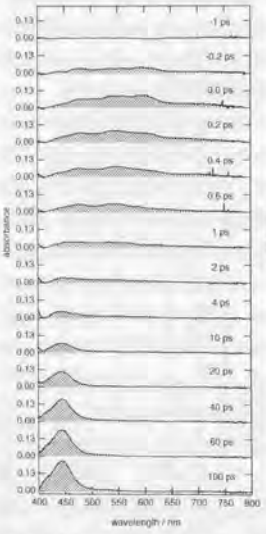

Fig. 3-2 Femtosecond time-resolved VIS absorption spectra of all-trans retinal in hexane at various time delays.

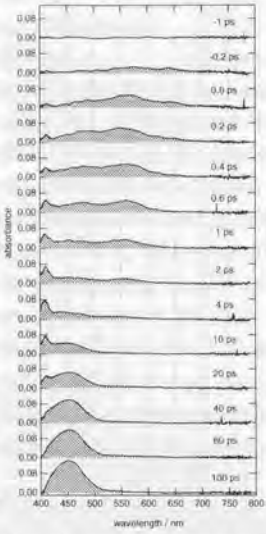

Fig. 3-3 Femtosecond time-resolved VIS absorption spectra of 9-cis retinal in hexane at various time delays.

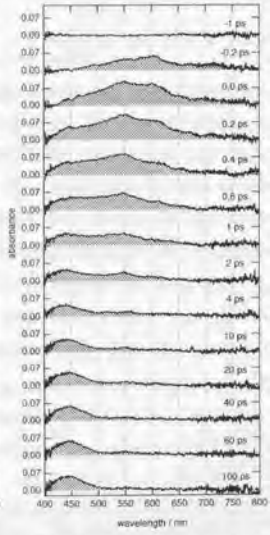

Fig. 3-4 Femtosecond time-resolved VIS absorption spectra of 13-cis retinal in hexane at various time delays.

S_0 9-cis isomer is the starting material, as reviewed in 3-1-1, the T_1 species directly generated from an excited singlet species by way of intersystem crossing has the 9-cis configuration, and further it isomerizes adiabatically to give the T_1 all-trans isomer with a time constant of 880 ps [11]. Then, it is concluded that the T_1 9-cis isomer contributes to about 90% of the absorption band at 100 ps around 450 nm in Fig. 3-3. The band shape and the peak position of this band agree well with those in the literature [10]. When S_0 13-cis retinal is the starting isomer, the absorption band at 100 ps around 450 nm in Fig. 3-4 reproduces the results reported by Mukai et al. [12]. However the configuration of the T_1 species in the picosecond time range generated through the photoexcitation of the 13-cis isomer has not yet been clarified. The normalized VIS absorption spectra of the all-trans, 9-cis, and 13-cis isomers in hexane at 100 ps after the photoexcitation are simultaneously shown in Fig. 3-5 for the sake of comparison. The $T_n \leftarrow T_1$ absorption band generated through the photoexcitation of the 13-cis isomer is clearly different from the other two bands, but it is impossible to determine only from Fig. 3-5 the configuration and the electronic state of transient species contributing to this band: For instance, the T_1 13-cis isomer, both of the T_1 13-cis and all-trans isomers, and a perpendicular excited state are all possible candidates.

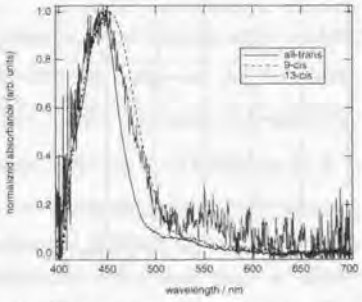

Fig. 3-5 $T_n \leftarrow T_1$ absorption spectra of the retinal isomers in hexane at 100 ps.

Broad absorption bands in the subpicosecond time range are another feature common to the three sets of the spectra in Fig. 3-2 ~ 4. These bands of all-trans retinal were observed first by Hochstrasser et al. in 1976 [23], and there has been no further reports until my letter was published in 1996 [25]. It is likely that the excited singlet states contribute to these broad bands, but any detailed assignments have not yet been performed. It is due to that the three congested excited singlet states (B_u^+ (π, π^*), A_g^- (π, π^*), (n, π^*)) make the electronic structure and the excited-state dynamics of all-trans retinal complicated. As regards the 9-cis and 13-cis isomers, corresponding three excited singlet states are expected to exist, though the meanings of the symbols such as A_g and B_u are even more approximate. The time-resolved VIS absorption spectra of 9-cis and 13-cis retinal as the starting isomer in the subpicosecond time range have never been reported so far. A detailed kinetics analysis is necessary to obtain more insight into the singlet electronic structure of retinal from the time-resolved spectra in Fig. 3-2 ~ 4.

When two or more transient species are involved in one set of time-resolved spectra just like the present case, the singular value decomposition (SVD) analysis combined with fitting procedures is sometimes useful for its kinetics analysis. The methods and the

advantages of SVD have been briefly reviewed by Chen and Braiman [49] and besides theirs there are many examples in various fields which show the usefulness of SVD [22, 25, 50-53]. In SVD, a set of time-resolved spectra is treated as a matrix. Let this matrix be written as $\mathbf{A}$ of which the ith row vector corresponds to the spectrum at the ith time delay point. The SVD analysis yields several SVD components from $\mathbf{A}$, and each SVD component has its singular value (scalar), its spectrum (column vector), and its temporal evolution (column vector). $\mathbf{A}$ is expressed as follows:

$$\mathbf{A} = \sum_{i=1} V_i \mathbf{t}_i {}^t\mathbf{s}_i , \tag{3-1}$$

where V_i is the singular value of the ith SVD component, $\mathbf{s}_i$ is the spectrum of the ith SVD component, and $\mathbf{t}_i$ is the temporal evolution of the ith SVD component. All the singular values are positive, and $V_i > V_j$ if $i < j$. $\{\mathbf{s}_i\}$ and $\{\mathbf{t}_i\}$ are both normalized orthogonal sets; ${}^t\mathbf{s}_i\mathbf{s}_j = \delta_{ij}$ and ${}^t\mathbf{t}_i\mathbf{t}_j = \delta_{ij}$. In Eq. (3-1), the contribution of the ith SVD component to $\mathbf{A}$ is determined by V_i. The ith SVD component is not important if V_i is small, and it is reasonable only to take account of the SVD components of which the singular value is significantly large. The omission of the SVD components with a small singular value is effective in simplifying an analysis and removing noise. This is one of the advantages of the SVD analysis. However, it is always arbitrary to determine a boundary singular value for taking the corresponding SVD component into account, and it is sometimes difficult to determine it.

The SVD of the three sets of the time-resolved spectra in Fig. 3-2 ~ 4 yielded the three series of the singular values shown in Fig. 3-6. The 5th and the higher singular values are almost constant and independent of the samples. It is presumed that these higher singular values are dominated not by signals but by noise. Therefore it is meaningless to take account of the 5th and the higher SVD components. In order to obtain physically meaningful temporal evolutions and the corresponding spectra from the SVD components, let us start with the following kinetics scheme for the photophysics of all-trans retinal:

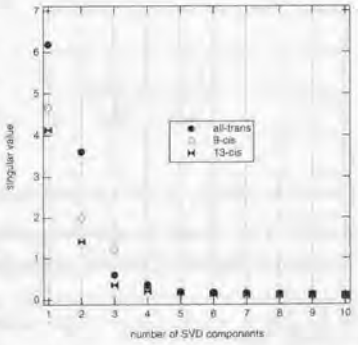

Fig. 3-6 Singular values obtained from the time-resolved spectra of the retinal isomers (Fig. 3-2 ~ 4).

Kinetics Scheme (I), $S_0 \xrightarrow[h\nu]{} S_3 \xrightarrow{\phi_3\gamma_3} S_2 \xrightarrow{\phi_2\gamma_2} S_1 \xrightarrow{\phi_1\gamma_1} T_1$.

Here it is assumed that only the $S_3 \leftarrow S_0$ transition is one-photon allowed. This is based on the results of femtosecond time-resolved fluorescence up-conversion spectroscopy performed by Takeuchi and Tahara [43]. According to their conclusion, the S_3 state of all-trans retinal is of B_u^+ (π, π^*) character and the $S_3 \leftarrow S_0$ transition contribute to about 96% of the ground-state absorption band around 370 nm. In Kinetics Scheme (I), the simplest relaxation schemes are assumed among the three excited singlet states: The S_3 state relaxes to the S_2 state with the quantum efficiency ϕ_3 and the lifetime γ_3^{-1}, S_2 to S_1 with ϕ_2 and γ_2^{-1}, and S_1 to T_1 with ϕ_1 and γ_1^{-1}. Since the maximum time delay after the photoexcitation in the present femtosecond experiments is about 100 ps, it is unnecessary to take into account the relaxation of the T_1 state [11]. According to Kinetics Scheme (I), the time-delay dependence of the population of each electronic state is expressed as follows:

$$[S_3] = e^{-\gamma_3 t}, \tag{3-2}$$

$$[S_2] = \frac{\phi_3\gamma_3}{\gamma_3 - \gamma_2}\left(e^{-\gamma_2 t} - e^{-\gamma_3 t}\right), \tag{3-3}$$

$$[S_1] = \frac{\phi_2\phi_3\gamma_2\gamma_3}{(\gamma_2 - \gamma_1)(\gamma_3 - \gamma_1)}\left(e^{-\gamma_1 t} - \frac{\gamma_3 - \gamma_1}{\gamma_3 - \gamma_2}e^{-\gamma_2 t} + \frac{\gamma_2 - \gamma_1}{\gamma_3 - \gamma_2}e^{-\gamma_3 t}\right), \tag{3-4}$$

$$[T_1] = \phi_1\phi_2\phi_3\left\{1 - \frac{\gamma_2\gamma_3 e^{-\gamma_1 t}}{(\gamma_2 - \gamma_1)(\gamma_3 - \gamma_1)} + \frac{\gamma_1\gamma_3 e^{-\gamma_2 t}}{(\gamma_2 - \gamma_1)(\gamma_3 - \gamma_2)} - \frac{\gamma_1\gamma_2 e^{-\gamma_3 t}}{(\gamma_3 - \gamma_1)(\gamma_3 - \gamma_2)}\right\}, \tag{3-5}$$

where δ-function-like photoexcitation at $t = 0$ is assumed and the S_3 population directly generated by the photoexcitation is set to be 1. All the populations are zero if $t < 0$. There is a relation among the populations of the five electronic states involved in Kinetics Scheme (I):

$$[S_0] = -[S_3] - [S_2] - [S_1] - [T_1], \tag{3-6}$$

where the S_0 population $[S_0]$ is always negative. The term "population" in this thesis stands for the difference between the population with and without photoexcitation. Though the five

electronic states are included in Kinetics Scheme (I), it is enough to take into account only four SVD components. It is because $[S_0]$ is expressed as the linear combination of the other four populations and only four populations in Eq. (3-2) ~ (3-6) are linearly independent. The number of SVD components that have to be taken into account does not always coincide with that of transient species, since all the populations of transient species are not always linearly independent just like the present case while all the temporal behaviors of SVD components have to be linearly independent.

Let us derive the populations and the spectra of the transient species (S_3, S_2, S_1, T_1) from $\{\mathbf{t}_i\}_{1\le i\le 4}$ and $\{\mathbf{s}_i\}_{1\le i\le 4}$ of the SVD components. The product of the ith singular value and the temporal evolution of the ith SVD component, $V_i\mathbf{t}_i$, is fitted to the following model function:

$$c_{i4}[S_3]+c_{i3}[S_2]+c_{i2}[S_1]+c_{i1}[T_1]\,. \tag{3-7}$$

of which the fitting parameters are γ_1, γ_2, γ_3, c_{i1}, c_{i2}, c_{i3}, c_{i4}. The parameters γ_1, γ_2, γ_3 have to be common to all the four SVD components. The quantum efficiencies, ϕ_1, ϕ_2, ϕ_3, are not determined by the fitting procedure. In the practical fitting procedure, the model function of Eq. (3-7) is convoluted with a Gaussian function which represents the instrumental response. V_i which $\mathbf{t}_i$ is multiplied by serves as a fitting weight. The relation between $\{\mathbf{t}_i\}_{1\le i\le 4}$ and the populations of the transient species is expressed by using the converged fitting parameters c_{ij} as follows:

$$\begin{pmatrix} V_1{}^t\mathbf{t}_1 \\ V_2{}^t\mathbf{t}_2 \\ V_3{}^t\mathbf{t}_3 \\ V_4{}^t\mathbf{t}_4 \end{pmatrix} = \mathbf{C}\begin{pmatrix} {}^t\mathbf{T}_{1pop} \\ {}^t\mathbf{S}_{1pop} \\ {}^t\mathbf{S}_{2pop} \\ {}^t\mathbf{S}_{3pop} \end{pmatrix}, \tag{3-8}$$

where $\mathbf{C}$ is a matrix of which the (i,j) component is c_{ij}, $\mathbf{S}_{3pop}$ is a column vector of which the ith component is the S_3 population at the ith time delay point, and so are $\mathbf{S}_{2pop}$, $\mathbf{S}_{1pop}$, $\mathbf{T}_{1pop}$. The populations of the transient species are finally recomposed from $\{\mathbf{t}_i\}_{1\le i\le 4}$ as follows:

$$\begin{pmatrix} {}^{t}\mathbf{T}_{1pop} \\ {}^{t}\mathbf{S}_{1pop} \\ {}^{t}\mathbf{S}_{2pop} \\ {}^{t}\mathbf{S}_{3pop} \end{pmatrix} = \mathbf{C}^{-1} \begin{pmatrix} V_1{}^{t}\mathbf{t}_1 \\ V_2{}^{t}\mathbf{t}_2 \\ V_3{}^{t}\mathbf{t}_3 \\ V_4{}^{t}\mathbf{t}_4 \end{pmatrix}, \tag{3-9}$$

The spectra of the transient species have to satisfy the following equation:

$$\mathbf{A} = \mathbf{S}_{3pop}{}^{t}\mathbf{S}_{3spe} + \mathbf{S}_{2pop}{}^{t}\mathbf{S}_{2spe} + \mathbf{S}_{1pop}{}^{t}\mathbf{S}_{1spe} + \mathbf{T}_{1pop}{}^{t}\mathbf{T}_{1spe}, \tag{3-10}$$

where $\mathbf{S}_{3spe}$ is a column vector and stands for the absorption spectrum of the S_3 state. The ith component of $\mathbf{S}_{3spe}$ corresponds to absorbance at the ith wavelength point, and the same for $\mathbf{S}_{2spe}$, $\mathbf{S}_{1spe}$, $\mathbf{T}_{1spe}$. By using Eq. (3-1), (3-9), (3-10), the spectra of the transient species are recomposed from $\{\mathbf{s}_l\}_{1\le l\le 4}$:

$$\begin{pmatrix} {}^{t}\mathbf{T}_{1spe} \\ {}^{t}\mathbf{S}_{1spe} \\ {}^{t}\mathbf{S}_{2spe} \\ {}^{t}\mathbf{S}_{3spe} \end{pmatrix} = {}^{t}\mathbf{C} \begin{pmatrix} {}^{t}\mathbf{s}_1 \\ {}^{t}\mathbf{s}_2 \\ {}^{t}\mathbf{s}_3 \\ {}^{t}\mathbf{s}_4 \end{pmatrix}, \tag{3-11}$$

The SVD analysis combined with the fitting procedure is summarized as follows: The SVD of the set of the spectra yields V_l, $\mathbf{s}_l$, $\mathbf{t}_l$. The temporal evolution $\mathbf{t}_l$ is fitted to the kinetics model function (Eq. (3-7)) to give $\mathbf{C}$, and finally the absorption spectra ($\mathbf{S}_{3spe}$, $\mathbf{S}_{2spe}$, $\mathbf{S}_{1spe}$, $\mathbf{T}_{1spe}$) and the populations ($\mathbf{S}_{3pop}$, $\mathbf{S}_{2pop}$, $\mathbf{S}_{1pop}$, $\mathbf{T}_{1pop}$) of the transient species are recomposed by means of Eq. (3-9) and (3-11). The most important procedure in this SVD analysis is to make a kinetics model, and the others are just routine. The primary purpose of SVD is to simplify an analysis and to remove noise.

The absorption spectra and the population changes of the transient species (S_3, S_2, S_1, T_1) of all-trans retinal in hexane recomposed from Fig. 3-2 by way of the SVD analysis are shown in Fig. 3-7 (a) ~ (h). In the actual calculations, ϕ_2 was fixed to 0.74, and ϕ_1 and ϕ_3 were put equal to unity. Note that the triplet quantum yield (which is equal to $\phi_1\phi_2\phi_3$) of all-trans retinal in hexane at room temperature is going to be determined later in this thesis to be 0.74 at room temperature. It is also shown later that ϕ_1 is equal to 1. In fact, the values of ϕ_1, ϕ_2, and ϕ_3 do not affect the time constants (γ_1, γ_2, γ_3) and the spectral band shapes at all,

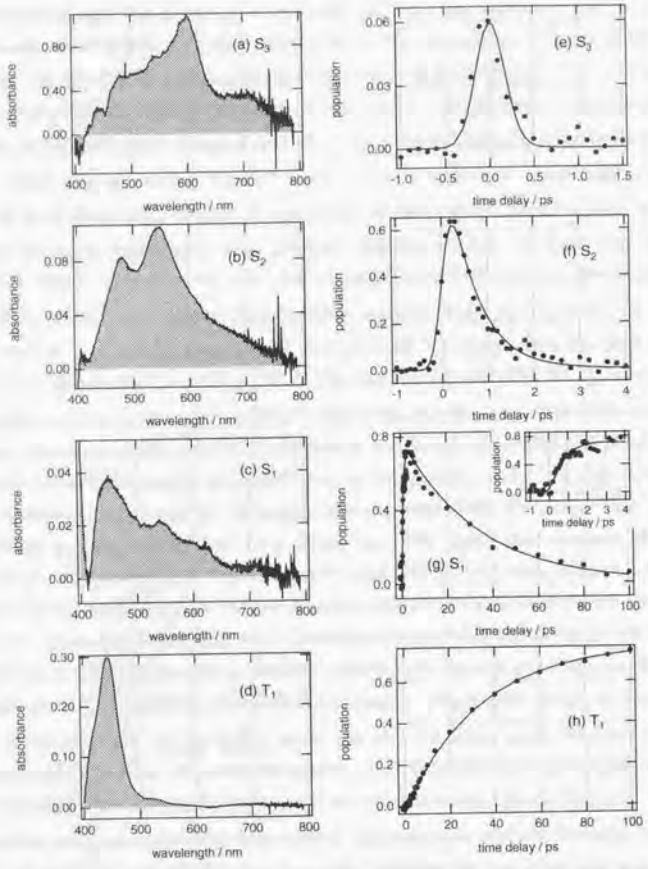

Fig. 3-7 Spectra ((a) ~ (d)) and populations ((e) ~ (h)) of the four transient species of all-trans retinal in hexane.

but only change the ratio of the magnitude of the spectra (Fig. 3-7 (a) ~ (d)) to that of the populations (Fig. 3-7 (e) ~ (h)). Nearly identical spectra and populations were also obtained in the case of all-trans retinal in cyclohexane. This means that hexane and cyclohexane provide similar environments for the excited-state dynamics of retinal. Twelve independent measurements and analyses yielded the averaged time constants and the errors (standard deviations) as summarized in Table 3-3. The rise time constant of T_1 or the S_1 lifetime, 32 ± 2 ps, is in

state	lifetime
S_3	0.03 ps (fixed)
S_2	0.75 ± 0.2 ps
S_1	32 ± 2 ps
T_1	∞ (fixed)

Table 3-3 Excited-state lifetimes of all-trans retinal in hexane at 293 ± 2 K obtained from the femtosecond time-resolved VIS absorption data.

good agreement with the reported values [10, 23, 24]. The spectrum in Fig. 3-7 (d) is identical with the known $T_n \leftarrow T_1$ absorption spectrum of all-trans retinal in nonpolar solvents [10, 12, 15, 16, 25, 48]. It is thus confirmed that the population in Fig 32 (h) is regarded as the temporal evolution of the T_1 all-trans isomer. The transient species showing the population in Fig. 3-7 (g) is assigned to S_1 all-trans retinal, because it is the precursor of T_1 all-trans retinal. The spectrum in Fig. 3-7 (c) corresponds to the $S_n \leftarrow S_1$ absorption spectrum, though the band shape looks strange. It will be shown later that the main band of the $S_n \leftarrow S_1$ absorption lies in the wavelength range 350 nm ~ 400 nm, and only the band edge appears in Fig. 3-7 (c). The S_2 lifetime or the rise time constant of S_1, 0.73 ± 0.2 ps, determined in the present study (Table 3-3) is shorter than the value reported in my previous letter (1.2 ps) [25] and that recently reported by Larson et al. (1.8 ps) [42], but longer than that determined by Takeuchi and Tahara (0.37 ± 0.02 ps) [43]. The discrepancy between the S_2 lifetime in the present study and that in my previous letter is due to the fact that only three SVD components were taken into account previously [25] because of a relatively lower signal to noise ratio and a narrower wavelength range measured than in the present study. An exponential time constant is strongly influenced by the number of components [49]. The author believe that the present value is more reliable than the previous one. The longer time constant obtained by Larson et al. was probably brought about by their method of data analysis [42]: They performed fitting procedures for several transient absorption data of different wavelengths without any constraint of time constants. Consequently they obtained different time constants from converged fitting parameters at different wavelengths for one physical process. The rise time constant of T_1 which they obtained, for example, ranged from 24 ps to 45 ps. In the present SVD analysis, on the other hand, one rise or decay time constant definitely corresponds to one lifetime of a transient species. The SVD analysis is essentially superior to their data-analysis method which seems to be nevertheless more popular [54]. The S_2 lifetime in the present study and that in the fluorescence up-conversion study by Takeuchi and Tahara [43] do not perfectly coincide even if the experimental errors are taken into account. Any clear idea for this discrepancy has not yet been figured out. The transient species exhibiting the spectrum in Fig. 3-7 (b) and the population in Fig. 3-7 (f) is the precursor of S_1 all-trans retinal and is naturally assigned to the S_2 all-trans isomer. The broad absorption bands in the subpicosecond time region in Fig. 3-2 is due to principally the $S_n \leftarrow S_2$ absorption spectrum. The S_2 rise time or the S_1 lifetime is too short to be determined by the present analysis. It is fixed to the value, 0.03 ps, reported by Takeuchi and Tahara [43]. This means that there is no clear evidence in the present study that the S_2 state is generated only from the S_1 state, as assumed in Kinetics Scheme (I). There remains a possibility that some portion of the S_2 population is directly generated by the photoexcitation. The spectrum in Fig. 3-7 (a) is assigned to the $S_n \leftarrow S_1$ absorption spectra. The small downward band at wavelength 454 nm

in Fig. 3-7 (a) is due to the impulsive stimulated Raman gain signal assigned to the CH stretching modes of hexane. The Raman gain process is also instantaneous in the present time resolution and has the same temporal evolution as that of the S_3 population. Two possibilities are considered for the negative signals around 407 nm in Fig. 3-7 (a); the ground-state bleaching or the stimulated emission gain. The former is possible in the wavelength range 400 nm ~ 430 nm. Since it has been revealed that the S_1 state is fluorescent [43], the stimulated emission gain is also possible in the wavelength range 400 nm ~ 450 nm. It will be shown later in the femtosecond time-resolved UV spectra that negative signals due to the ground-state bleaching is not so large in the wavelength range longer than 400 nm. Therefore the stimulated emission gain is more likely than the bleaching.

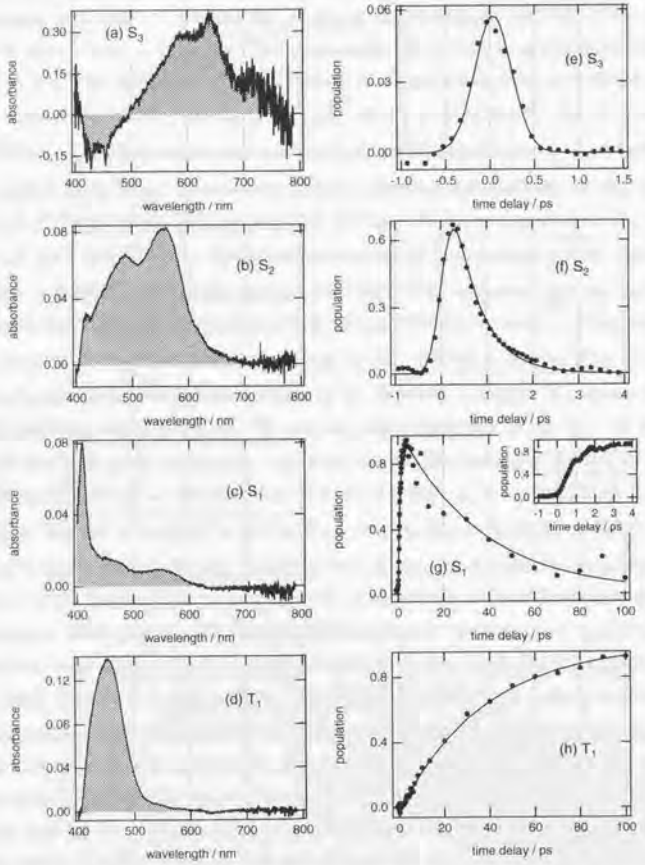

Fig. 3-8 Spectra ((a) ~ (d)) and populations ((e) ~ (h)) of the four transient species of 9-cis retinal in hexane.

The time-resolved VIS absorption spectra of 9-cis retinal in hexane (Fig. 3-3) were also successfully analyzed in the same way based on Kinetics Scheme (I). The absorption spectra and the populations of the transient species (S_3, S_2, S_1, T_1) of 9-cis retinal recomposed from Fig. 3-3 by way of the SVD analysis are shown in Fig. 3-8 (a) – (h). In the analysis, ϕ_1, ϕ_2, and ϕ_3 were all put equal to unity on trial, because the main pathway of the 9-cis → all-trans photoisomerization reaction lies on the adiabatic potential surface of T_1 [11] and no isomerization reaction pathway has been found in the singlet manifold. Independent five measurements and analyses yielded the averaged time constants and the errors (standard deviations) summarized in Table 3-4. The spectrum in Fig. 3-8 (d) is nearly identical with the $T_n \leftarrow T_1$ absorption spectrum of 9-cis retinal in degassed hexane at 100 ps after the photoexcitation reported by Hirata et al. [10]. As mentioned above, the T_1 species just generated from an excited singlet state has the 9-cis configuration when S_0 9-cis retinal is the starting isomer [11]. Then, the transient species showing the spectrum in Fig. 3-8 (d) is assigned to T_1 9-cis retinal. The population in Fig. 3-8 (h) is regarded as the temporal evolution of the T_1 9-cis isomer. The rise time constant of T_1 9-cis retinal is 34 ± 4 ps (Table 3-4) which is determined exactly for the first time. The transient species showing the population in Fig. 3-8 (g) is assigned to S_1 9-cis retinal, because its decay corresponds well to the rise of the T_1 9-cis isomer. The spectrum in Fig. 3-8 (c) is assigned to the $S_n \leftarrow S_1$ absorption spectrum of 9-cis retinal. Hirata et al. observed a similar absorption band and suggested the same assignment [10]. The present peak wavelength of the $S_n \leftarrow S_1$ absorption band, 410 nm, is in good agreement with their result. The transient species showing the population in Fig. 3-8 (f) is the precursor of S_1 9-cis retinal as recognized from the inset of Fig. 3-8 (g). Then, it is assigned to the S_2 9-cis isomer. The S_2 lifetime or the S_1 rise time constant of 9-cis retinal is 0.72 ± 0.2 ps (Table 3-4). It was found in the fitting procedures that the lifetime of the fastest transient species of 9-cis retinal was much shorter than the present time resolution. Since any other femtosecond time-resolved spectroscopic experiments of 9-cis retinal has never been performed so far, it is necessary to assume that the transient species of the shortest lifetime is S_2 9-cis retinal. The S_2 lifetime of the 9-cis isomer was fixed to be 0.03 ps throughout the fitting procedures as shown in Table 3-4 in correspondence with that of the all-trans isomer. The spectrum in Fig. 3-8 (a) is assigned to the $S_n \leftarrow S_0$ absorption spectrum of 9-cis retinal. The small downward band at wavelength 454 nm and that at 427 nm in Fig. 3-8 (a) are the impulsive stimulated Raman gain signals assigned to the CH stretching modes of hexane and the C=C stretching mode of S_0 9-cis retinal respectively. The

state	lifetime
S_2	0.03 ps (fixed)
S_1	0.72 ± 0.2 ps
S_1	34 ± 4 ps
T_1	∞ (fixed)

Table 3-4 Excited-state lifetimes of 9-cis retinal in hexane at 293 ± 2 K obtained from the femtosecond time-resolved VIS absorption data.

negative signals in the wavelength range 400 nm ~ 490 nm in Fig. 3-8 (a) probably correspond to the stimulated emission gain rather than the ground-state bleaching. The fluorescence spectrum of 9-cis retinal in nonpolar solvents has never been reported, but it has already been shown that the solid film of 9-cis retinal exhibited a fluorescence spectrum similar to that of all-trans retinal [55]. Therefore, the stimulated emission gain of 9-cis retinal is possible in the wavelength range 400 nm ~ 490 nm while the ground-state bleaching is expected only in the wavelength range shorter than 420 nm.

In the case of the time-resolved VIS absorption spectra of 13-cis retinal (Fig. 3-4), the SVD analysis based on Kinetics Scheme (I) was not successful because of the lower signal to noise ratio. It was impossible to obtain a unique S_1 spectrum. It is likely that Kinetics Scheme (I) is not applicable to 13-cis retinal. Instead the curves of time-delay dependence of absorbance at several wavelengths were derived from the spectra in Fig. 3-4 and are shown in Fig. 3-9 (a) ~ (d). The fast decay in the subpicosecond time range at 500 nm ~ 600 nm (Fig. 3-9 (b) ~ (d)) probably corresponds to the deactivation of the excited singlet states. The obtained decay time constants varied from 0.3 ps to 3 ps. The gradual increase of absorbance in the time range 10 ps ~ 50 ps at 450 nm (Fig. 3-9 (a)) corresponds to the rise of the T_1 population. The time constant of the T_1 rise was about 12 ps which is definitely shorter than that of the all-trans and 9-cis isomers (Table 3-3, 4). Therefore, it is highly likely that the absorption signals of the excited singlet and triplet states in Fig. 3-4 and Fig. 3-9 are primarily due to the 13-cis isomer. There is no evidence for any contribution of the other isomers to the spectra in Fig. 3-4 within the present experimental accuracy.

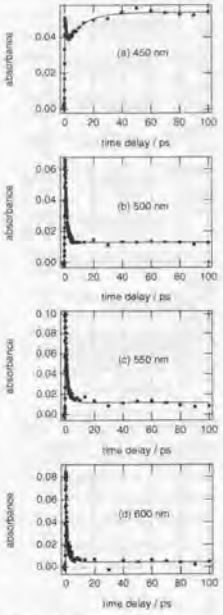

Fig. 3-9 Transient absorbance of 13-cis retinal in hexane at several wavelengths.

3-1-3-2. Femtosecond time-resolved UV absorption spectra

Fourteen representative femtosecond time-resolved UV absorption spectra of all-trans retinal in hexane at 298 K are shown in Fig. 3-10. The femtosecond time-resolved absorption spectra in the near UV region were measured for the first time to the best of my knowledge. Since the ground-state absorption bands of all-trans retinal exist in this wavelength range 310 nm ~ 390 nm, negative signals due to the ground-state bleaching dominated the spectra of Fig. 3-10. The bleaching band shape at 100 ps after the photoexcitation is in agreement with that measured by Veyret et al. with nanosecond time-resolution [16]. In the time range 0.6 ps ~ 20 ps, positive signals were observed in the

wavelength range longer than 370 nm. Similar measurements were performed with the hexane solutions of all-trans retinal at 273 K and 269 K and the cyclohexane solution at 293 K. The femtosecond UV absorption spectra in cyclohexane at 293 K were nearly identical with those in hexane at 298 K. This once again confirms our idea that hexane and cyclohexane give similar environments for all-trans retinal in the electronic excited states. The time-resolved UV spectra at 269 K are shown in Fig. 3-11. The features of the absorption bands in Fig. 3-11 are the same as those in Fig. 3-10.

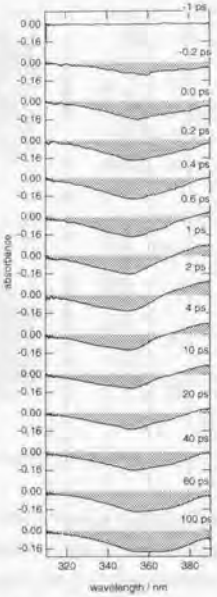

Fig. 3-10 Femtosecond time-resolved UV absorption spectra of all-trans retinal in hexane at 298 K.

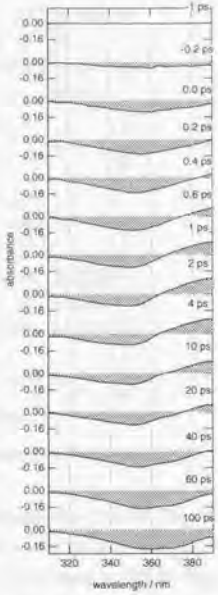

Fig. 3-11 Femtosecond time-resolved UV absorption spectra of all-trans retinal in hexane at 269 K.

The SVD analysis of the femtosecond time-resolved UV absorption spectra was performed in order to clarify transient species appearing in the spectra and the temperature dependence of the kinetics parameters. The two series of the singular values thus derived from the spectra in Fig. 3-10 and 11 are shown in Fig. 3-12. Both of them clearly indicate that two SVD components should be taken into account. The third and higher SVD components were disregarded. In the previous section, the time-resolved VIS absorption spectra of all-trans retinal have been successfully interpreted in terms of Kinetics Scheme (I). The five transient species of which four are linearly independent are involved in Kinetics Scheme (I). It is now necessary to identify the two transient species that contribute to the time-resolved UV spectra. One is definitely the S_0 state, because the negative signals in Fig. 3-10 and 11 must be due to the ground-state bleaching. The other is most likely to be the S_1 state which has a 32-ps

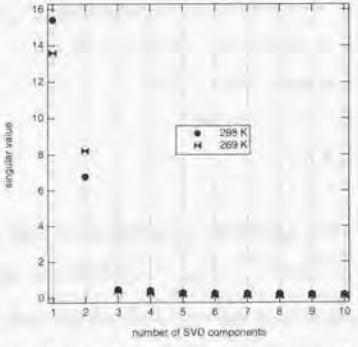

Fig. 3-12 Singular values obtained from the time-resolved UV spectra of all-trans retinal at 298 K and 269 K of Fig. 3-10 and 11 respectively.

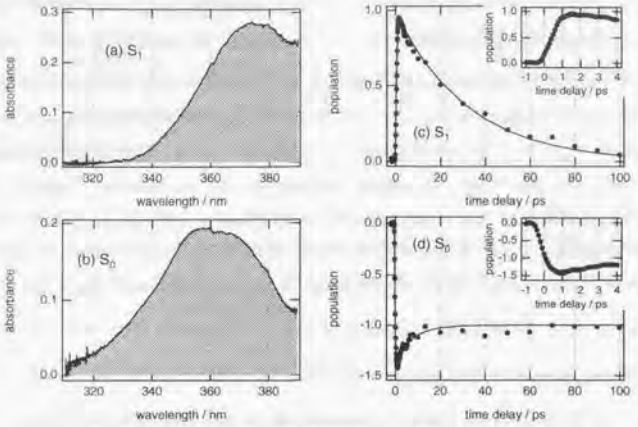

Fig. 3-13 Spectra ((a), (b)) and populations ((c), (d)) of the two transient species obtained from the time-resolved UV spectra of all-trans retinal in hexane at 298 K.

lifetime that corresponds to the observed positive signals. By using the sum of single-exponential functions for the fitting procedures, the absorption spectra and the populations of the two transient species were recomposed from the time-resolved UV spectra at 298 K (Fig. 3-10) by way of the SVD analysis and are shown in Fig. 3-13 (a) ~ (d). It was found in the actual fitting procedures that a new rate constant γ_p which did not appear in Kinetics Scheme (I) was necessary while γ_3 was unnecessary. The kinetics equations of the two transient species were finally reduced to the following simple forms:

$$f_{S1}(t) = e^{-\gamma_1 t} - e^{-\gamma_2 t}, \tag{3-12}$$

$$f_{S0}(t) = -1 - Ae^{-\gamma_p t}, \tag{3-13}$$

The population of Fig 38 (c) and that of Fig. 3-13 (d) correspond to Eq. (3-12) and (3-13) respectively. The averaged values of the three time constants (γ_2^{-1}, γ_1^{-1}, γ_p^{-1}) and the parameter A with their errors (standard deviations) were obtained from the eight independent measurements of all-trans retinal in hexane as follows: $\gamma_2^{-1} = 0.56 \pm 0.05$ ps, $\gamma_1^{-1} = 31 \pm 3$ ps, $\gamma_p^{-1} = 7.2 \pm 2$ ps, $A = 0.36 \pm 0.08$. The value of γ_1^{-1} is in good agreement with the S_1 lifetime (Table 3-3) obtained from the preceding femtosecond time-resolved VIS absorption measurements. The value of γ_2^{-1} is shorter than the S_2 lifetime determined in the preceding

measurements (0.73 ± 0.2 ps), but there is overlap between them when the errors are taken into account. The S_1 population $[S_1]$ (Eq. (3-4)) can be reduced to $f_{S1}(t)$ (Eq. (3-12)) because the lifetime of S_3 is much shorter than that of S_2. Therefore, the transient species showing the spectrum of Fig. 3-13 (a) and the population of Fig. 3-13 (c) is assigned to the same S_1 all-trans isomer as that identified in the VIS spectra. As seen from Fig. 3-13 (a), a strong $S_0 \leftarrow S_1$ absorption band is located in the wavelength range 360 nm ~ 390 nm. The negative population in Fig. 3-13 (d) is ascribed to the ground-state bleaching. Though the instantaneous decrease of the S_0 population in the inset of Fig. 3-13 (d) is consistent with the depletion of the S_0 all-trans isomer by the photoexcitation, its recovery with the time constant of 7.2 ps ($= \gamma_p^{-1}$) has to be accounted for. The S_0 population $[S_0]$ of Eq. (3-6) is not reduced to $f_{S0}(t)$ of Eq. (3-13) which includes γ_p. The most simple and reasonable modification of Kinetics Scheme (I) is to assume that an intermediate of which the lifetime is γ_p^{-1} exists and it exclusively decays to S_0. The symbol p* is hereafter used to designate this intermediate. As discussed later, the p* state is considered to be the "perpendicular excited singlet state" which plays an essential role in the process of isomerization. Either the S_3 or S_2 state can be the precursor of p*, since the lifetime of p* is longer than that of S_3 and S_2 but shorter than that of S_1 and T_1. First, let us assume that S_2 is the precursor of p*. This is to assume that the isomerization proceeds from the S_2 state. Then, we need to add to Kinetics Scheme (I) an extra relaxation pathway of the S_2 state:

Kinetics Scheme (II), $S_0 \xrightarrow[h\nu]{} S_3 \xrightarrow{\gamma_3} S_2 \xrightarrow{\phi_2\gamma_2} S_1 \xrightarrow{\gamma_1} T_1$

$$S_2 \xrightarrow{(1-\phi_2)\gamma_2} p^* \xrightarrow{\gamma_p} S_0.$$

The S_3, S_2, S_1, and T_1 populations in Kinetics Scheme (II) are the same as those in Kinetics Scheme (I) (Eq. (3-2) ~ (3-5)) with the condition $\phi_1 = \phi_3 = 1$. The population of p* and that of S_0 in Kinetics Scheme (II) are written as follows:

$$[p^*] = \frac{(1-\phi_2)\gamma_2\gamma_3}{(\gamma_2-\gamma_p)(\gamma_3-\gamma_p)}\left(e^{-\gamma_p t} - \frac{\gamma_3-\gamma_p}{\gamma_3-\gamma_2}e^{-\gamma_2 t} + \frac{\gamma_2-\gamma_p}{\gamma_3-\gamma_2}e^{-\gamma_3 t}\right). \tag{3-14}$$

$$[S_0] = -[S_3] - [S_2] - [S_1] - [T_1] - [p^*]. \tag{3-15}$$

Eq. (3-15) is reduced to Eq. (3-13) on the condition that $\gamma_3 >> \gamma_p$ and $\gamma_2 >> \gamma_p$ that are really satisfied. We also have a relation between ϕ_2 and A as follows::

$$\phi_2 = \frac{1}{1+A} . \tag{3-16}$$

Secondly, when S_3 is assumed to be the precursor of p*, Kinetics Scheme (I) is modified in the similar way as follows:

Kinetics Scheme (III), $S_0 \xrightarrow[h\nu]{} S_3 \xrightarrow{\phi_3\gamma_3} S_2 \xrightarrow{\gamma_2} S_1 \xrightarrow{\gamma_1} T_1$

$$S_3 \xrightarrow{\left(1-\phi_3\right)\gamma_3} p^* \xrightarrow{\gamma_p} S_0 .$$

The S_3, S_2, S_1, and T_1 populations in Kinetics Scheme (III) are the same as those in Kinetics Scheme (I) with the condition $\phi_1 = \phi_2 = 1$. The S_0 population in Kinetics Scheme (III) is also written as Eq. (3-15). The population of p* in Kinetics Scheme (III) is written as follows:

$$[p^*] = \frac{\left(1-\phi_3\right)\gamma_3}{\gamma_3 - \gamma_p}\left(e^{-\gamma_p t} - e^{-\gamma_3 t}\right), \tag{3-17}$$

By substituting Eq. (3-17) for Eq. (3-15) and using the realized condition $\gamma_3 >> \gamma_p$, Eq. (3-15) is again reduced to Eq. (3-13), and the following equation is obtained:

$$\phi_3 = \frac{1}{1+A} . \tag{3-18}$$

The SVD analysis which yielded Fig. 3-13 (a) ~ (d) can be based on either Kinetics Scheme (II) or (III). Note that the parameter A of $f_{S0}(t)$ (Eq. 35) determines the quantum yield of S_1, T_1, and p* in both Kinetics Scheme (II) and (III). The S_1 and T_1 quantum yields are given by $\frac{1}{1+A}$, and that of p* is given by $\frac{A}{1+A}$. There is no $S_1 \rightarrow S_0$ relaxation pathway ($\phi_1 = 1$) as indicated by the constant S_0 population for $t > 20$ ps in Fig. 3-13 (d).

The femtosecond time-resolved UV absorption spectra of all-trans retinal at 293 K, 273 K, and 269 K (Fig. 3-11) were also analyzed in the same way except for the following point: It was found in the actual fitting procedures that γ_p was almost independent of temperature while A was not. Both γ_p and A were determined by a small fraction of the data in the time range 0 ps ~ 20 ps (see Fig. 3-13 (d)), and it was not possible to determine these two quantities simultaneously with small uncertainties. Therefore, γ_p^{-1} was fixed at 7.2 ps throughout these analyses in order to determine the temperature dependence of A as exact as possible. The spectra and the populations of S_1 and S_0 at 269 K obtained by way of the SVD analysis are shown in Fig. 3-14. It is noticed that the data were fitted well for S_0 even with γ_p fixed. The S_1 decay in Fig. 3-14 (c) is slower than that in Fig. 3-13 (c). The amount of the S_0 recovery in Fig. 3-14 (d) is smaller than that in Fig. 3-13 (d). The averaged values of γ_2^{-1}, γ_1^{-1}, and A with their errors (standard deviations) obtained from several independent measurements at each temperature are summarized in Table 3-5. The temperature dependence of the quantum yield derived from the parameter A in Table 3-5 will be discussed later.

temperature / K	S_2 lifetime / ps	S_1 lifetime / ps	A
298	0.56 ± 0.05	31 ± 3	0.36 ± 0.08
293	0.47 ± 0.05	31 ± 1	0.29 ± 0.04
273	0.53 ± 0.05	42 ± 2	0.21 ± 0.01
269	0.49 ± 0.02	42 ± 1	0.18 ± 0.02

Table 3-5 Converged fitting parameters in the analyses of the femtosecond time-resolved UV absorption spectra of all-trans retinal in aerated nonpolar solvents at four different temeperatures.

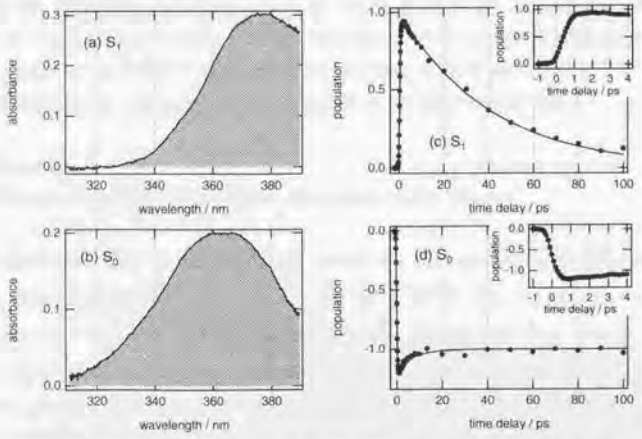

Fig. 3-14 Spectra ((a), (b)) and populations ((c), (d)) of the two transient species obtained from the time-resolved UV spectra of all-trans retinal in hexane at 269 K.

3-1-3-3. Nanosecond time-resolved UV absorption spectra

The nanosecond time-resolved UV absorption spectra of all-trans retinal in cyclohexane are shown in Fig. 3-15. The dominant negative signals are ascribed to the ground-state bleaching. The bleaching recovery in the nanosecond time region corresponds to the $T_1 \rightarrow S_0$ decay. The T_1 lifetime of all-trans retinal in aerated cyclohexane is obtained from the present nanosecond spectra as 74 ns which is in good agreement with the nanosecond CARS data [11] and is about hundred times shorter than that in degassed nonpolar solvents (5 ~ 10 μs) [15, 22]. The bleaching band shape in Fig. 3-15 is nearly identical with that in femtosecond UV spectrum at 100 ps (Fig. 3-10, 11).

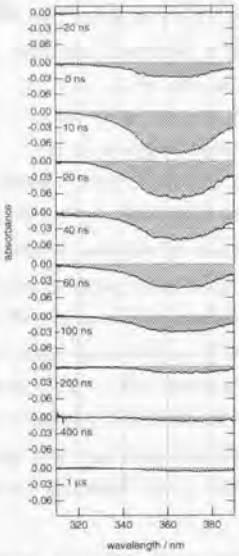

Fig. 3-15 Nanosecond time-resolved UV absorption spectra of all-trans retinal in cyclohexane.

No population of T_1 all-trans retinal in aerated cyclohexane is expected at 1 μs after the photoexcitation. Nevertheless the time-resolved absorption spectrum at 1 μs in Fig. 3-15 slightly deviates from zero in the longer wavelength range 350 nm ~ 390 nm. It is due to the all-trans → 13-cis·9-cis photoisomerization. In fact, the spectrum at 1 μs in Fig. 3-15 is in good agreement with the difference spectrum between the molar absorption spectra of the S_0 13-cis and all-trans isomers. It is unnecessary to take account of 9-cis retinal for calculating the difference molar absorption spectrum, because the ground-state absorption spectrum of 13-cis retinal is nearly identical with that of 9-cis retinal and the quantum yield of the 13-cis isomer is about 5 ~ 10 times larger than that of the 9-cis isomer (Table 3-1). The absorption spectrum at 1 μs in Fig. 3-15 is regarded as the photoproduct band.

3-1-4. Discussion

3-1-4-1. Comparison of the excited-state absorption of the isomers

Considering both all-trans and 9-cis retinal, the correspondence between the T_1 rise and the S_1 decay and that between the S_1 rise and the S_2 decay were simultaneously found in the femtosecond time-resolved VIS absorption spectra for the first time. The S_1 temporal evolution of all-trans retinal was confirmed also in the femtosecond time-resolved UV absorption spectra. These findings strongly support Kinetics Scheme (I). However the correspondence between the S_2 rise and the S_1 decay was not confirmed exactly because of insufficient time resolution. It was impossible to determine the S_1 lifetime from the present

measurements. It is admitted that the assignment of S_3 is less unequivocal than that of S_2, S_1, and T_1. There may be some other plausible interpretations. The most important one is probably that the species of the shortest lifetime, that is, what is assigned to S_3 above, is ascribed to the vibrationally excited S_2 state (S_2*). However this particular interpretation is rejected for the following three reasons: One is that all the transient species in the all-trans and 9-cis isomers have the distinct absorption spectra, though it is expected that vibrational excitation brings about only broadening and/or vibrational structures of an absorption band [56-58]. The second is that there is possibly no substantial Franck-Condon overlapping between S_0 and S_2, and accordingly substantial vibrational excitation is not expected to be brought about by the photoexcitation of S_0. It is because any vibrational structure has never been observed in the UV-VIS absorption and fluorescence spectra of retinal even at low temperature [29-32, 59, 60]. In the last place, it is unlikely that the vibrationally excited S_2 band of 9-cis retinal is located energetically below that of all-trans retinal by as much as 1000 cm^{-1} which corresponds to the difference between the two peak wavelengths of the spectra of Fig. 3-7 (a) and 8 (a). It is noted that the S_2 band of 9-cis retinal is located at nearly the same energy as that of all-trans retinal (Fig. 3-7 (b), 8 (b)). Accordingly it is very likely that the transient species of the shortest lifetime in all-trans and 9-cis retinal is assigned to the S_3 state which is the precursor of S_2.

Some general correspondence between the transient species of all-trans retinal and those of 9-cis retinal was found. Especially the S_2 and S_1 lifetimes of all-trans retinal (Table 3-3) approximately coincide with those of 9-cis retinal (Table 3-4). It is also pointed out that the $S_n \leftarrow S_3$ and $S_n \leftarrow S_2$ absorption spectra of both of the isomers are similar (Fig. 3-7 (a), (b), 8 (a), (b)). This correspondence is probably ascribed to the fact that the all-trans and 9-cis isomers have similar excited electronic structures. Then it is natural to consider that the corresponding excited states of the all-trans and 9-cis isomers are of the nearly same character. However the symbols A_g and B_u should not be used for characterizing the excited states of 9-cis retinal even in an approximate meaning, because the 9-cis isomer is never of C_{2h} symmetry but of only C_s symmetry even if the cyclohexene ring, the carbonyl group, and the methyl groups are all neglected. Kinetics Scheme (I) was originally made on the assumption that the S_3 state of all-trans retinal is of B_u^+ (π, π^*) character which has recently been verified by femtosecond time-resolved fluorescence up-conversion spectroscopy [43]. It is likely that the S_3 state of 9-cis retinal corresponds to the S_3 all-trans isomer of B_u^+ (π, π^*) character because of the similarity of the absorption bands and the temporal behaviors. The other two remaining, namely A_g^- (π, π^*) and (n, π^*) are assigned to S_2 and S_1. The coincidence of the S_2 and S_1 lifetimes in the two isomers can help the characterization of these states. The S_2 and S_1 lifetimes are primarily determined by the rate of the $S_2 \rightarrow S_1$ internal

conversion process and that of the $S_1 \rightarrow T_1$ intersystem crossing process respectively. It has been shown by an electron spin echo experiment that the T_1 state of all-trans retinal is of (π, π^*) character [61]. Since the $T_n \leftarrow T_1$ absorption spectrum of 9-cis retinal (Fig. 3-8 (d)) is very similar to that of all-trans retinal (Fig. 3-7 (d)), it is probable that the T_1 state of 9-cis retinal is also of (π, π^*) character. The $S_1 \rightarrow T_1$ intersystem crossing in all-trans and 9-cis retinal is presumed to be a direct process of $^1(n, \pi^*) \rightarrow {}^3(\pi, \pi^*)$, because it is unlikely that a $^1(\pi, \pi^*) \rightarrow {}^3(\pi, \pi^*)$ process which is only induced by vibronic coupling brings about the nearly equal rise time constants of T_1 for the all-trans (31 ps) and 9-cis (34 ps) isomers. A $^1(n, \pi^*) \rightarrow {}^3(\pi, \pi^*)$ process is more tenable to account for the similar temporal evolution of T_1, because all-trans and 9-cis retinal are expected to have a similar structure as regards the C_{10}-C_{11}=C_{12}-C_{13}=C_{14}-C_{15}=O part which strongly influences the overlap between the non-bonding and π orbitals. Therefore it is likely that the S_1 state is of (n, π^*) character in both of the isomers, and consequently the S_2 state is of A_g^- (π, π^*) character in the all-trans isomer and of (π, π^*) character in the 9-cis isomer. Note that the experimental fact that all-trans retinol (vitamin A) which has no nonbonding electrons has a much lower T_1 quantum yield (0.03) [62] than all-trans retinal (0.74 in the present study) also suggests that the S_1 state which is the precursor of T_1 is of (n, π^*) character.

In the analysis of the femtosecond VIS absorption spectra of all-trans retinal (Fig. 3-2), Kinetics Scheme (I) starts from the S_0 state with the all-trans configuration and ends with the T_1 state having the same configuration. It is therefore natural to assume that the three excited singlet states also have the all-trans configuration. In order to check whether other cis excited states are involved in the all-trans VIS spectra as minor components, the products of the spectra and the populations of the S_3, S_2, S_1, and T_1 states (Fig. 3-7) were subtracted from the raw all-trans VIS spectra (Fig. 3-2). The resultant residual spectra are shown in Fig. 3-16. There are no meaningful bands in the residual spectra. Especially any transient absorption bands observed in the 13-cis VIS spectra (Fig. 3-4) never appear in the residual spectra. The residual spectra show that the femtosecond time-resolved VIS absorption spectra of all-trans retinal were fully explained by Kinetics Scheme (I). This means that no 13-cis excited-state species as a photoisomerization product is observed in the all-trans VIS spectra. It is concluded that an all-trans $\rightarrow$ 13-cis·9-cis

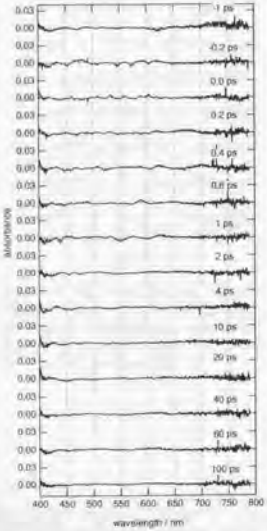

Fig. 3-16 Residual spectra of all-trans retinal in hexane at various time delays obtained by subtracting the contribution of the four transient species in Fig. 3-7 from the raw spectra in Fig. 3-2.

photoisomerization reaction pathway which is complete in the electronic excited states was not found within the present experimental accuracy. It is possible to estimate this accuracy as follows: The standard deviation of the residual spectrum at each time delay was calculated at about 0.002. The S - S absorption peak coefficient of 13-cis or 9-cis retinal at 0 ps ~ 0.6 ps in the present condition is about 0.07 (Fig. 3-3, 4). Then the possible maximum total quantum yield of the all-trans → 13-cis·9-cis isomerization reaction which is complete in the excited singlet states is the ratio of 0.002 to 0.07, that is, 0.03. Note that the all-trans → 13-cis·9-cis total quantum yield is about 0.12 (Table 3-1). It is necessary to figure out another reaction mechanism that is not complete in the excited singlet states.

The residual spectra of 9-cis retinal were obtained in the same way as those of all-trans retinal and are shown in Fig. 3-17. The residual spectra show that the 9-cis VIS spectra (Fig. 3-3) was fully explained by Kinetics Scheme (I). Only the transient species of the 9-cis configuration are included in Kinetics Scheme (I) applied to 9-cis retinal. Nothing like the transient absorption bands observed in the all-trans VIS spectra (Fig. 3-2) appears in the 9-cis residual spectra. Therefore, it is concluded that a 9-cis → all-trans photoisomerization reaction pathway which produces all-trans species in the electronic excited singlet states was not found within the present experimental accuracy. The accuracy can be estimated in the same way as just above. The standard deviation of the residual spectrum of 9-cis retinal at each time delay was calculated at about 0.002. The S - S absorption peak coefficient of all-trans retinal at 0 ps ~ 0.5 ps in the present condition is about 0.1 (Fig. 3-2). Then the possible maximum quantum yield of the 9-cis → all-trans isomerization reaction which is complete in the excited singlet states is the ratio of 0.002 to 0.1, that is, 0.02. Since the 9-cis → all-trans quantum yield is about 0.2 (Table 3-1), the possible contribution of this particular singlet mechanism to the total 9-cis → all-trans quantum yield is less than 10%.

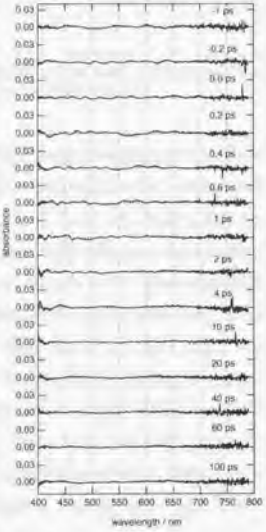

Fig. 3-17 Residual spectra of 9-cis retinal in hexane at various time delays obtained by subtracting the contribution of the four transient species in Fig. 3-8 from the raw spectra in Fig. 3-3.

3-1-4-2. Photoisomerization reaction scheme

The intermediate p* was introduced in Kinetics Scheme (II) or (III) to understand the femtosecond UV data. The precursor of p* can be either the S_1 or S_2 states of all-trans retinal,

and p* decays exclusively to S_0. The most evident assignment for p* is to the perpendicular excited singlet state as schematically shown in Fig. 3-18. The isomerization scheme in Fig. 3-18 is based on Kinetics Scheme (II) or (III), and they are compatible with each other as shown later in this section. All-trans retinal in nonpolar solvents undergoes isomerization to both the 13-cis and 9-cis isomers. Therefore, strictly speaking, two different perpendicular configurations of which one is twisted about the C_{13}=C_{14} double bond and the other about the C_9=C_{10} double bond should be considered. However it is sufficient to assume only the former perpendicular state because (i) the 13-cis quantum yield is about 5 ~ 10 times higher than the 9-cis quantum yield, and (ii) the signal to noise ratio in the present femtosecond time-resolved UV absorption data is not sufficient to assume two different perpendicular states with different lifetimes. Therefore, the isomerization scheme in Fig. 3-18 does not distinguish the 13-cis and 9-cis isomers. The reaction mechanism in the scheme is then the same as the trans → cis photoisomerization mechanism of stilbene. The p* state decays to the perpendicular ground state, p, and p is deactivated to give the trans and cis isomers in the ground state in an equal ratio. The decay rate of p is assumed to be much larger than that of p*, $(7.2\ \text{ps})^{-1}$. The lifetime of the perpendicular excited singlet state of stilbene is thought to be much shorter than a picosecond [26, 63, 64] while that of trans-1, 1'-biindanylidene (stiff stilbene) is about 10 ps [65]. The excited singlet state of tetraphenylethylene, for which the perpendicular configuration is confirmed by nanosecond time-resolved Raman spectroscopy [66], has a lifetime of 3 ns [67]. The 7-ps lifetime of the p* state of retinal is well in the range of the reported lifetimes of the excited singlet perpendicular states of olefins.

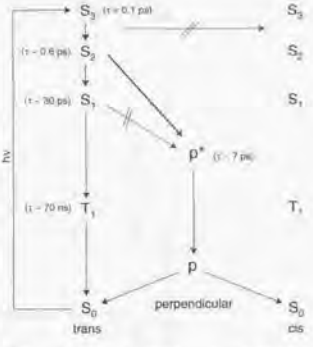

Fig. 3-18 All-trans → mono-cis photoisomerization reaction scheme of retinal in aerated nonpolar solvents.

According to the scheme in Fig. 3-18, the total quantum yield of the all-trans → 13-cis·9-cis photoisomerization of retinal can be derived from the femtosecond UV absorption data as follows:

$$\phi_{tm} = \frac{1}{2} \cdot \frac{A}{1+A} \quad , \tag{3-19}$$

where ϕ_{tm} is the total quantum yield and A is the parameter in Eq. (3-13) representing the S_0 population change. Note that ϕ_{tm} is half of the quantum yield of p*. The temperature dependence of the all-trans → 13-cis·9-cis photoisomerization total quantum yield is obtained from Eq. (3-19) and Table 3-5, and is shown in Fig. 3-19. The total quantum yields upon

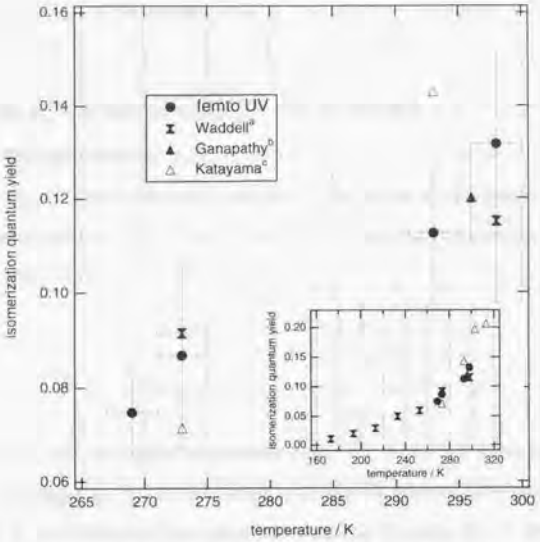

Fig. 3-19 Temperature dependence of all-trans → 13-cis·9-cis photoisomerization total quantum yield obtained from the femtosecond UV data.
HPLC-determined quantum yield values upon direct photoexcitation are together shown. In the inset, the temeperature range is extended. a) Ref. [17], b) Ref. [7], c) Ref. [20].

direct photoexcitation measured by means of HPLC [7, 17, 20] are also together shown in Fig. 3-19. It is noted that the quantum yield in the temperature range lower than 260 K have been given only by Waddell and Chihara [17], and the data of Katayama are due to supplementary experiments performed in our group [20]. The total quantum yields at the four temperature points obtained in the present time-resolved spectroscopic measurements agree well with the literature values by HPLC. This agreement strongly supports the present isomerization scheme in Fig. 3-18.

Both of Kinetics Scheme (II) and (III) give the same isomerization quantum yield or Eq. (3-19). This means that we cannot unequivocally determine the isomerization pathway solely from the present femtosecond UV data. However, the fact that the isomerization quantum yield becomes lower with a decrease in temperature means that thermal excitations are involved in the process of the p* formation. The S_1 lifetime which has been reported as 0.03 ps [43] is too short to be associated with any kind of thermal excitations. It is considered that the precursor of p* is the S_2 state; in other words, we adopt Kinetics Scheme (II) rather than (III). Then, the total quantum yield is determined by two rate constants as follows:

$$\phi_{iso} = \frac{1}{2} \cdot \frac{\gamma_{2\to p^*}}{\gamma_{2\to 1} + \gamma_{2\to p^*}} , \tag{3-20}$$

where $\gamma_{2\to 1}$ is the $S_2 \to S_1$ internal conversion rate constant and $\gamma_{2\to p^*}$ is the $S_2 \to p^*$ decay rate constant, and the equation $\gamma_2 = \gamma_{2\to 1} + \gamma_{2\to p^*}$ has to be satisfied. The temperature dependence of ϕ_{iso} in Fig. 3-19 means that $\gamma_{2\to p^*}$ decreases as the temperature becomes lower. The most straightforward way to introduce the temperature dependence of $\gamma_{2\to p^*}$ is to use a transition state expression as follows:

$$\gamma_{2\to p^*} = a_{2\to p^*} \exp\left(-\frac{E_a}{k_B T}\right), \tag{3-21}$$

where $a_{2\to p^*}$ is the rate at a high-temperature limit, E_a is an activation energy, and the temperature is expressed as T. On the assumption that the internal conversion rate $\gamma_{2\to 1}$ is independent of T, an Arrhenius-type relation is obtained by using Eq. (3-20) and (3-21) in the following way:

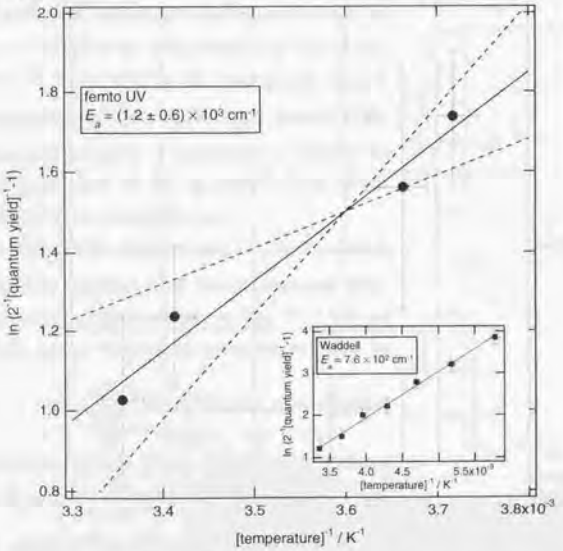

Fig. 3-20 Arrhenius plot to obtain the activation energy of all-trans → 13-cis-9-cis isomerization.
Dashed lines correspond to the error range of the activation energy. In the inset, the data of Waddell and Chihara (Ref. [17]) are plotted for the sake of comparison.

$$\log\left(\frac{1}{2\phi_{iso}}-1\right)=\frac{E_a}{k_BT}+\log\left(\frac{\gamma_{2\to1}}{a_{2\to p^*}}\right). \qquad (3\text{-}22)$$

The activation energy E_a can be derived by plotting $\log\left(2^{-1}\phi_{iso}^{-1}-1\right)$ versus T^{-1} as shown in Fig. 3-20. The data of Waddell and Chihara are also plotted in the same way in the inset of Fig. 3-20. E_a was roughly estimated at $(1.2 \pm 0.6) \times 10^3$ cm^{-1} (14 ± 7 kJ mol^{-1}) from the present data, while the data of Waddell and Chihara yielded 7.6×10^2 cm^{-1}. These two E_a values do overlap when the error is taken into account, and the present E_a value is comparable to the activation energy along the trans → perpendicular reaction pathway of S_1 stilbene (1200 cm^{-1}) [68-72]. However, $\gamma_{2\to p^*}$ at 293 K ~ 298 K is estimated to be about (2 ps)$^{-1}$ which is more than ten times larger than the trans → perpendicular reaction rate of S_1 stilbene [69, 71, 72]. It is quite possible that the present E_a value is being overestimated, and the lower value of Waddell and Chihara may be more trustworthy. Though the present reaction scheme of retinal is a replica of that of stilbene, the fact that the nearly equal values of the activation energy were obtained for retinal and stilbene does not necessarily mean the validity of applying the transition state theory to such an ultrafast reaction. However the present data are not enough in their quantity and quality to figure out a new temperature-dependence expression of $\gamma_{2\to p^*}$ instead of Eq. (3-21). At the present stage, it is appropriate to ascribe the temperature dependence of the quantum yield to the existence of the activation energy barrier.

The temperature dependence of the S_2 and S_1 lifetimes (Table 3-5) obtained from the femtosecond time-resolved UV absorption data is shown in Fig. 3-21 (a) and (b). In Fig. 3-21 (a), a theoretical curve represented by $\gamma_2=\gamma_{2\to1}+a_{2\to p^*}\exp\left(-\frac{E_a}{k_BT}\right)$ based on the isomerization scheme and Kinetics Scheme (II) is together shown. Since $\gamma_{2\to1}$ is about four times larger than $\gamma_{2\to p^*}$, the S_2 lifetime depends on T only weakly. The experimental errors of the S_2 lifetime in Fig. 3-21 (a) are too large compared to the S_2 lifetime change on going from 269 K to 298 K calculated

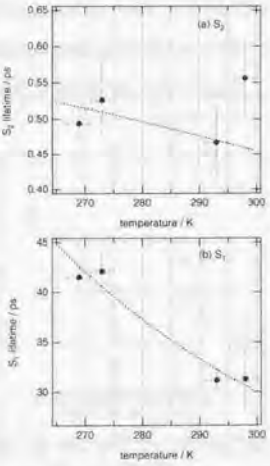

Fig. 3-21 Temperature dependence of the S_2 and S_1 lifetimes obtained from the femtosecond UV data.
A dotted line in Fig. (a) is a theoretical curve based on the reaction scheme assuming that S_2 is the p* precursor. A dotted line in Fig. (b) is a fitting curve by a transition state expression.

theoretically to know whether the S_2 lifetime depends on T or not. In Fig. 3-21 (b), the observed S_1 lifetime change is larger than the experimental errors. The S_1 lifetime becomes longer with a decrease in T. This T dependence of the S_1 lifetime is natural. In fact, it is well-known that a nonradiative $T_1 \rightarrow S_0$ intersystem crossing rate constant generally decreases with a decrease in temperature. On the assumption of $\gamma_1 \propto \exp\left(-\frac{E_{S1\rightarrow T}}{k_B T}\right)$, the activation energy of the $S_1 \rightarrow T_1$ intersystem crossing ($E_{S1\rightarrow T}$) was estimated as 6×10^2 cm^{-1}. It is presumed that the intersystem crossing process from S_1 to T_1 in all-trans retinal is accompanied with a structural change along a coordinate other than that of the double-bond isomerization.

There are two independent methods to derive the S_1 quantum yield ϕ_{S1} from the femtosecond UV data. One method is to use Table 3-5 and the following equation:

$$\phi_{S1} = \frac{1}{1+A} = 1 - 2\phi_{iso} \,. \tag{3-23}$$

that is based on the isomerization scheme in Fig. 3-18. The other is to calculate the ratio of the area of the S_1 absorption band to that of the S_0 absorption band in Fig. 3-13 or 14. In the former method, ϕ_{S1} is determined only by the S_0 temporal evolution and the absolute value of ϕ_{S1} can be obtained. However only relative value of ϕ_{S1} is obtained in the latter method, because the molar absorption coefficient of the $S_n \leftarrow S_1$ absorption is not known. The ϕ_{S1} temperature dependence obtained by way of the former method and that by way of the latter with an adequate scaling factor are simultaneously shown in Fig. 3-22. They approximately coincide with each other. The coincidence of the independently obtained ϕ_{S1} values supports the present isomerization scheme. Note that ϕ_{S1} in the present scheme is equal to the triplet quantum yield ϕ_T. The ϕ_T or ϕ_{S1} value at 298 K obtained by way of the former method is 0.74 ± 0.04 which is slightly higher than the reported ϕ_T values which ranged from 0.43 to 0.7 [13-16, 73]. All the reported ϕ_T values were obtained by means of the T_n

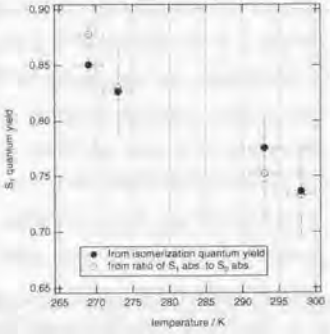

Fig. 3-22 Temperature dependence of the S_1 quantum yield obtained from the femtosecond UV data by means of two different methods. One affords absolute values using isomerization quantum yields (solid circles), and the other gives relative values from absorbance ratio of S_1 to S_0 (open circles).

$\leftarrow T_1$ absorption measurements with nano- and microsecond time resolution. In the analysis of the $T_n \leftarrow T_1$ absorption spectrum, it was necessary to assume the molar absorption coefficient of T_1 all-trans retinal and the effects of multiple excitation had to be taken into account. The femtosecond UV absorption analysis does not need any assumption and therefore the present ϕ_T value is more trustworthy than the previously reported values.

In the nanosecond time-resolved UV absorption spectra of all-trans retinal in cyclohexane at 298 K (Fig. 3-15), both the ground-state bleaching band and the photoproduct band have been observed. The former is ascribed to the T_1 population, and the latter is due to the all-trans → 13-cis-9-cis isomerization. Then, it is possible to obtain the ratio of ϕ_{iso} to ϕ_T from the nanosecond spectra by using the molar absorption coefficients of the all-trans and 13-cis isomers. The ratio $\frac{\phi_{iso}}{\phi_T}$ is calculated at 0.21 ± 0.05. By substituting this ratio for Eq. (3-23), ϕ_{iso} and ϕ_T are calculated at 0.15 ± 0.03 and 0.70 ± 0.06 respectively. These values agree well with those obtained from the femtosecond UV data. This agreement provides additional support to the present isomerization scheme.

We now consider how the isomerization scheme in Fig. 3-18 becomes compatible with Kinetics Scheme (II). In Kinetics Scheme (II) or (III), the intermediate p* decays exclusively to the S_0 all-trans isomer, and isomerization is not included at all. In the isomerization scheme, on the other hand, the p* decay is accompanied with the formation of the S_0 all-trans and 13-cis isomers in a 50/50 ratio. An ideal SVD analysis of the femtosecond UV data based on the isomerization scheme in Fig. 3-18 requires three components, the S_1 all-trans, S_0 all-trans, and S_0 13-cis isomers, but in fact only two SVD components were obtained experimentally. It is already shown by the present SVD analysis of the UV data that the S_1 and S_0 all-trans species contribute to the two leading SVD components. It is unlikely that all the contribution of the S_0 13-cis isomer to the SVD components was neglected in the present SVD analysis, because the S_0 absorption spectra of the all-trans and 13-cis isomers are nearly identical (Fig. 3-1). On the contrary, it is highly likely that most of the contribution of the S_0 13-cis isomer has already been taken into account in the present SVD analysis, and what was neglected is only the contribution of the difference spectrum between the S_0 absorption spectra of the 13-cis and all-trans isomers. When the temporal evolution of the S_0 all-trans isomer is expressed as $f_{S0}(t)$ of Eq. (3-13), that of the difference spectrum between the 13-cis and all-trans isomers is written as follows:

$$f_{diff}(t) = \frac{A}{2}\left(1 - e^{-\gamma_T t}\right). \qquad (3\text{-}24)$$

The contribution of each transient species to the SVD components is determined by the product of the area of its absorption spectrum and that of its temporal evolution. The ratio of the area of the S_0 all-trans spectrum to that of the 13-cis - all-trans difference spectrum is obtained from the ground-state molar absorption spectra in Fig. 3-1 as 22.5. The ratio of the area of the S_0 all-trans temporal evolution to that of the temporal evolution of the 13-cis - all-trans difference spectrum is obtained from Eq. (3-13) and (3-24) as 14.5. Accordingly the ratio of the contribution of the S_0 all-trans isomer to that of the 13-cis - all-trans difference spectrum is calculated to be 326. The ratio of the contribution of the S_0 all-trans isomer to that of the S_1 all-trans isomer is calculated in the same way to be 1.77 from the spectra and the populations in Fig. 3-13. Consequently the contributions of the S_0 all-trans isomer, that of the S_1 all-trans isomer, and that of the 13-cis - all-trans difference spectrum are in the ratio 1 : 0.57 : 0.0031. The 1st ~ 4th singular values derived from the femtosecond UV data (Fig. 3-12) are in the ratio 1 : 0.44 : 0.030 : 0.026, and the 3rd and higher SVD components are dominated by noise. The expected contribution of the 13-cis - all-trans difference spectrum is ten times smaller than the present noise level. Therefore, the signal to noise ratio has to be improved at least ten times better than in the present experiment, in order to include the contribution of the 13-cis - all-trans difference spectrum correctly in the SVD analysis with the three components. Owing to both the small difference between the S_0 all-trans and 13-cis spectra and the low quantum yield of the all-trans $\rightarrow$ 13-cis·9-cis photoisomerization, the SVD analysis of the UV data has been soundly performed with only two components.

No transient absorption band ascribable to p* was observed either in the VIS region (400 nm ~ 800 nm) or in the near UV region (310 nm ~ 390 nm), though it has been known that the p* absorption band of tetraphenylethylene is located at 420 nm [67], and that of stiff stilbene is located at 350 nm [65]. It is possible that a p* absorption band of retinal lies in the wavelength range shorter than 300 nm or longer than 800 nm. It is also noted that the p* quantum yield of retinal has proved to be as small as 0.22 at 293 K and 0.15 at 269 K, while that of tetraphenylethylene or stiff stilbene is nearly equal to 1. Such a small quantum yield makes it difficult to detect the p* retinal absorption. Since the molar absorption coefficient of p* is neither known nor predicted, it is not possible to estimate the signal to noise ratio of time-resolved spectra which enables the identification of the p* absorption by means of the SVD analysis.

Two additional remarks are made on the proposed isomerization scheme in Fig. 3-18. First, it is possible to ascribe the 7-ps lifetime to the perpendicular ground state, p. A potential minimum at the perpendicular configuration is necessary to account for the lifetime as long as 7 ps. However, existence of such a potential minimum in the ground state has never been rationalized either theoretically or experimentally. The perpendicular ground state whose lifetime is 7.2 ps is much less likely than the perpendicular excited state. Secondly, it

is also possible to ascribe the 7-ps lifetime to the vibrationally-excited electronic ground state (S_0*). Since no vibrational structure has ever been observed in the absorption and fluorescence spectra of all-trans retinal even at low temperature [29-32, 59, 60], the S_0* spectrum is expected to be nearly identical with the S_0 spectrum. Then, the S_0* $\rightarrow$ S_0 relaxation does not bring about the observed temporal evolution of the bleaching recovery shown in Fig. 3-13 (d). In addition, the assignment of p* to the S_0* state is not consistent with Fig. 3-19, which leads to an excellent agreement between the isomerization quantum yields determined by the two independent methods. Therefore, the S_0* state is also much less likely.

3-1-4-3. Relation between isomerization mechanism and electronic structure

On the basis of the above arguments, it is most likely that p* is assigned to the perpendicular excited singlet state which is a bottleneck state on the way from the all-trans to the mono-cis configuration. It is also likely that an energy barrier exists on the reaction pathway from the S_2 state in the all-trans configuration to the p* state and brings about the activation energy E_a which was estimated as $(1.2 \pm 0.6) \times 10^3$ cm^{-1}.

The origin of the energy barrier and the bottleneck perpendicular state is related with the electronic characters of S_1, S_2, and p*. Roughly speaking, there are two routes to consider the origin of the energy barrier. One is to assume the participation of two different excited states and attribute the energy barrier to the crossing of these two states [74-76]. The other is to regard the energy barrier as an intrinsically adiabatic one and assume the electronic configuration to be unchanged during the barrier crossing process [77]. If p* is identified electronically with an excited state of the same character as the S_2 state, that is, A_g (π, π*), the S_2 $\rightarrow$ p* reaction pathway is presumed to be adiabatic. If p* is identified electronically with an excited state of B_u^+ (π, π*) character, on the other hand, the energy barrier is presumed to be attributed to the crossing of the S_1 and S_2 states. The participation of these two states in the isomerization process is quite possible since they are very close in energy (~ 2000 cm^{-1}) [35]. The crossing of the S_1 and S_2 states can bring about the energy barrier as high as 1.2×10^3 cm^{-1}. As regards the photoisomerization reaction of stilbene, both adiabatic and nonadiabatic mechanisms have been proposed from a theoretical point of view [74, 75, 77], and a lot of extensive experimental studies do not unanimously support one mechanism [26, 64, 72, 78]. In the case of retinal in nonpolar solvents, potential energy surfaces of the ground and excited states have not yet been calculated in detail. At least the elucidation of p* electronic character is necessary to fully explain the all-trans $\rightarrow$ 13-cis-9-cis isomerization mechanism of retinal in the singlet states.

There is one clue to elucidate p* electronic character in the present results; the p* lifetime, 7.2 $\pm$ 2 ps. It has been assumed in the isomerization scheme that p* decays

exclusively to the perpendicular ground state, p, and this assumption has been strongly supported by the agreement of the isomerization quantum yields. Then, the p* lifetime is determined exclusively by the p* → p conversion rate. Since p is on the ground-state potential energy surface, the electronic character of p is regarded as A_g in a very approximate meaning. It is very unlikely that p* is of (n, π*) character because of the following two reasons: One is that neither S_1 (n, π*) → p* nor p* → T_1 (π, π*) conversion process has been observed in the present study. Both of the processes should exist if p* is of (n, π*) character. The other is that it is unlikely that an (n, π*) state takes part in a double-bond isomerization reaction, since an n → π* transition is presumed to be localized to a certain extent in the carbonyl group. In fact, an isomerization reaction where an (n, π*) state participates has never been reported so far to the best of my knowledge, and it has been clarified in this study that the S_1 all-trans isomer of (n, π*) character does not really take part in the all-trans → 13-cis-9-cis isomerization. If p* is approximately of A_g (π, π*) character, the p* → p decay process is internal conversion between electronic singlet states of the same character. Since nonadiabatic radiationless transitions are induced by vibronic perturbations, the p* → p process is "forbidden" and may be slow though it is difficult to estimate its rate [76]. The time scale of the "forbidden" p* → p process is probably too slow for stilbene [26], but may be in an acceptable range for tetraphenylethylene (3 ns) [67], stiff stilbene (10 ps) [65], and retinal in this study (7 ps). If p* is identified with a minimum on the B_u^+ (π, π*) state surface, the time scale of the p* → p conversion may be much faster. In the cis → trans photoisomerization reactions of rhodopsin and isorhodopsin, internal conversion processes between electronic singlet states of different characters take only hundreds of femtoseconds or less than a few picoseconds [79-82]. However, a larger energy gap between p* and p can make the nonadiabatic p* → p conversion rate smaller [76]. In the present case, the energy gap between p* and p is not known at all. The assignment of p* to B_u^+ (π, π*) character does not conflict with the 7-ps lifetime of the p* state.

Though we have obtained the activation energy of the isomerization and the lifetime of the perpendicular intermediate, these data are still not sufficient to unequivocally determine the origin of the energy barrier and p* electronic character. Further theoretical and experimental efforts will be necessary to understand fully the all-trans → 13-cis-9-cis isomerization mechanism of retinal.

3-1-5. Summary

The excited-state dynamics and the photoisomerization reactions of the retinal isomers in aerated nonpolar solvents were studied by using femtosecond time-resolved UV-VIS absorption spectroscopy.

Four transient species (S_3, S_2, S_1, T_1) were found in the time-resolved VIS spectra of

all-trans retinal. The correspondence between the S_2 decay and the S_1 rise and that between the S_1 decay and the T_1 rise were simultaneously confirmed. On the assumption that S_3 is of B_u^+ (π, π^*) character, S_2 and S_1 were characterized as A_g^- (π, π^*) and (n, π^*) respectively. The relaxation sequence and the excited-state lifetimes of 9-cis retinal were found to be nearly identical with those of the all-trans isomer. As regards 13-cis retinal, the kinetics data of the S - S and $T_n \leftarrow T_1$ absorption distinct from those of the all-trans and 9-cis isomers were obtained. On the basis of the comparison of the time-resolved VIS spectra of these three isomers, the possible maximum quantum yields of the all-trans $\rightarrow$ 13-cis·9-cis and 9-cis $\rightarrow$ all-trans isomerization reactions that complete in the excited singlet manifold were estimated to be sufficiently lower than the known quantum yields. In other words, the femtosecond VIS data did not provide any evidence for an isomerization reaction complete in the excited singlet states.

The femtosecond UV spectra of all-trans retinal were successfully analyzed in terms of an isomerization scheme involving a perpendicular excited singlet state, p*. The p* lifetime was found to be 7.2 ± 2 ps and was much longer than the S_3 and S_2 lifetimes but was shorter than the S_1 lifetime. It is proposed that the precursor of p* is most likely the S_2 state. The S_1 state does not take part in the isomerization reaction. The quantum yield values of the all-trans $\rightarrow$ 13-cis·9-cis isomerization in the temperature range 269 K ~ 298 K obtained from the femtosecond UV data were in good agreement with the reported values measured by HPLC. The S_1 quantum yields obtained from the femtosecond UV absorption data by way of the two independent methods were also in good agreement. The quantum yield derived on the basis of the present isomerization scheme from the nanosecond UV spectra was also in agreement with the reported values. All these agreements present evidence in favor of the proposed isomerization scheme. The height of the energy barrier on the way from S_2 to p* was roughly estimated as $(1.2 \pm 0.6) \times 10^3$ cm^{-1}, but it is still not clear whether it is proper to apply the transition state theory to such ultrafast reactions. The origin of the activation energy barrier has been discussed in terms of the electronic character of the S_3, S_2, and p* states. The detection of the p* UV-VIS absorption band will be useful for securing the proposed reaction scheme and further discussing the isomerization mechanism.

3-2. All-trans retinal in protic solvents

3-2-1. Introduction

The electronic structure and the photochemical properties of retinal strongly depend on its surroundings. Especially the properties of retinal in protic solvents are quite different from those in nonpolar solvents because of hydrogen-bonding interactions. The fluorescence and isomerization quantum yields of all-trans retinal generally increases on H-bond formation, whereas the triplet quantum yield decreases. The fluorescence quantum yield ϕ_F of all-trans retinal in hexane or 3-methylpentane has been reported to be about 10^{-4} or less [29, 36, 43], while ϕ_F in alcohol or acid solutions is much higher and the fluorescence is easily detected [83, 84]. The triplet quantum yield ϕ_T of all-trans retinal in nonpolar solvents has been reported to be as high as 0.4 ~ 0.7 [13-16] and was determined to be 0.74 by way of femtosecond time-resolved UV absorption spectroscopy in the previous section, while ϕ_T in alcohol solutions is about 0.1 or less [15, 16].

The solvent dependence of ϕ_F and ϕ_T has been quite often ascribed to a change in the state order upon H-bond formation [29, 36-38]: It seems that the notion that the lowest excited singlet (n, π^*) state brings about low ϕ_F and high ϕ_T in nonpolar solvents while high ϕ_F and low ϕ_T in protic solvents is caused by the lowest excited singlet (π, π^*) state has been generally accepted. In fact, it is consistent that an electron spin echo experiment has revealed T_1 all-trans retinal to be of (π, π^*) character [61]. However, no direct concrete evidence for the singlet state order change upon H-bond formation in all-trans retinal has been given so far. Takemura et al. confirmed H-bond formation between all-trans retinal and phenol, but the grounds they presented for concluding the state order change or a strong solvent-induced mixing of the energy levels (n, π^*) and (π, π^*) were nothing but the ϕ_F increase and the ϕ_T decrease on H-bond formation [29]. Papanikolas et al. performed stationary spectroscopy of all-trans decatetraenal which is one of the model molecules of all-trans retinal. They found difference between the absorption and fluorescence excitation spectra of decatetraenal in ethanol/methanol glass, and they ascribed the difference to the existence of fluorescent H-bonded species and nonfluorescent free species. In their discussion, it was assumed *a priori* that the ϕ_F increase on H-bond formation was brought about by the state order change along a proton transfer coordinate [38]. Alex et al. concluded in the similar way that ϕ_F was determined by the state order [37]. One major point to remember at this stage is the fact that an excited state which fluorescence originates from is not always the S_1 state. In addition, a criterion to judge whether fluorescent or nonfluorescent is always equivocal. For example, ϕ_F of all-trans retinal in methanol has been reported to be as small as 4×10^{-3} [16], but its laser-excited fluorescence can be easily observed by eye.

Though all-trans retinal in methanol can be regarded as fluorescent, such a small ϕ_F value does not necessitate a one-photon allowed state as the lowest excited singlet state. In general, stationary spectroscopy which either provides an exact ϕ_F value or enables comparison between absorption and fluorescence excitation spectra does not give enough data to determine a state order.

Time-resolved spectroscopy, on the other hand, reveals excited-stated relaxation dynamics and lifetimes which are essential in considering a state order and an electronic structure. As regards free all-trans retinal in nonpolar solvents, femtosecond time-resolved fluorescence up-conversion spectroscopy has revealed the S_2 state to be of B_u^+ (π, π^*) character [43], and the relaxation sequence in the excited singlet manifold has been clarified by femtosecond time-resolved UV-VIS absorption spectroscopy in the previous section of this thesis. On the basis of these results, it was concluded that the most tenable assignments for the S_2 and S_1 states of free all-trans retinal are to A_g^- (π, π^*) and (n, π^*), respectively. On the other hand, only a very few time-resolved spectroscopic studies of H-bonded retinal in protic solvents have been performed so far. Dawson and Abrahamson measured the methanol concentration dependence of the T_1 lifetime of all-trans retinal and determined the equilibrium constant between the free and H-bonded species of T_1 all-trans retinal in their pioneering flash illumination study [48]. Hamaguchi et al. showed that the Raman spectra of the T_1 all-trans and 9-cis isomers in methanol were nearly identical with each other and similar to those in hexane [28]. These two studies have proved that the photoexcitation of all-trans retinal in alcohol solvents affords the T_1 species in the all-trans configuration. Larson et al. reported the femtosecond time-resolved absorption data of all-trans retinal in ethanol for the first time [42]. Although they did not present any transient spectrum, they observed the excited-state absorption including not only the triplet but also singlet states, the stimulated emission gain, and the ground-state bleaching. They also reported the time-resolved absorption data upon two-photon excitation in the same paper and observed the singlet excited-state absorption. Unfortunately, they concluded that the S_1 state of all-trans retinal in ethanol was of A_g^- (π, π^*) character without any experimental grounds. The kinetics model they proposed seems very unlikely since a state with a 1.8 ps lifetime is located energetically above a state with a subpicosecond lifetime. It is almost impossible to search in their results for reasons why they located the B_u^+ (π, π^*) and (n, π^*) states energetically above the A_g^- (π, π^*) state. It is asserted here that the state order change upon H-bond formation has not yet been experimentally proved.

The quantum yields and the product distribution of the retinal photoisomerization also depend on solvents. The photoexcitation of free all-trans retinal in aerated nonpolar solvents at room temperature affords the 13-cis and 9-cis isomers of which the quantum yields (ϕ_{13}^{free} and ϕ_9^{free}) are about 0.1 and 0.02 respectively, while that of H-bonded all-trans

retinal in aerated alcohol solvents gives not only the 13-cis and 9-cis isomers but also the 11-cis isomer with the quantum yield (ϕ_{11}^{Hbond}) lower than ϕ_{13}^{Hbond} but higher than ϕ_{9}^{Hbond} [17, 45]. Furthermore ϕ_{13}^{Hbond} is about twice as large as ϕ_{13}^{free}. Deckert et al. recently explained qualitatively the solvent dependence of the all-trans → mono-cis photoisomerization quantum yields [85], but an isomerization reaction pathway in protic solvents has not yet been clarified at all.

The purpose of this section 3-2 is to study the excited-state dynamics of all-trans retinal in protic solvents: chemical equilibria between free and H-bonded species in the excited singlet and triplet states, the excited singlet electronic structure of H-bonded species, and the isomerization mechanism. In Sect. 3-2-3, the femtosecond time-resolved VIS absorption spectra of all-trans retinal in mixed solvents of 1-butanol and cyclohexane are presented. The addition of 1-butanol was accompanied with the appearance of stimulated emission gain signals which were ascribed not to the S_1 state but to the S_2 state. No evidence for the state order change of (π, π^*) and (n, π^*) states upon H-bond formation was found. The linear-combination fitting analyses of the excited-state absorption and gain bands indicated that free and H-bonded species coexist in the S_2 and T_1 states, while no free species exists in the S_2 and S_1 states. No conclusion has been reached for the all-trans → mono-cis isomerization reaction pathway in H-bonding solvents. However, it was confirmed that the longer lifetime of the H-bonded S_2 species is consistent with the higher isomerization quantum yield than in nonpolar solvents.

3-2-2. Experimental

3-2-2-1. Materials

Cyclohexane and 1-butanol were purchased from Wako Chemical Co. and used as received. No precautions were taken to dry these solvents. All the solvents were aerated. Commercial all-trans retinal (Sigma Chemical Co.) was used without further purification. Retinal samples were analyzed for isomeric composition as explained in Sect. 3-1-2-1. The same criterion of isomeric composition as in Sect. 3-1-2-1 was satisfied throughout the study.

The stationary UV-VIS absorption spectra of all-trans retinal in mixed solvents of cyclohexane and 1-butanol were measured at room temperature by using a commercial UV-VIS spectrometer (HITACHI, U-3500) in order to investigate the H-bonding equilibrium in the ground state. The concentration of 1-butanol was varied from 0 to 8.56 mol dm^{-3}, while that of all-trans retinal was fixed at 1.7×10^{-5} mol dm^{-3}. All the seven spectra are shown in Fig. 3-23. When the 1-butanol concentration is between 0 and 3.06 mol dm^{-3}, an isosbestic point is clearly seen at wavelength 380.6 nm. Accordingly, it is concluded that two species are equilibrated in the mixed solvents of cyclohexane and 1-butanol in this concentration

range. One is definitely free all-trans retinal, and it is highly likely that the other is the 1:1 H-bonded complex of all-trans retinal and 1-butanol. In the higher-concentration region, the absorption spectra do not intersect the low-concentration spectra at the isosbestic point. This kind of deviation has been also reported by Das and Hug who used 1,1,1,3,3,3-hexafluoro-2-propanol (HFIP) instead of 1-butanol [83]. They proposed formation of another species such as a 1:n (n > 1) H-bonded complex or a protonated form. However it is also possible to ascribe the superfluous red shift of the absorption bands in the higher-concentration region to a solvent-environmental effect [86]. In any case, the deviation is so small that all the mixed-solvent absorption spectra were well fitted with a linear combination of two basis spectra: One was the spectrum in neat cyclohexane and the other was that in the mixed solvent of the 3.05-mol dm^{-3} 1-butanol concentration. The former spectrum (Basis 1) is ascribed to only free all-trans retinal, but the latter (Basis 2) is contributed to by not only the H-bonded species but also the free species even with such a high 1-butanol concentration. It is because 1-butanol is a weak H-bonder in contrast with acid solvents such as phenol and HFIP [29, 83]. The linear-combination fitting procedure yielded the coefficient of Basis 1 (c_1) and that of Basis 2 (c_2) for each mixed-solvent spectrum. The isosbestic point guarantees the condition $c_1 + c_2 = 1$ for the low-concentration spectra. The well-known Benesi-Hildebrand method [87] is modified to afford the following equation:

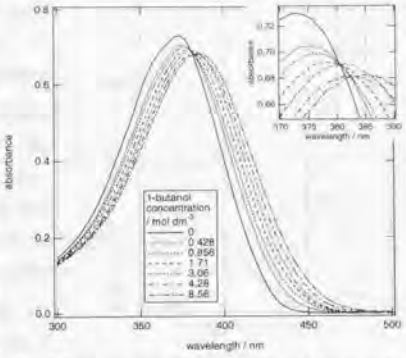

Fig. 3-23 Ground-state absorption spectra of all-trans retinal in the mixed solvents of 1-butanol and cyclohexane. The 1-butanol concentrations are indicated as a legend in the figure.

$$c_2^{-1} = \alpha\left(K^{-1}C^{-1} + 1\right), \tag{3-25}$$

where α is the ratio of [H-bonded retinal] to the sum of [H-bonded retinal] and [free retinal] (i.e. the total retinal concentration) in the mixed solvent of which [1-butanol] is equal to 3.05 mol dm^{-3}, K is the equilibrium constant given by [H-bonded retinal]·[free retinal]$^{-1}$·[1-butanol]$^{-1}$, and C is [1-butanol]. The linear relation between c_2^{-1} and C^{-1} shown in Fig. 3-24 gave the following results: α = 0.84, K = 1.2 dm^3 mol^{-1}. If a stronger H-bonder is used instead of 1-butanol, K becomes larger and α approaches unity. The tendency of the Benesi-Hildebrand-plot deviation from linearity in the high-concentration region is the same as that reported by Das and Hug (i.e. bend downwards) [83]. There may also exist effect of

self-association of alcohols [88]. Self-association effectively reduces [1-butanol] which is available to form an H-bonding complex [38], and is expected to bend the c_2^{-1} - C^{-1} plot upwards in the high-concentration region. The moderate linearity in the low-concentration region indicates that self-association is not so effective in this region. It has been reported that stronger H-bonders such as phenol (pK_a 10), HFIP, and methanol (pK_a 15) make H-bonded all-trans retinal with much larger K values of 6×10^3 dm^3 mol^{-1} [29], 4×10^2 dm^3 mol^{-1} [83], and 7 dm^3 mol^{-1} [48], respectively.

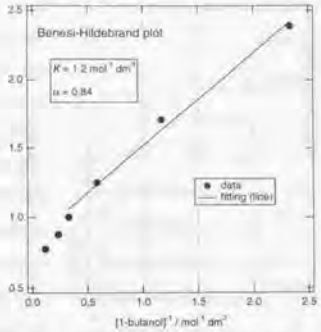

Fig. 3-24 Benesi-Hildebrand plot based on the linear-combination fitting of the absorption spectra in Fig. 3-23 (see text).

3-2-2-2. Femtosecond time-resolved VIS absorption spectroscopy

The femtosecond time-resolved VIS absorption spectra of all-trans retinal in mixed solvents of cyclohexane and 1-butanol were measured by using the spectrometer described in Chap. 2. All the solvents were of HPLC grade. The 1-butanol concentration was set at eleven different values of 0, 1.78, 3.06, 4.01, 4.76, 5.35, 5.94, 6.69, 7.64, 8.92, and 10.7 mol dm^{-3}. The last concentration value corresponds to neat 1-butanol. All the solutions had the same retinal concentration (2×10^{-3} mol dm^{-3}) and the same volume (0.2 dm^3). The temperature of the solutions just emitted from the jet nozzle was 293 ± 2 K. The pump pulse was characterized as follows: center wavelength, 400 nm; pulse energy, 5 μJ; excitation density, 2 × 10 J m^{-2}. The pulse energy of the VIS wide-band probe pulse was less than 0.1 μJ. In a set of time-resolved spectra, there were 96 time-delay points from -4 ps to 120 ps. The exposure time of the CCD was 1 s, and the number of the exposures at each time delay point was 10. Chirp correction described in Sect. 2-2-3-3 was performed to obtain the final time-resolved spectra.

3-2-3. Results and Discussion

3-2-3-1. Salient features of spectra

In Fig. 3-25 (a) ~ (d), the four sets of several representative femtosecond time-resolved VIS absorption spectra of all-trans retinal in the mixed solvents of cyclohexane and 1-butanol are shown. The 1-butanol concentration values are (a) 0, (b) 1.78, (c) 5.35, and (d) 10.7 mol dm^{-3}, respectively. In these figures, positive signals generally correspond to transitions from excited states to higher excited states, and negative signals correspond to ground-state bleaching, a stimulated emission gain, a Raman gain, and so on.

The time-resolved spectra of all-trans retinal in neat cyclohexane (Fig. 3-25 (a)) are nearly identical with those in hexane (Fig. 3-2). Therefore, on the basis of the kinetics analysis in Sect. 3-1-3-1, rough assignments can be performed for the free all-trans spectra in cyclohexane (Fig. 3-25 (a)). The absorption band around 600 nm in the spectrum at -0.2 ps is ascribed to the S_2 state which decays within the present time resolution. The broad absorption spectrum in the wavelength range 450 nm ~ 650 nm at 0.2 ps ~ 0.6 ps is ascribed to the S_2 state of which the lifetime was determined to be 0.7 ps in Sect. 3-1-3-1. The intense band of which the peak wavelength is 445 nm at 40 ps ~ 100 ps is assigned to the T_1 state. All these transient species are of the free (i.e. no H-bond) all-trans isomer.

As shown in Sect. 3-2-2-1, the free and H-bonded S_0 species are equilibrated in the protic solvents, and accordingly both of the S_0 species are photoexcited by the 400-nm pump pulses. In Fig. 3-25 (b), an absorption band in

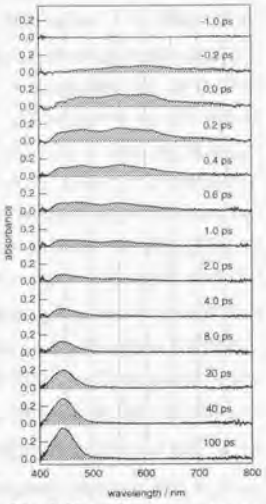

Fig. 3-25 (a) Femtosecond time-resolved VIS absorption spectra of all-trans retinal in neat cyclohexane.

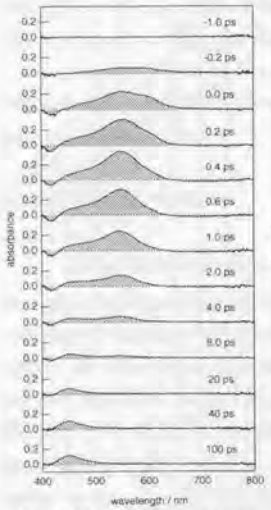

Fig. 3-25 (b) Femtosecond time-resolved VIS absorption spectra of all-trans retinal in the mixed solvent of 1-butanol and cyclohexane.
The 1-butanol concentration was 1.78 mol dm^{-3}.

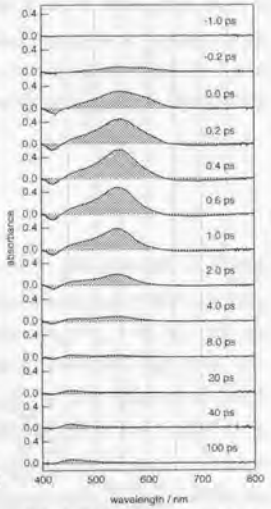

Fig. 3-25 (c) Femtosecond time-resolved VIS absorption spectra of all-trans retinal in the mixed solvent of 1-butanol and cyclohexane.
The 1-butanol concentration was 5.35 mol dm^{-3}.

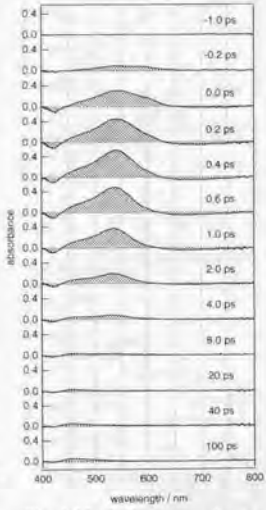

Fig. 3-25 (d) Femtosecond time-resolved VIS absorption spectra of all-trans retinal in neat 1-butanol.
The 1-butanol concentration was 10.7 mol dm^{-3}.

550 nm ~ 600 nm at -0.2 ps appears first. This band is tentatively assigned to the $S_n \leftarrow S_1$ absorption band because of the correspondence between Fig. 3-25 (a) and (b). After the S_1 state decays very fast, an intense absorption band around 550 nm is observed in the spectra at 0.2 ps ~ 0.6 ps. The correspondence presumably allows a tentative assignment of this band to the S_2 state. The $S_n \leftarrow S_2$ absorption band is accompanied with negative signals in the wavelength ranges 400 nm ~ 430 nm and 620 nm ~ 800 nm. In the former wavelength range, the ground-state bleaching may contribute to the negative signals, since the ground-state absorption exists there as shown in Fig. 3-23. However, those in the latter range are definitely ascribed solely to a stimulated emission gain, since there is no ground-state absorption in such a long wavelength range. The fact that a stimulated emission gain is brought about by the addition of 1-butanol is consistent with the fact that ϕ_F is far larger in protic solvents than in nonpolar solvents. At 40 ps ~ 100 ps, a weak absorption band is observed around 450 nm. This absorption band is ascribed to the T_1 state. The red shift of the $T_n \leftarrow T_1$ absorption band upon H-bond formation has been well-known [15, 48, 83]. The addition of 1-butanol caused the decrease of the $T_n \leftarrow T_1$ absorbance. It presumably corresponds to the fact that ϕ_F is smaller in protic solvents than in nonpolar solvents. The time-resolved spectra in Fig. 3-25 (c) and (d) have similar features to those in Fig. 3-25 (b). The increase of the 1-butanol concentration brings about the blue shift of the $S_n \leftarrow S_2$ absorption band at 0.4 ps (550 nm → 540 nm) and the red shift of the $T_n \leftarrow T_1$ absorption band at 100 ps (450 nm → 460 nm). Note that with an increase in the 1-butanol concentration, the intensity of the stimulated emission gain band increases while the $T_n \leftarrow T_1$ absorbance becomes smaller.

3-2-3-2. Kinetics analysis

The rise time constant of T_1 was estimated by fitting the time-delay dependence of the absorbance at 450 ± 2.5 nm with exponential functions as shown in Fig. 3-26 (a) ~ (d). As regards all-trans retinal in neat cyclohexane (Fig. 3-26 (a)), two time constants, 0.7 ps and 30 ps, were obtained of which the latter is the T_1 rise time constant. It is quite natural that these values agree with the results of all-trans retinal in hexane in Sect. 3-1-3-1. The former value corresponds to the S_2 lifetime. When 1-butanol is added, the fitting results of Fig. 3-26 (b) ~ (d) unanimously show that the T_1 rise time constant is about 20 ps (20 ps ~ 22 ps). This time constant is definitely

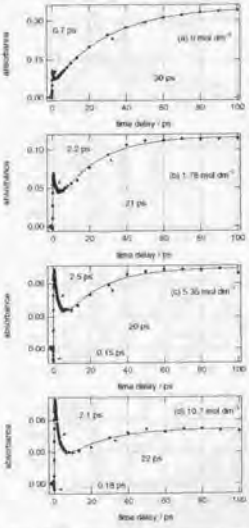

Fig. 3-26 Transient absorbance of all-trans retinal at 450 nm. The 1-butanol concentrations and exponential time constants are indicated as legends.

shorter than that of the free species (30 ps). In addition, two components were found: One is a 2-ps decay (2.1 ps ~ 2.5 ps), and the other is a 0.1-ps rise (0.12 ps ~ 0.18 ps). Both of these two components become more distinct with an increase in the 1-butanol concentration, while the T_1 rise becomes less prominent.

The time-delay dependence of the absorbance at 541 ± 2.5 nm where the $S_0 \leftarrow S_2$ absorption is dominant was analyzed in the similar way as shown in Fig. 3-27 (a) ~ (d). In the case of all-trans retinal in the protic solvents ((b) ~ (d)), a 2-ps decay (1.7 ps ~ 2.0 ps) as well as a subpicosecond decay (0.3 ps ~ 0.4 ps) were identified. The former decay time constant, 2 ps, is approximately regarded as the S_2 lifetime, and the latter presumably corresponds to the S_3 decay. The S_2 and S_3 lifetimes in the protic solvents appear to be longer than those in neat cyclohexane (Fig. 3-27 (a)).

In Fig. 3-28 (a) ~ (d), the time-delay dependence of the absorbance at 603 ± 2.5 nm where the $S_0 \leftarrow S_1$ absorption is dominant are shown along with the fitting results. Two decay components were found in the protic solvents data ((b) ~ (d)). One ranged from 1.2 ps to 2.7 ps, and the other was about 0.3 ps. Though the former time constants do not exactly coincide with those at 541 nm (Fig. 3-27 (b) ~ (d)), they can be roughly assigned to the S_2 state. The latter 0.3-ps component is presumed to correspond to the S_3 state.

In Fig. 3-29 (a) ~ (d), the time-delay dependence of the absorbance at 679 ± 2.5 nm

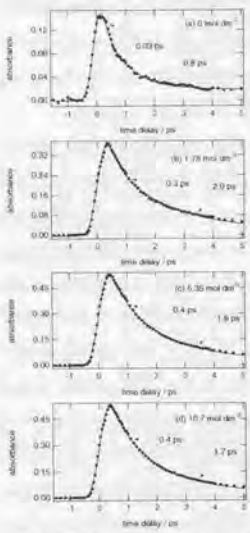

Fig. 3-27 Transient absorbance of all-trans retinal at 541 nm.
The 1-butanol concentrations and exponential time constantsare indicated as legends.

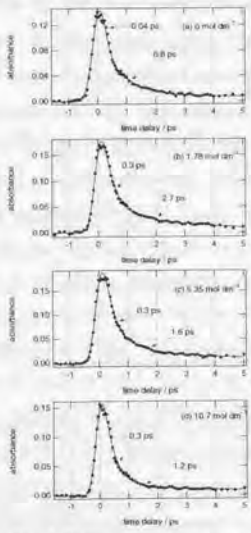

Fig. 3-28 Transient absorbance of all-trans retinal at 603 nm.
The 1-butanol concentrations and exponential time constants are indicated as legends.

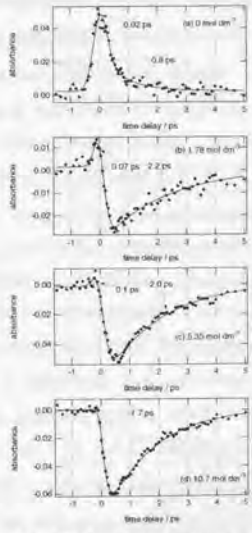

Fig. 3-29 Transient absorbance of all-trans retinal at 679 nm.
The 1-butanol concentrations and exponential time constants are indicated as legends.

where the stimulated emission gain is dominant in the protic solvents data are shown along with the fitting results. The decay time constants of the stimulated emission gain which ranged from 1.7 ps to 2.2 ps approximately agree with the S_2 lifetime obtained at 541 nm (Fig. 3-27 (b) ~ (d)). Therefore, the stimulated emission gain is ascribed to the $S_2 \rightarrow S_0$ transition. The decay time constants of the ultrafast positive signals in Fig. 3-29 (b) and (c) were 0.07 ps and 0.13 ps respectively. These are shorter than the time constants of the fastest components at 603 nm and 541 nm (Fig. 3-27, 28) but nearly equal to those at 450 nm (Fig. 3-26).

Since the time constants at different wavelengths do not exactly coincide with each other in Fig. 3-26 ~ 29, it is difficult to determine the excited-state lifetimes conclusively in each protic solvent. However, approximate time ranges where the lifetimes are located can be determined as follows: First of all, the T_1 rise time constant in the protic solvents is about 20 ps which is almost independent of the 1-butanol concentration, while that in neat cyclohexane is about 30 ps. It is highly likely that the precursor of T_1 in the protic solvents is an excited singlet state as in the case of the free species in nonpolar solvents. Accordingly an excited singlet state of which the lifetime is about 20 ps has to exist in the protic solvents. Secondly, the decay time constant of the $S_n \leftarrow S_2$ absorption and the $S_2 \rightarrow S_0$ gain in the protic solvents is about 2 ps which seems to become slightly shorter with an increase in the 1-butanol concentration. It is affirmed that the S_2 state is a one-photon allowed fluorescent state because of the existence of the stimulated emission gain. Lastly, the S_3 decay time constant in the protic solvents is about 0.3 ps or shorter but probably longer than that of the free S_3 species.

Though the above lifetimes are only approximate, it is impossible to assign the excited singlet state of which the lifetime is about 20 ps, that is, the precursor of the T_1 state, to the S_2 or S_3 state. A much more tenable assignment for the 20-ps singlet state is to the S_1 state. It is generally accepted that an electronic state of a longer lifetime is located energetically below a state of a shorter lifetime. Otherwise a longer-lifetime state decays to a shorter-lifetime state and it will be almost impossible to observe the shorter lifetime. Therefore it is concluded that the S_1 lifetime in the protic solvents is about 20 ps. Unfortunately the $S_n \leftarrow S_1$ absorbance of the free species is weak in the VIS wavelength region (400 ~ 800 nm) as shown in Sect. 3-1-3-1, and no $S_0 \leftarrow S_1$ absorption peak was found in the protic solvents data (Fig. 3-25 (b) ~ (d)). No stimulated emission gain of which the lifetime is about 20 ps was found. This fact strongly suggests that S_1 is not a fluorescence source in the protic solvents. Furthermore, the T_1 precursor is still S_1 as in the case of the free species in nonpolar solvents. The free T_1 all-trans isomer is of (π, π^*) character [61]. It was concluded in Sect. 3-1 that the free S_1 state is of (n, π^*) character. On the assumption that T_1 remains a (π, π^*) state on H-bond formation between retinal and 1-butanol, it is probable that

the S_1 state in the protic solvents also remains an (n, π^*) state. In fact, it is very unlikely that either S_2 or S_3 is of (n, π^*) character, because the S_2 state showed the stimulated emission gain and the S_3 state is deemed to be directly generated by the photoexcitation. Therefore it is concluded that the S_1 state in the protic solvents is of (n, π^*) character.

It seems that the meaning of the symbols A_g and B_u is much more approximate in the protic solvents than in nonpolar solvents, because both S_2 and S_3 are deemed to be one-photon allowed. It is inferred that a mixing of A_g^- and B_u^+ (π, π^*) states is induced by H-bonding interactions in S_2 and S_3. In nonpolar solvents, the radiative lifetime of the S_1 B_u^- (π, π^*) state has been estimated at 3 ns which is about fourty times shorter than that of the S_2 A_g^- (π, π^*) state [43]. In the protic solvents, on the other hand, it is likely that both S_2 and S_3 have comparable radiative lifetimes. Otherwise the $S_3 \rightarrow S_0$ stimulated emission gain can not be observed. The ground-state absorption spectra (Fig. 3-23) show that the radiative lifetime of the S_2 and S_3 states in the protic solvents is comparable to that of S_1 in nonpolar solvents. Unfortunately the ratio of the initial population of S_2 prepared by the photoexcitation to that of S_3 can not be estimated from the present results because of the insufficient time resolution. As regards the S_2 state, 20 ~ 30 times shortening of the radiative lifetime and 3 ~ 4 times lengthening of the lifetime on the addition of 1-butanol causes roughly a hundred times larger ϕ_F value. It is thus realized that the state order change of the (π, π^*) and (n, π^*) states is not necessary at all to account for the ϕ_F increase upon H-bond formation. It is concluded that S_2 and S_3 in the protic solvents are both one-photon allowed (π, π^*) states.

The fact that the S_2 lifetime is about three times longer in the protic solvents than in nonpolar solvents is consistent with the increase of the all-trans $\rightarrow$ mono-cis isomerization quantum yield on H-bond formation. It has been reported that the total quantum yield in ethanol is about 2 ~ 3 times higher than in nonpolar solvents [17]. In Sect. 3-1, it has been shown that the all-trans $\rightarrow$ mono-cis isomerization reaction in aerated nonpolar solvents proceeds most probably from the S_2 state by way of a perpendicular excited singlet state (p*). On the assumption that the $S_2 \rightarrow$ p* conversion rate remains unchanged upon H-bond formation, the S_2 lifetime lengthening corresponds well to the quantum-yield increase.

3-2-3-3. Equilibrium between H-bonded and free retinal

As regards the ground state, free and H-bonded all-trans retinal are equilibrated not only in the mixed solvents but also in neat 1-butanol as shown in Sect. 3-2-2-1. A Franck-Condon excited state prepared by the photoexcitation has the same atomic configuration as the ground state. The S_1 state of which the lifetime is shorter than about 0.3 ps can be approximately regarded as a Franck-Condon state. Therefore it is expected that free and H-

bonded species coexist also in the S_1 state. In Fig. 3-30 (a) ~ (d), the time-resolved absorption spectra of all-trans retinal at -0.2 ps are shown. The 1-butanol concentration values are (a) 0, (b) 1.78, (c) 5.35, and (d) 10.7 mol dm^{-3} respectively. At -0.2 ps, the $S_n \leftarrow S_1$ absorption band is predominant, and it is presumably unnecessary to take any S_2 contribution into account, because no negative signal of the stimulated emission gain is seen in the wavelength range 620 nm ~ 800 nm. The mixed-solvent S_1 spectra (Fig. 3-30 (b), (c)) were fitted with a linear combination of the two neat solvent S_1 spectra ((a), (d)). The fitting results are together shown there. The mixed-solvent S_1 spectra are well reproduced by the linear-combination fitting spectra. The fitting of all the other seven mixed-solvent S_1 spectra were also successful to the same extent. It means that the mixed-solvent S_1 spectra are composed of two species. One is definitely the free S_1 all-trans isomer, and the other is probably the 1:1 H-bonded S_1 all-trans isomer which is presumed to have nearly the same atomic configuration as the 1:1 H-bonded S_0 state. Since the S_1 lifetime is ultrashort, it is pertinent to conclude that the free

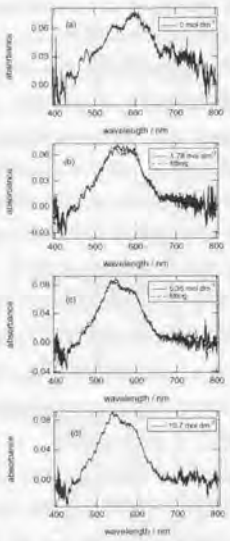

Fig. 3-30 Time-resolved VIS absorption spectra of all-trans retinal at -0.2 ps.
The 1-butanol concentrations are indicated as legends. In (b) and (c), the fitting spectra (linear-combination of (a) and (d)) are together shown.

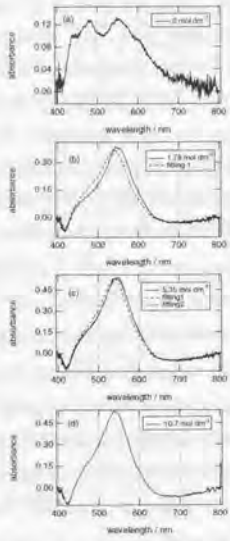

Fig. 3-31 Time-resolved VIS absorption spectra of all-trans retinal at 0.4 ps.
The 1-butanol concentrations are indicated as legends. In (b) and (c), the fitting spectra (linear-combination of (a) and (d)) are together shown (fitting 1). In (c), the fitting spectrum (linear-combination of (b) and (d)) is together shown (fitting 2).

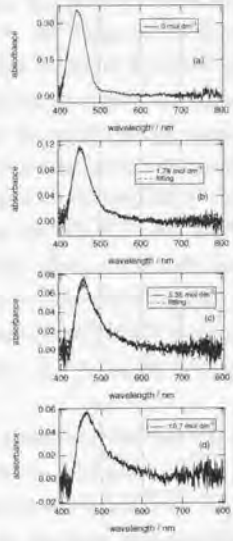

Fig. 3-32 Time-resolved VIS absorption spectra of all-trans retinal at 100 ps.
The 1-butanol concentrations are indicated as legends. In (b) and (c), the fitting spectra (linear-combination of (a) and (d)) are together shown.

and H-bonded species in the S_2 state are in coexistence rather than equilibrated. Strictly speaking, all-trans retinal in the mixed solvent cannot be regarded as a two-component system when the 1-butanol concentration is higher than about 4 mol dm^{-3} as shown in the previous section. However the present linear-combination fitting analysis is not accurate enough to assume more than two species. The above conclusion that the free and 1:1 H-bonded species in the S_2 state are in coexistence does not necessarily exclude the possibility of another minor species.

The time-resolved absorption spectra of all-trans retinal at 0.4 ps are shown in Fig. 3-31 (a) ~ (d): [1-butanol] is (a) 0, (b) 1.78, (c) 5.35, and (d) 10.7 mol dm^{-3} respectively. At 0.4 ps, the $S_n \leftarrow S_2$ absorption band is predominant in these spectra. The fitting of the mixed-solvent S_2 spectra ((b), (c)) with a linear combination of the two neat-solvent S_2 spectra ((a), (d)) resulted in failure as shown together. In fact, it turned out that the S_2 spectrum (a) in neat cyclohexane was useless for the linear-combination fitting. Therefore it is likely that no free S_2 species exists in the protic solvents. In Fig. 3-31 (c), another fitting result using a linear combination of the spectra (b) and (d) is shown together. Not only the spectrum (c) but also the other seven mixed-solvent spectra were well reproduced by the fitting with a linear combination of the spectra (b) and (d). It suggests that two different H-bonded S_2 species are in coexistence or equilibrated in the protic solvents. They could be 1:1 and 1:2 H-bonded complexes of all-trans retinal and 1-butanol. Since the spectra (b) and (d) are not greatly different, it is also presumably possible to ascribe the difference to not the multiple H-bonded species but a solvent environmental effect [86]. However at least no contribution of free species to the S_2 spectra in the protic solvents is possible. Though the idea of 1:1 and 1:2 H-bonded complexes is only speculative, it has to be emphasized that all the retinal molecules are H-bonded in the S_2 state at 0.4 ps. All-trans retinal appears to be a stronger base in the S_2 state than in the ground state. Since the free and H-bonded species coexist in the S_2 state at ~ 0.2 ps, it is deduced that the H-bond formation during or after the $S_2 \rightarrow S_1$ internal conversion process is complete within a few hundred femtoseconds or less.

Since the $S_n \leftarrow S_1$ absorption band in nonpolar solvents is relatively weak and that in the protic solvents is not distinct, the same linear-combination fitting procedure as above is not effective for the S_1 state. The S_1 lifetime in nonpolar solvents was determined to be 32 ± 2 ps by way of the SVD analysis in Sect. 3-1-3-1 and 30 ps in the simple fitting analysis of Fig. 3-26 (a). The absence of a 30-ps ~ 32-ps component in the protic solvents data in Fig. 3-26 ~ 29 strongly suggests that there is no free S_1 all-trans isomer in the protic solvents. It is probable that the T_1 rise time constant or the S_1 lifetime in the protic solvents which was estimated at 20 ps in Fig. 3-26 (b) ~ (d) is ascribed solely to H-bonded species. It is not clear whether multiple H-bonded complexes in S_1 exist or not.

In Fig. 3-32 (a) ~ (d), the time-resolved absorption spectra of all-trans retinal at 100

ps are shown: [1-butanol] is (a) 0, (b) 1.78, (c) 5.35, and (d) 10.7 mol dm^{-3} respectively. At 100 ps, the $T_n \leftarrow T_1$ absorption band is predominant in these spectra. The mixed-solvent T_1 spectra (Fig. 3-32 (b), (c)) were fitted with a linear combination of the two neat-solvent T_1 spectra ((a), (d)), and the fitting results are together shown there. The mixed-solvent T_1 spectra are well reproduced by the linear-combination fitting spectra. The fitting of all the other seven mixed-solvent T_1 spectra resulted in success to the same extent. Therefore it is concluded that the mixed-solvent T_1 spectra are composed of two species: One is definitely the free T_1 all-trans isomer, and the other is probably the 1:1 H-bonded T_1 all-trans isomer. The precursor of the T_1 state in the protic solvents is probably the H-bonded S_1 species. The appearance of the free T_1 species at 100 ps means that H-bond breakage takes place during or after the $S_1 \rightarrow T_1$ intersystem crossing process. It turned out through the fitting procedures that all the mixed-solvent $T_n \leftarrow T_1$ absorption bands at 40 ps ~ 90 ps were well reproduced by using nearly the same linear-combination coefficients as those at 100 ps. This means that the H-bond formation and breakage reaction rates are much larger than the reciprocal of the T_1 formation time. The T_1 lifetime is naturally much longer than the reciprocals of the H-bond formation and breakage reaction rates. Then, it is concluded that the free and H-bonded T_1 species are fully equilibrated in the protic solvents at 40 ps ~ 100 ps.

Finally, it is noted that the above conclusions are against those of Das and Hug [83]. They performed stationary UV-VIS absorption and fluorescence spectroscopy and nanosecond time-resolved VIS absorption spectroscopy of all-trans retinal in mixed solvents of HFIP and cyclohexane. They observed a transient absorbance decrease at wavelength 445 nm and a corresponding increase at 480 nm in the nanosecond time region. Note that the $T_n \leftarrow T_1$ absorption band shifts to the red side on H-bond formation. They concluded that H-bond formation and breakage reactions were slower than the S_1 decay, and an equilibration process between free and H-bonded species took place in the T_1 state with the time constant of a few tens of nanoseconds. The present results and analyses which has shown the ultrafast H-bond formation and breakage reactions are not compatible with their conclusions. HFIP is a stronger H-bonder than 1-butanol, and it is expected that the replacement of 1-butanol with HFIP makes the H-bond formation rate larger. Then, the difference of the H-bonding strength of these two solvents probably does not explain this incompatibility. However it is possible that the incompatibility is due to the difference of the H-bonder concentration. In their measurements, [HFIP] is about a hundred times smaller than [1-butanol] in the present study. Such a low H-bonder concentration may bring about a slower H-bond formation reaction. It may be also possible that what they called an H-bonded complex of all-trans retinal and HFIP was actually a protonated form, and a proton transfer reaction might be much slower. In any case, a time-resolved IR spectroscopic study will be effective to solve this problem, since the

C=O stretching frequency is strongly influenced by H-bond formation and protonation.

3-2-4. Conclusions

Femtosecond time-resolved VIS absorption spectroscopy of all-trans retinal in the mixed solvents of 1-butanol and cyclohexane was performed. Three distinct ranges of the exponential time constants of H-bonded all-trans retinal were obtained from the mixed-solvents data: First, the shortest time constants were about 0.3 ps or less which correspond to the S_3 state. Secondly, both the intense absorption band at about 540 nm and the stimulated emission gain band at 630 nm ~ 800 nm decayed with the time constant of 1 ps ~ 2 ps. These bands were assigned to the S_2 state. Lastly, the T_1 rise time constant was about 20 ps. The precursor of T_1 was identified as the S_1 (n, π^*) state, and the S_2 and S_3 states were both assigned to one-photon allowed (π, π^*) states. No evidence for the state order change of (n, π^*) and (π, π^*) states upon H-bond formation was found. It was confirmed that the free and H-bonded species coexist in the S_3 state. On the contrary, all the retinal molecules were presumed to be H-bonded in the S_2 and S_1 states. The existence of multiple H-bonded species in the S_2 state was suggested. In the T_1 state, the equilibrium between the free and H-bonded species was confirmed. The present study gives the first example of subpicosecond H-bond formation and breakage reactions.

3-3. References

[1] R. M. Hochstrasser and C. K. Johnson, *Biological Processes Studied by Ultrafast Laser Techniques*, in *Ultrashort Laser Pulses - Generation and Applications*, W. Kaiser, Editor. 1993, Springer-Verlag: Berlin. p. 396.

[2] R. A. Mathies, *The femtosecond cis-trans isomerization in vision: a classic barrierless photochemical reaction*, in *Ultrafast Processes in Chemistry and Photobiology*, M. A. El-Sayed, I. Tanaka and Y. Molin, Editor. 1995, Blackwell Science: Oxford. p. 215.

[3] J. P. Corsetti and B. E. Kohler, *J. Chem. Phys.* **67** (1977) 5237.

[4] A. B. Myers and R. R. Birge, *J. Am. Chem. Soc.* **103** (1981) 1881.

[5] S. Ganapathy and R. S. H. Liu, *Photochem. Photobiol.* **56** (1992) 959.

[6] S. Ganapathy, A. Trehan and R. S. H. Liu, *J. Chem. Soc.-Chem. Commun.* (1990) 199.

[7] S. Ganapathy and R. S. H. Liu, *J. Am. Chem. Soc.* **114** (1992) 3459.

[8] W. H. Waddell, R. Crouch, K. Nakanishi and N. J. Turro, *J. Am. Chem. Soc.* **98** (1976) 4189.

[9] H. Hamaguchi, H. Okamoto, M. Tasumi, Y. Mukai and Y. Koyama, *Chem. Phys. Lett.* **107** (1984) 355.

[10] Y. Hirata, N. Mataga, Y. Mukai and Y. Koyama, *Chem. Phys. Lett.* **134** (1987) 166.

[11] T. Tahara, B. N. Toleutaev and H. Hamaguchi, *J. Chem. Phys.* **100** (1994) 786.

[12] Y. Mukai, Y. Koyama, Y. Hirata and N. Mataga, *J. Phys. Chem.* **92** (1988) 4649.

[13] R. Bensasson, E. J. Land and T. G. Truscott, *Photochem. Photobiol.* **21** (1975) 419.

[14] T. Rosenfeld, A. Alchalel and M. Ottolenghi, *J. Phys. Chem.* **78** (1974) 336.

[15] M. M. Fisher and K. Weiss, *Photochem. Photobiol.* **20** (1974) 423.

[16] B. Veyret, S. G. Davis, M. Yoshida and K. Weiss, *J. Am. Chem. Soc.* **100** (1978) 3283.

[17] W. H. Waddell and K. Chihara, *J. Am. Chem. Soc.* **103** (1981) 7389.

[18] N.-H. Jensen, R. Wilbrandt and R. V. Bensasson, *J. Am. Chem. Soc.* **111** (1989) 7877.

[19] H. Hamaguchi, *Transient and time-resolved Raman spectroscopy of short-lived intermediate species*, in *Vibrational spectra and structure*, J. R. During, Editor. 1987, Elsevier: Amsterdam. p. 227.

[20] Y. Katayama, Graduation Thesis, Kitazato Univ., 1997.

[21] R. Wilbrandt, N.-H. Jensen and C. Houee-Levin, *Photochem. Photobiol.* **41** (1985) 175.

[22] T. Yuzawa and H. Hamaguchi, *J. Mol. Struct.* **352-353** (1995) 489.

[23] R. M. Hochstrasser, D. L. Narva and A. C. Nelson, *Chem. Phys. Lett.* **43** (1976) 15.

[24] T. Tahara and H. Hamaguchi, *Chem. Phys. Lett.* **234** (1995) 275.

[25] S. Yamaguchi and H. Hamaguchi, *J. Mol. Struct.* **379** (1996) 87.

[26] R. J. Sension, S. T. Repinec, A. Z. Szarka and R. M. Hochstrasser, *J. Chem. Phys.* **98** (1993) 6291.

[27] T. Arai and K. Tokumaru, *Present status of the photoisomerization about ethylenic bonds*, in *Advances in photochemistry*, D. C. Neckers, D. H. Volman and G. V. Bünau,

Editor. 1995, John Wiley & Sons: New York. p. 1.
[28] H. Hamaguchi, H. Okamoto and M. Tasumi, *Chem. Lett.* (1984) 549.
[29] T. Takemura, P. K. Das, G. Hug and R. S. Becker, *J. Am. Chem. Soc.* **100** (1978) 2626.
[30] G. Drikos, P. Morys and H. Rüppel, *Photochem. Photobiol.* **40** (1984) 133.
[31] G. Drikos and H. Rüppel, *Photochem. Photobiol.* **40** (1984) 93.
[32] G. Drikos, H. Rüppel, W. Sperling and P. Morys, *Photochem. Photobiol.* **40** (1984) 85.
[33] W. H. Waddell, A. M. Schaffer and R. S. Becker, *J. Am. Chem. Soc.* **95** (1973) 8223.
[34] R. R. Birge, J. A. Bennett, B. M. Pierce and T. M. Thomas, *J. Am. Chem. Soc.* **100** (1978) 1533.
[35] R. R. Birge, J. A. Bennett, L. M. Hubbard, H. L. Fang, B. M. Pierce, D. S. Kliger and G. E. Leroi, *J. Am. Chem. Soc.* **104** (1982) 2519.
[36] R. S. Becker, *Photochem. Photobiol.* **48** (1988) 369.
[37] S. Alex, H. L. Thanh and D. Vocelle, *Can. J. Chem.* **70** (1992) 880.
[38] J. Papanikolas, G. C. Walker, V. A. Shamamian, R. L. Christensen and J. C. Baum, *J. Am. Chem. Soc.* **112** (1990) 1912.
[39] M. Merchan and R. Gonzalez-Luque, *J. Chem. Phys.* **106** (1997) 1112.
[40] R. Pariser, *J. Chem. Phys.* **24** (1956) 250.
[41] A. G. Doukas, M. R. Jnnarkar, D. Chandra, R. R. Alfano and R. H. Callender, *Chem. Phys. Lett.* **100** (1983) 420.
[42] E. J. Larson, L. A. Friesen and C. K. Johnson, *Chem. Phys. Lett.* **265** (1997) 161.
[43] S. Takeuchi and T. Tahara, *J. Phys. Chem. A* **101** (1997) 3052.
[44] R. S. H. Liu and A. E. Asato, *Methods Enzymol.* **88** (1982) 506.
[45] N. Ohtsuka, Graduation Thesis, Kitazato Univ., 1996.
[46] B. Honig, U. Dinur, R. R. Birge and T. G. Ebrey, *J. Am. Chem. Soc.* **102** (1980) 488.
[47] P. K. Das and R. S. Becker, *J. Phys. Chem.* **82** (1978) 2081.
[48] W. Dawson and E. W. Abrahamson, *J. Phys. Chem.* **66** (1962) 2542.
[49] W. G. Chen and M. S. Braiman, *Photochem. Photobiol.* **54** (1991) 905.
[50] T. Iwata and J. Koshoubu, *Appl. Spectrosc.* **48** (1994) 1453.
[51] M. Lupu and D. Todor, *Chemometrics and Intelligent Laboratory Systems* **29** (1995) 11.
[52] W. H. A. M. Vandenbroek, D. Wienke, W. J. Melssen, C. W. A. Decrom and L. Buydens, *Anal. Chem.* **67** (1995) 3753.
[53] K. Mohanalingam and H. Hamaguchi, *Chem. Lett.* (1997) 157.
[54] S. L. Logunov, L. Song and M. A. El-Sayed, *J. Phys. Chem.* **100** (1996) 18586.
[55] S. Hotchandani, P. Paquin and R. M. Leblanc, *Can. J. Chem.* **56** (1978) 1985.
[56] A. Samanta, C. Devadoss and R. W. Fessenden, *J. Phys. Chem.* **94** (1990) 7106.
[57] S. Yamaguchi and H. Hamaguchi, *Chem. Phys. Lett.* **227** (1994) 255.
[58] H. Miyasaka, M. Hagihara, T. Okada and N. Mataga, *Chem. Phys. Lett.* **188** (1992) 259.
[59] R. R. Birge, D. F. Bocian and L. M. Hubbard, *J. Am. Chem. Soc.* **104** (1982) 1196.
[60] R. L. Christensen and B. E. Kohler, *Photochem. Photobiol.* **18** (1973) 293.

[61] M. Ros, M. A. Hogenboom, P. Kok and E. J. J. Groenen, *J. Phys. Chem.* **96** (1992) 2975.

[62] T. Rosenfeld, A. Alchalel and M. Ottolenghi, *Intersystem crossing, ionic dissociation, and cis trans isomerization of retinol and related molecules*, in *Excited States of Biological Molecules*, J. B. Birks, Editor. 1976. Wiley, New York: p. 540.

[63] S. Abrash, S. Repinec and R. M. Hochstrasser, *J. Chem. Phys.* **93** (1990) 1041.

[64] J. Saltiel, A. S. Walker and J. Donald F. Sears, *J. Am. Chem. Soc.* **115** (1993) 2453.

[65] F. E. Doany, E. J. Heilweil, R. Moore and R. M. Hochstrasser, *J. Chem. Phys.* **80** (1984) 201.

[66] T. Tahara and H. Hamaguchi, *Chem. Phys. Lett.* **217** (1994) 369.

[67] B. I. Greene, *Chem. Phys. Lett.* **79** (1981) 51.

[68] J. A. Syage, P. M. Felker and A. H. Zewail, *J. Chem. Phys.* **81** (1984) 4706.

[69] H. P. Good, U. P. Wild, E. Haas, E. Fischer, E.-P. Resewitz and E. Lippert, *Ber. Bunsenges. Phys. Chem.* **86** (1982) 126.

[70] J. Saltiel and J. T. D'Agostino, *J. Am. Chem. Soc.* **94** (1972) 6445.

[71] M. Sumitani, N. Nakashima, K. Yoshihara and S. Nagakura, *Chem. Phys. Lett.* **51** (1977) 183.

[72] H. Hamaguchi and K. Iwata, *Chem. Phys. Lett.* **208** (1993) 465.

[73] R. Bensasson, E. J. Land and T. G. Truscott, *Photochem. Photobiol.* **17** (1973) 53.

[74] G. Orlandi and W. Siebrand, *Chem. Phys. Lett.* **30** (1975) 352.

[75] G. Orlandi, P. Palmieri and G. Poggi, *J. Am. Chem. Soc.* **101** (1979) 3492.

[76] G. Orlandi and F. Zerbetto, *J. Mol. Struct.* **138** (1986) 185.

[77] J. Troe and K.-M. Weitzel, *J. Chem. Phys.* **88** (1988) 7030.

[78] J. Saltiel, A. Walker, Y.-P. Sun and J. Donald F. Sears, *J. Am. Chem. Soc.* **112** (1990) 4580.

[79] R. W. Schoenlein, L. A. Peteanu, Q. Wang, R. A. Mathies and C. V. Shank, *J. Phys. Chem.* **97** (1993) 12087.

[80] M. Taiji, K. Bryl, M. Nakagawa, M. Tsuda and T. Kobayashi, *Photochem. Photobiol.* **56** (1992) 1003.

[81] R. W. Schoenlein, L. A. Peteanu, R. A. Mathies and C. V. Shank, *Science* **254** (1991) 412.

[82] M. Yan, D. Manor, G. Weng, H. Chao, L. Rothberg, T. M. Jedju, R. R. Alfano and R. H. Callender, *Proc. Natl. Acad. Sci. USA* **88** (1991) 9809.

[83] P. K. Das and G. L. Hug, *Photochem. Photobiol.* **36** (1982) 455.

[84] T. Takemura, P. K. Das, G. Hug and R. S. Becker, *J. Am. Chem. Soc.* **98** (1976) 7099.

[85] V. Deckert, K. Iwata and H. Hamaguchi, *J. Photochem. Photobiol. A:Chem.* **102** (1996) 35.

[86] M. J. Kamlet, C. Dickinson and R. W. Taft, *Chem. Phys. Lett.* **77** (1981) 69.

[87] H. A. Benesi and J. H. Hildebrand, *J. Am. Chem. Soc.* **71** (1949) 2703.

[88] A. N. Fletcher, *J. Phys. Chem.* **76** (1972) 2562.

4. Ultrafast vibrational relaxation in terthiophene

Ultrafast vibrational population redistribution dynamics and subsequent cooling processes have been identified and quantified for photogenerated S_1 α-terthiophene in solution by using femtosecond time-resolved absorption/emission spectroscopy combined with picosecond time-resolved Raman spectroscopy. The population redistribution among the S_1 vibrational levels dominates the dynamics for the first few picoseconds after the photoexcitation. The cooling of the solvent-solute system then takes place in the time scale of a few tens of picosecond.

4-1. Introduction

The pathway through which the excess energy flows and dissipates from photoexcited molecules influences critically the photophysics and photochemistry in the solution phase. Information on this pathway may be obtained from the observation of the vibrational population redistribution that follows the photoexcitation. Since the vibrational population redistribution occurs in femto-picosecond time scale in the solution phase, ultrafast time-resolved spectroscopies are necessary to identify and quantify this process. Recently developed femtosecond time-resolved absorption/emission spectroscopy have a potential to observe the vibrational population redistribution as time-dependent changes of the vibrational structure [1]. However, the absorption and emission spectra in the solution phase tend to be broadened by fast electronic dephasing and are often structureless. This is particularly the case with large organic molecules, for which congested vibrational levels make the observation of the vibrational structure even more difficult.

In this chapter, the observation of femto-picosecond time-dependent changes of the vibrational structure of the $S_n \leftarrow S_1$ absorption of α-terthiophene in cyclohexane is reported. The $S_n \leftarrow S_1$ absorption spectrum of α-terthiophene has already been observed by Charra et al. with 30-ps time-resolution [2]. Lap et al. recently reported a marked subpicosecond temporal changes of the $S_n \leftarrow S_1$ absorption spectrum of α-terthiophene [3]. In the present study, time-resolved absorption spectra measured in the 40 ~ 100 ps time range agree very well with those of Charra et al. On the other hand, the measured spectra at the early stage (0 ~ 5 ps) differ radically from those reported by Lap et al. We do not observe large shifts of the absorption maximum that was reported by them. Instead, we observe a regular vibrational structure existing only for the first few picoseconds after the photoexcitation. The vibrational mode responsible for this structure has been identified by the picosecond time-resolved Raman spectra in resonance with the $S_n \leftarrow S_1$ transition.

4-2. Experimental

The sample of α-terthiophene (2,2':5',2"-terthiophene) was purchased from Tokyo Kasei and used without further purification. All the spectroscopic measurements were carried out for dilute cyclohexane solutions (2×10^{-3} mol dm^{-3}) at room temperature. In the time-resolved absorption measurements, the sample solution was flowed through a quartz cell (optical path length 0.5 mm) with a magnet-gear pump. In the time-resolved Raman measurement, the sample solution was ejected as a thin film jet flow (thickness 0.2 mm) from a CW dye laser nozzle.

The femtosecond time-resolved VIS absorption/emission measurement was carried out using the spectrometer described in Chap. 2. The center wavelength of the pump pulse was 388 nm, and its pulse energy was 8 μJ. The wavelength 388 nm is at the longer wavelength side of the $S_1 \leftarrow S_0$ absorption spectrum of α-terthiophene.

The transform-limited picosecond time-resolved Raman system has been described elsewhere [4]. The fundamental output from an amplified picosecond dye laser system (588 nm, 10 μJ, 3.2 ps, 3.5 cm^{-1}, 2 kHz) is frequency doubled and used for pumping (294 nm, 1.5 μJ) α-terthiophene. The residual of the fundamental output is attenuated (100 nJ; higher probe energy results in power-broadened Raman spectra) and is used for probing resonance Raman scattering of S_1 α-terthiophene in resonance with the $S_n \leftarrow S_1$ transition. Raman scattering is analyzed by a single spectrograph (HR320, Instruments SA) with a 1800 lines/mm grating and is detected by a liquid nitrogen cooled CCD (LN/CCD-1024 TKB, Princeton Instruments; 1024 × 1024 pixels). Typical exposure time was 30 min for each time delay.

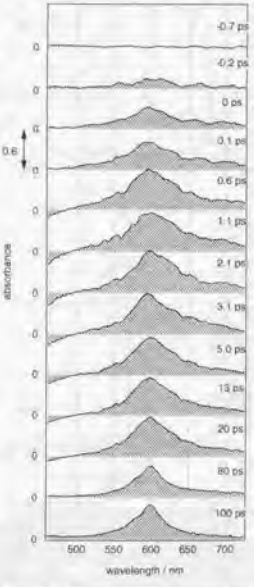

Fig. 4-1 Femtosecond time-resolved VIS absorption spectra of α-terthiophene in cyclohexane.

4-3. Results and Discussion

4-3-1. Femtosecond Time-resolved Absorption/Emission Spectra

Fig. 4-1 shows the femtosecond time-resolved pump-probe absorption/emission spectra of α-terthiophene in cyclohexane. The positive signals centered around 600 nm are due to the photoinduced absorption, while the negative signals in the 450 nm ~ 500 nm region are ascribed to the $S_1 \rightarrow S_0$ stimulated emission gain. The absorption spectrum in the 40 ps ~ 100 ps time range agrees very well with the $S_n \leftarrow S_1$ absorption spectrum reported by Charra et al. [2]. The

absorption rises with time-dependent structures in the subpicosecond time range, retains the structure until about 5 ps after the photoexcitation, and then gradually narrows down toward the final spectrum at 80 ps and later. The absorption peak stays around 600 nm throughout the time course. This observation is contrary to that by Lap et al. [3], who reported a large shift of the absorption peak with time (520 nm at 0.0 ps to 605 nm at 10.2 ps). I think that their result might be affected by the chirp in the probe continuum. In our data processing, the effect of chirp is adequately corrected. Since the structures in the present spectra can be seen until 5 ps after the photoexcitation, they are not ascribable to any coherent artifacts arising from the interaction of the pump and probe pulses. These structures disappear entirely in the spectra after 40 ps. This means that they are not the artifacts due either to the detecting system or to the data processing procedure. We ascribe these time-dependent structures of the absorption band to the vibrational population redistribution as discussed in the following.

4-3-2. Picosecond Time-resolved Raman Spectra

The picosecond time-resolved resonance Raman spectra of α-terthiophene in cyclohexane is shown in Fig. 4-2. The fluorescence background is subtracted in these spectra. A very strong band around 670 cm^{-1} (hereafter called the 671-cm^{-1} band corresponding to the Raman shift at 10 ps) and other several weak bands are observed at all time delays. Apart from the time-dependent shift of the position of the 671-cm^{-1} band, which will be discussed in the following, the spectra at all time delays look the same with one another, indicating that only one species is observed in the picosecond time range. This species is undoubtedly the S_1 state of α-terthiophene, for the Raman spectrum is observed under a resonance with the $S_n \leftarrow S_1$ transition. Of the weak bands in the higher Raman shift region, the bands at 1341 cm^{-1} is assigned to the overtone of the 671-cm^{-1} band. The weaker bands at 1311 cm^{-1} and 1324 cm^{-1} are assigned to the overtone of the 658-cm^{-1} band and the combination of the 671- and 658-cm^{-1} modes, respectively. The existence of the combination band indicates that the 671-cm^{-1} and 658-cm^{-1} bands are due to the vibrations of the same species. This is contrary to what was suggested for the ground state, for which a few Raman bands in the 700 cm^{-1} ~ 650 cm^{-1} region were ascribed to different conformational isomers [5]. It is

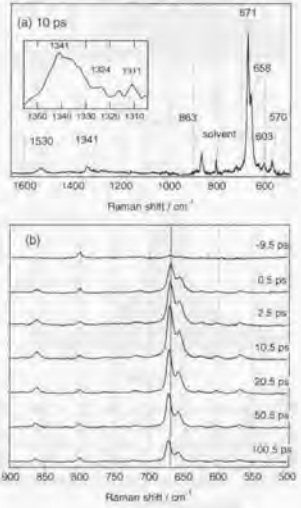

Fig. 4-2 Picosecond time-resolved Raman spectra of S_1 α-terthiophene in cyclohexane. (a) Spectrum at 10 ps after the photoexcitation with Raman shifts indicated. The overtone region is enlarged in the inset. (b) Spectra with time delays increasing from the top to the bottom as indicated in the figure.

most likely that the 671-cm^{-1} mode in the S_1 states corresponds to the 691-cm^{-1} mode in the ground state which is assigned to a ring deformation vibration [5].

4-3-3. Discussion

The fact that the S_1 resonance Raman spectrum is dominated by one strong band at 671 cm^{-1} indicates that there is only one strongly Franck-Condon active mode for the $S_0 \leftarrow S_1$ transition and that the 671-cm^{-1} mode represents this active mode in the S_1 potential [6]. The very weak overtone at 1341 cm^{-1} suggests that the potential displacement along this mode between the S_1 and S_0 states is small. A small potential displacement should lead to a strong 0-0 absorption without distinct vibrational structures. In harmony with this thought, the observed $S_n \leftarrow S_1$ absorption spectrum at 80 ps and later shows a sharp, nearly symmetric profile. The peak position at the later time, 600 nm, can be regarded as the position of the 0-0 transition of the $S_n \leftarrow S_1$ absorption of α-terthiophene.

In order to look into the details of the structures observed in the earlier time, we compare in Fig. 4-3 the absorption spectrum at 0.6 ps (a) with that at 100 ps (b). In the 0.6-ps spectrum, two shoulders are observed at 625 and 653 nm in the longer wavelength side of the 0-0 band. Since only the 671-cm^{-1} mode possesses appreciable Franck-Condon activity in the $S_n \leftarrow S_1$ transition, vibrational structures that are able to accompany the $S_n \leftarrow S_1$ absorption must be related to this mode. In fact, the shoulders at 625 nm and 653 nm correspond very well with the hot transitions with one (Δv=-1) and two (Δv=-2) quanta of the 671-cm^{-1} vibration. These shoulders become weaker as the time goes on and disappear after about 5 ps from the photoexcitation. It is most likely that this time-dependent change of the structure reflects the population redistribution among the vibrational levels of the 671-cm^{-1} mode in the S_1 state and that the time constant of this redistribution is on the order of a few picoseconds. There are also shoulders in the shorter wavelength side of the 0.6-ps spectrum. They are ascribable to the vibrational structures from vibrationally excited S_1 molecules. Note the fact that the Franck-Condon overlaps are larger for the transitions starting from higher vibrational levels and that the vibrational structures are more enhanced for absorption starting

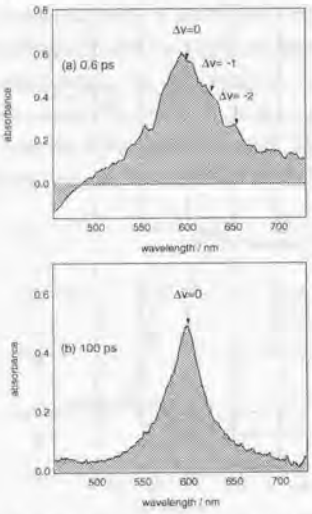

Fig. 4-3 Femtosecond time-resolved VIS absorption spectra of α-terthiophene in cyclohexane at (a) 0.6 ps and (b) 100 ps. The small peak at 460 nm in the spectrum (b) is ascribed to the $T_n \leftarrow T_1$ absorption.

from higher vibrational levels. The disappearance of these structures with time is also explainable in terms of the population decay among the vibrational levels of the 671-cm^{-1} mode.

As noted above, the position of the 671-cm^{-1} band changes with time. This change is quantitatively studied in Fig. 4-4, where the accurate peak position of the 671-cm^{-1} band obtained by the Lorentzian band fitting procedure is plotted against the time delay. Except for the first few picosecond, where the overlapping pump field affects the Raman shift [7], the peak position gradually shifts toward the higher frequency as the time goes on. An exponential fit to the data after 5 ps gives a time constant of 18 ± 2 ps. Similar shifts of the Raman band have been found for S_1 trans-stilbene [8-12] and S_1 *p*-terphenyl [7] and have recently been attributed to the cooling of the solvent-solute system which follows the dissipation of the excess energy from the photoexcited solute molecule to the solvent [10]. We also note that the gradual narrowing of the absorption spectrum in Fig. 4-1 occurs in the same time scale. We conclude that the shift of the peak position of the 671-cm^{-1} Raman band and the gradual narrowing of $S_n \leftarrow S_1$ absorption band are both due to the cooling of the solvent-solute system.

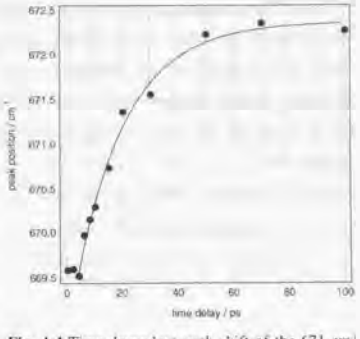

Fig. 4-4 Time dependent peak shift of the 671-cm^{-1} Raman band of S_1 α-terthiophene (circle). A fitting curve with a time constant of 18 ps is together shown.

Finally, the delay in the rise of the stimulated emission gain signal needs to be mentioned. Fig. 4-5 shows the rise curves of the negative signals due to the gain at 460 nm and 480 nm together with that of the $S_n \leftarrow S_1$ absorption. There are clear wavelength dependent delays in the rise of the gain signals. The 460 nm signal rises with a delay of 0.5 ps, while the 480 nm signal shows a delay of 0.6 ps. The stimulated emission gain is caused by population inversion between optically coupled S_0 and S_1 level pairs. The wavelength dependent delay in the rise of the gain signal provides information on the dynamics through which the vibrational population is redistributed from the phtolytically produced Franck-Condon state.

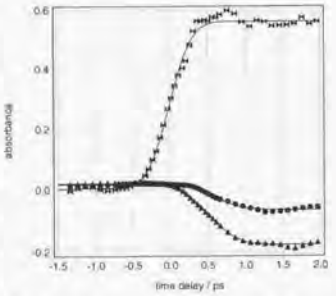

Fig. 4-5 Temporal changes of the $S_n \leftarrow S_1$ absorbance at 600 nm (ribbon) and the $S_n \rightarrow S_1$ stimulated emission gain at 460 nm (triangle), 480 nm (circle).
Fitting curves with delays of 0.5 ps (stimulated emission at 460 nm) and 0.6 ps (stimulated emission at 480 nm) are together shown.

In summary, two distinct relaxation processes have been identified for photoexcited

α-terthiophene in cyclohexane. One is the intramolecular vibrational population redistribution occurring in the subpicosecond/picosecond time region, which is detected by femtosecond time-resolved absorption/emission spectroscopy and is substantiated by picosecond time-resolved Raman spectroscopy. The other is the cooling process of the solvent-solute system in the time range of a few tens of picosecond. This process manifests itself in the shift of the peak position of the Raman spectrum and also in the narrowing of the $S_n \leftarrow S_1$ absorption spectrum. The observation of the time-dependent change of the vibrational structure has been made possible by a rather unusual situation in which only one vibrational mode (671 cm^{-1}) is Franck-Condon active, leading to a very simple vibrational structure of the $S_n \leftarrow S_1$ absorption spectrum.

4-4. References

[1] C. H. B. Cruz, R. L. Fork, W. H. Knox and C. V. Shank, *Chem. Phys. Lett.* **132** (1986) 341.

[2] F. Charra, D. Fichou, J.-M. Nunzi and N. Pfeffer, *Chem. Phys. Lett.* **192** (1992) 566.

[3] D. V. Lap, D. Grebner, S. Rentsch and H. Naarmann, *Chem. Phys. Lett.* **211** (1993) 135.

[4] K. Iwata, S. Yamaguchi and H. Hamaguchi, *Rev. Sci. Instrum.* **64** (1993) 2140.

[5] Y. Furukawa, M. Akimoto and I. Harada, *Synth. Met.* **18** (1987) 151.

[6] A. C. Albrecht, *J. Chem. Phys.* **34** (1961) 1476.

[7] K. Iwata and H. Hamaguchi, *J. Raman Spectrosc.* **25** (1994) 615.

[8] J. Qian, S. L. Schultz, G. R. Bradburn and J. M. Jean, *J. Phys. Chem.* **97** (1993) 10638.

[9] R. E. Hester, P. Matousek, J. N. Moore, A. W. Parker, W. T. Toner and M. Towrie, *Chem. Phys. Lett.* **208** (1993) 471.

[10] H. Hamaguchi and K. Iwata, *Chem. Phys. Lett.* **208** (1993) 465.

[11] K. Iwata and H. Hamaguchi, *Chem. Phys. Lett.* **196** (1992) 462.

[12] W. L. Weaver, L. A. Huston, K. Iwata and T. L. Gustafson, *J. Phys. Chem.* **96** (1992) 8956.

5. Concluding remarks

In this dissertation, the construction of the femtosecond time-resolved pump-probe UV-VIS absorption spectrometer and its application to ultrafast photochemistry and photophysics in solution have been described.

In Chap. 2, the construction of the femtosecond absorption spectrometer and the development of the OKE cross-correlation method were described. The spectrometer enabled the measurements of transient spectra such as excited-state absorption spectra and ground-state bleaching spectra in the wavelength range of 300 nm ~ 800 nm with time-resolution of about 300 fs. Further improvements to acquire faster time resolution by using pulse compression technique and to extend the measurable wavelength range to the shorter wavelength side will be needed in the future. The OKE method was established as a chirp-structure measurement technique for the purpose of chirp correction of time-resolved UV-VIS absorption spectra. The OKE method required still shorter measurement time and afforded much more data points on the wavelength axis than the conventional SFG or DFG method. It will become a standard method of chirp correction in the future.

In Chap. 3, the femtosecond time-resolved UV-VIS absorption spectroscopy of retinal was described. Sect. 3-1 reported the all-trans → 13-cis·9-cis photoisomerization reaction in nonpolar solvents. In Fig. 5-1, what was already established before the present study and what has been newly clarified in this thesis are summarized. Four transient species (S_3, S_2, S_1, T_1) were found in the time-resolved VIS spectra of all-trans retinal. On the assumption that S_3 is of B_u^+ (π, π^*) character, S_2 and S_1 were characterized as A_g^- (π, π^*) and (n, π^*) respectively. The relaxation sequence and the excited-state lifetimes of 9-cis retinal were found to be nearly identical with those of the all-trans isomer. The possible maximum quantum yields of the all-trans → 13-cis·9-cis and 9-cis → all-trans isomerization reactions that complete in the excited singlet manifold were estimated to be sufficiently lower than the known quantum yields. The femtosecond VIS data did not provide any evidence for an isomerization reaction complete in the excited singlet states. The femtosecond UV spectra of all-trans retinal were successfully analyzed in terms of an isomerization scheme involving a perpendicular excited singlet state, p*. The p* lifetime was found to be 7.2 ± 2 ps. It was

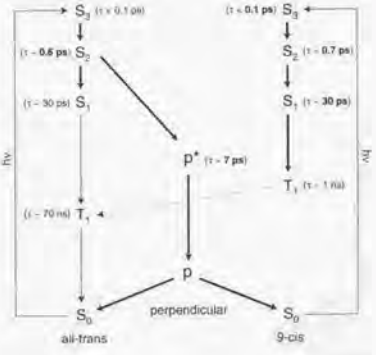

Fig. 5-1 Photochemical and photophysical processes of retinal in aerated nonpolar solvents.
Lifetimes in bold letters and thick lines with arrows correspond to what have been newly clarified in this thesis. Lifetimes in plain letters and thin lines with arrows correspond to what was already established before the present study.

concluded that the precursor of p* was most likely the S_2 state. The quantum yield values of the all-trans → 13-cis·9-cis isomerization in the temperature range 269 K ~ 298 K obtained from the femtosecond UV data were in good agreement with the reported values measured by HPLC. The height of the energy barrier on the way from the S_2 state to the p* state was roughly estimated as $(1.2 \pm 0.6) \times 10^3$ cm^{-1}. In Sect. 3-2, H-bonding dynamics between all-trans retinal and 1-butanol was described. No evidence for the state order change of (n, π^*) and (π, π^*) states upon H-bond formation was found. It was confirmed that the free and H-bonded species coexist in the S_1 state. On the contrary, all the retinal molecules were presumed to be H-bonded in the S_2 and S_3 states. The existence of multiple H-bonded species in the S_2 state was suggested. In the T_1 state, the equilibrium between the free and H-bonded all-trans retinal was confirmed. The first example of subpicosecond H-bond formation and breakage reactions was given in the present study.

In Chap. 4, ultrafast vibrational relaxation of α-terthiophene in cyclohexane was described. Two distinct relaxation processes were identified by using femtosecond time-resolved VIS absorption and picosecond time-resolved Raman spectroscopies. One was the intramolecular vibrational population redistribution and relaxation occurring in the subpicosecond/picosecond time region. The other was the cooling process of the solvent-solute system in the time range of a few tens of picosecond.

This thesis has illustrated good examples which show the usefulness of ultrafast time-resolved spectroscopy in probing chemical reaction dynamics. Time-resolved spectroscopy will continue to play an important role in the future for studying interesting photochemical and photophysical subjects.

Acknowledgments

I would like to express my sincerest gratitude to Prof. Hiro-o Hamaguchi for his guidance throughout the present research and for giving me the opportunity to study ultrafast time-resolved spectroscopy in Kanagawa Academy of Science and Technology (KAST) and in the Univ. of Tokyo, Komaba.

I am very grateful to Prof. Koichi Iwata for teaching me a lot of experimental techniques and giving me fruitful advice, to Prof. Tahei Tahara for his encouragement and stimulating discussion, to Dr. Taka-aki Ishibashi for his precise discussion and helpful advice, to Dr. Tetsuro Yuzawa for advising me on the SVD analysis and retinal photochemistry, and to Dr. Mamoru Hashimoto for offering me a lot of valuable advice and helping me in many ways.

I show my sincere gratitude to Dr. K. Mohanalingam for his critical reading of the present manuscript and friendly encouragement. I am indebted to Mr. Natsuhiko Ohtsuka and Mr. Yusuke Katayama for their HPLC measurements. I thank all the other members of Hamaguchi Project of KAST.

I am grateful to Dr. Satoshi Takeuchi and Dr. Taro Sekikawa for affording me their papers and many valuable e-mail pieces of advice.

Finally, I wish to thank my wife and parents.

This dissertation was prepared by making use of the following:
Hardware: PowerBook 540c, Nupowr167 plus, Microline 600PSII, BINDOMATIC 1000
Software: QuarkXPress 3.31J, Nisus Writer 5.0.4J, MathType 3.1, EndNote Plus 2.0.1,
Igor Pro 3.03, Adobe Illustrator 7.0.1J, CS ChemDraw Pro 3.5.1

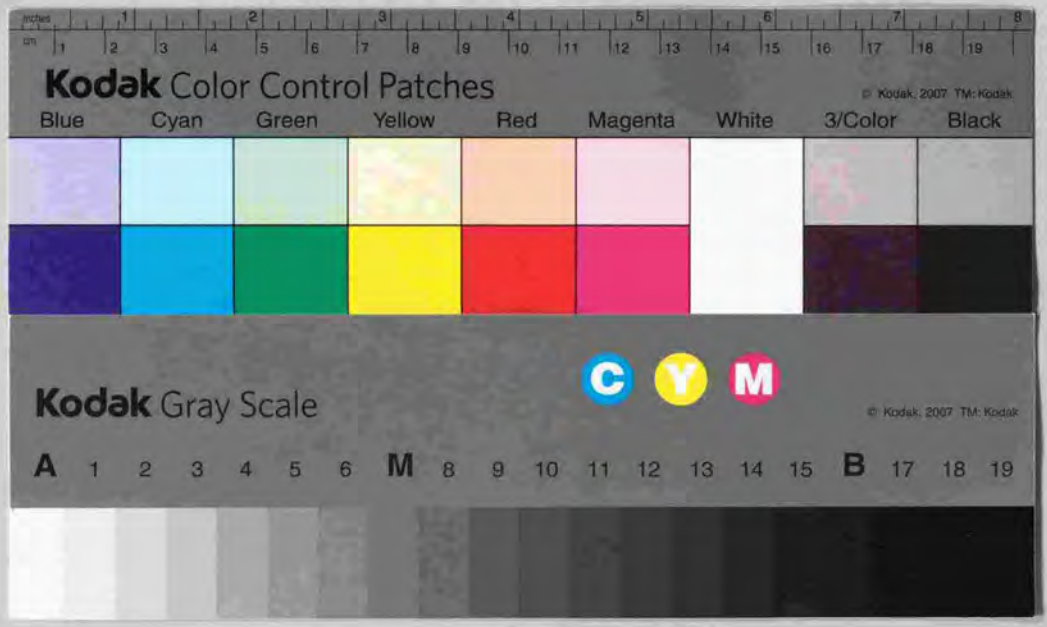
inches
cm
Kodak Color Control Patches
© Kodak, 2007 TM: Kodak
Blue
Cyan
Green
Yellow
Red
Magenta
White
3/Color
Black
Kodak Gray Scale
C
Y
M
© Kodak, 2007 TM: Kodak
A 1 2 3 4 5 6 M 8 9 10 11 12 13 14 15 B 17 18 19